

Multicarrier Transceivers using DFT Filter Banks with Perfect Reconstruction

François Duplessis Beaulieu



Department of Electrical & Computer Engineering
McGill University
Montreal, Canada

August 2007

A thesis submitted to McGill University in partial fulfillment of the requirements for the degree of Doctor of Philosophy.

© 2007 François Duplessis Beaulieu

Abstract

In recent years, multicarrier modulation techniques have stirred great interest among engineers and researchers working in the field of telecommunications. Multicarrier systems are characterized by the fact that constellation symbols are modulated in parallel onto several distinct subcarriers. One specific form of multicarrier modulation, referred to as OFDM (orthogonal frequency division multiplexing), has been deployed in many applications, such as in wireless LAN routers, in high-definition television tuners, and in DSL modems. Multicarrier and OFDM systems have proved to be much more robust against impairments such as impulse noise and sudden channel fadings than their single carrier counterparts. Moreover, channel equalization in OFDM systems can be performed quite easily by a set of per-subcarrier one-tap equalizers.

Despite their many advantages, OFDM systems have a few, but important, drawbacks. In particular, OFDM relies on the inverse FFT for modulation purposes, which leads to a very poor spectral containment and a high susceptibility to narrowband noise. To mitigate this problem, we propose in this thesis to perform multicarrier modulation using a perfect reconstruction (PR) DFT filter bank instead of employing the inverse FFT. The design of such filter banks is addressed using a novel method that guarantees the PR property to be satisfied while the spectral containment is being maximized. Equalization in the proposed DFT filter bank transceiver takes advantage of the fact that the filter banks do not contribute to any distortion due to its PR nature. Two equalization schemes are presented. The first one is based on a zero-padded block linear equalization approach, and the second one utilizes a one-tap per subcarrier configuration. The estimation of the channel coefficients in the proposed transceiver is also addressed. A blind estimation method that exploits the inherent cyclostationarity of the transmitted signal is derived.

Computer experiments presented in this thesis indicate that the spectral containment of the proposed PR DFT filter bank transceiver is indeed superior to that of the OFDM system. Moreover, simulations conducted in a DSL-like environment contaminated by a narrowband noise show that the achievable bit rate of the proposed transceiver is much higher than that of a conventional OFDM system.

Résumé

Depuis quelques années, les techniques de modulation multi-porteuse ont suscité beaucoup d'intérêts parmi les ingénieurs et les chercheurs travaillant dans le domaine des télécommunications. Les systèmes à ondes porteuses multiples se distinguent par le fait que les symboles de constellation sont modulés en parallèle sur plusieurs ondes sous-porteuses. Une technologie particulière de modulation multi-porteuse, appelée OFDM (multiplexage par répartition orthogonale de la fréquence), est présentement déployée dans plusieurs applications telles que les routeurs sans fil pour réseaux locaux, les récepteurs numériques pour la télévision haute définition et les modems de lignes d'abonnés numériques (DSL). Les systèmes à ondes porteuses multiples s'avèrent être beaucoup plus robustes que les systèmes à onde porteuse unique pour combattre les dégradations telles que le bruit impulsif et les évanouissements soudains du canal. De plus, l'égalisation du canal dans les systèmes OFDM peut être facilement accomplie à l'aide d'un ensemble d'égalisateurs à un seul coefficient.

Malgré leurs nombreux avantages, les systèmes OFDM présentent quelques inconvénients importants. Entre autres, OFDM se sert de la FFT inverse pour des fins de modulation, ce qui engendre un mauvais confinement spectral et une grande susceptibilité au bruit à bande étroite. Pour résoudre ce problème, nous proposons dans cette thèse de moduler les symboles de constellation en utilisant un banc de filtres DFT à reconstruction parfaite (RP) au lieu d'employer la FFT inverse. La conception de ces bancs de filtres s'effectue en utilisant une nouvelle méthode qui garantit que la RP soit satisfaite tout en maximisant le confinement spectral. L'égalisation de l'émetteur-récepteur proposé tire avantage du fait que les bancs de filtres utilisés ne contribuent à aucune distorsion grâce à la propriété de RP. Deux techniques d'égalisation sont présentées. La première méthode est basée sur

l'utilisation de la méthode de remplissage de zéros et d'un égalisateur à bloc linéaire. La seconde méthode repose sur l'utilisation d'un égalisateur n'ayant qu'un seul coefficient par onde sous-porteuse. L'estimation des coefficients du canal est également considérée. Une méthode aveugle qui exploite la cyclostationnarité inhérente du signal transmis est développée. Les résultats expérimentaux présentés dans cette thèse indiquent que le confinement spectral de l'émetteur-récepteur proposé est effectivement supérieur à celui du système OFDM. De plus, des simulations effectuées dans un environnement contaminé par un bruit à bande étroite, ressemblant à celui que l'on trouve en DSL, démontrent que le débit binaire réalisable de l'émetteur-récepteur proposé est beaucoup plus rapide que celui d'un système OFDM conventionnel.

Acknowledgments

First and foremost, I would like to convey my sincere gratitude to my advisor, Prof. Benoît Champagne. Through his helpful guidance, I have certainly become today a better researcher and scientist. Furthermore, I would like to thank the other members of my Ph. D. committee, Prof. Peter Caines and Prof. Tho Le-Ngoc. I also acknowledge *le Fonds québécois de la recherche sur la nature et les technologies*, Prof. Benoît Champagne and *l'Aide financière aux études* of the Québec government for providing financial support to complete this research.

I am grateful to my fellow colleagues in the Telecommunications and Signal Processing Laboratory. They all contributed to the creation of a pleasant and stimulating work environment. In particular, I would like to express my gratitude to Benoît, Joachim (Joe) and Mohamed for their friendship. I enjoyed our numerous discussions about our research and life in general. Sharing the lunch hour with you was one of the highlights of my day!

I would like to thank my family for their love and kindness. They have always supported me throughout my studies, and I am forever indebted to them. *À ma mère, France, mon père, Laurent, et ma soeur, Isabelle, merci énormément.*

Last but not least, I would like to extend my thanks to the woman with whom I share my life, Geneviève. Your cheerful nature, generosity and love are very precious to me. I look forward to many years of joy and happiness together!

Contents

| | | |
|----------|---|-----------|
| 1 | Introduction | 1 |
| 1.1 | Filter Banks in Digital Communications | 1 |
| 1.1.1 | Multicarrier Modulation and Filter Bank Transceivers | 2 |
| 1.1.2 | Application to DSL Communications | 4 |
| 1.2 | Literature Survey | 5 |
| 1.2.1 | Filter Banks for Multicarrier Communications | 5 |
| 1.2.2 | Design of DFT Filter Bank Transceivers | 8 |
| 1.3 | Thesis Objectives and Contributions | 10 |
| 1.3.1 | Key Contributions | 10 |
| 1.3.2 | List of Publications | 13 |
| 1.4 | Thesis Organization and Notation | 14 |
| 2 | Overview of Multicarrier Modulation and DFT Filter Banks | 17 |
| 2.1 | Multicarrier Modulation | 17 |
| 2.1.1 | Multicarrier Modulation Overview | 18 |
| 2.1.2 | OFDM and Discrete Multitone | 19 |
| 2.2 | Filter Bank Transceivers | 23 |
| 2.2.1 | General Concepts | 24 |

| | | |
|----------|---|-----------|
| 2.2.2 | Polyphase Representation and Perfect Reconstruction | 26 |
| 2.3 | DFT Filter Banks | 31 |
| 2.3.1 | DFT Modulation | 32 |
| 2.3.2 | Implementation and Computational Complexity | 34 |
| 2.4 | Chapter Summary | 35 |
| 3 | Design of Perfect Reconstruction DFT Filter Banks | 41 |
| 3.1 | Parametrization of the Prototype Filter | 42 |
| 3.1.1 | The Two-Step Parametrization Method | 42 |
| 3.1.2 | Parametrization of the Polyphase Matrix for M and K Coprime . . . | 45 |
| 3.1.3 | Parametrization of the Polyphase Matrix for M and K Non-Coprime | 47 |
| 3.2 | Prototype Filter Design | 48 |
| 3.2.1 | Optimization Problem | 49 |
| 3.2.2 | Computation of the Stopband Energy | 50 |
| 3.3 | Chapter Summary | 52 |
| 4 | Channel Equalization Techniques | 55 |
| 4.1 | Zero-Padded Block Linear Equalizer | 57 |
| 4.1.1 | Zero-Forcing Solution | 58 |
| 4.1.2 | MMSE Solution | 61 |
| 4.1.3 | MMSE with Insufficient Guard Length | 65 |
| 4.2 | One-Tap Equalizer | 67 |
| 4.2.1 | Intrablock and Interblock ISI | 68 |
| 4.2.2 | Zero-Forcing and MMSE Solutions | 72 |
| 4.2.3 | Optimal Solution for Non-Ideal Prototype Filters | 74 |
| 4.3 | Performance of the Proposed Equalizers | 77 |

| | | |
|----------|---|-----------|
| 4.3.1 | Computational Complexity | 78 |
| 4.3.2 | Subchannel SNR | 79 |
| 4.4 | Chapter Summary | 82 |
| 5 | Blind Channel Identification | 83 |
| 5.1 | Cyclostationarity and Redundant Filter Banks | 85 |
| 5.1.1 | General Considerations on Cyclostationarity | 85 |
| 5.1.2 | Statistical Properties of the DFT Filter Bank Transceiver | 86 |
| 5.2 | Channel Identification | 89 |
| 5.2.1 | Homogeneous System of Linear Equations | 89 |
| 5.2.2 | Channel Coefficients Estimation | 92 |
| 5.3 | Chapter Summary | 96 |
| 6 | Computer Simulations and Experimental Results | 99 |
| 6.1 | Design of Perfect Reconstruction Prototype Filters | 100 |
| 6.1.1 | Design Examples | 100 |
| 6.1.2 | Comparison with OFDM and Other Non-PR Design | 103 |
| 6.2 | Channel Equalization | 105 |
| 6.2.1 | Simulation Parameters | 106 |
| 6.2.2 | Equalization with Zero-Padding | 109 |
| 6.2.3 | Equalization with One-Tap per Subcarrier | 112 |
| 6.2.4 | Comparison Between the Proposed Equalization Schemes | 114 |
| 6.3 | Blind Channel Identification | 116 |
| 6.3.1 | Simulation Parameters | 116 |
| 6.3.2 | Channel Coefficient Estimation | 117 |
| 6.4 | Chapter Summary | 123 |

| | |
|--|------------|
| 7 Conclusion | 125 |
| 7.1 Summary of our Work | 125 |
| 7.2 Future Work | 128 |
| A Entries of the Polyphase Matrix $U(z)$ | 131 |
| References | 135 |

List of Figures

| | | |
|------|--|----|
| 1.1 | DSL Topology. | 4 |
| 2.1 | Multicarrier modulator. | 18 |
| 2.2 | OFDM transmitter. | 20 |
| 2.3 | OFDM receiver. | 21 |
| 2.4 | Channel model. | 22 |
| 2.5 | A filter bank transceiver. | 25 |
| 2.6 | Frequency response of OFDM subchannels for $M = 64$ | 26 |
| 2.7 | Polyphase representation of a filter bank transceiver. | 28 |
| 2.8 | Polynomial matrix representation of a filter bank transceiver. | 31 |
| 2.9 | Modulated filter. | 32 |
| 2.10 | DFT filter bank transceiver with $\mathbf{S}(z) = \tilde{\mathbf{G}}(z)$ | 35 |
| 2.11 | Implementation of the DFT filter bank transmitter. | 36 |
| 2.12 | Implementation of the DFT filter bank receiver. | 37 |
| 3.1 | Outline of the prototype filter design process. | 53 |
| 4.1 | A zero-padded DFT filter bank transceiver. | 58 |

| | | |
|------|---|-----|
| 4.2 | Polyphase representation of a DFT filter bank transceiver with a one-tap per subcarrier equalizer. | 68 |
| 4.3 | Alternate (non-polyphase) representation of the DFT filter bank transceiver with a one-tap per subcarrier equalizer. | 70 |
| 4.4 | Subchannel frequency response for a large M | 71 |
| 6.1 | Frequency responses of PR DFT filter bank prototype filters with $M = 64$ | 101 |
| 6.2 | Frequency responses of PR DFT filter bank prototype filters with $M = 128$ | 102 |
| 6.3 | Frequency responses of the PR DFT filter bank with $M = 128$, $K/M = 1.25$ and $D/M = 20$ and of the OFDM prototype filter with $M = 128$ | 104 |
| 6.4 | Frequency responses of the first few sidelobes of the PR and non-PR DFT filter banks with $M = 128$, $K/M = 1.25$ and $D/M = 20$ | 105 |
| 6.5 | Frequency response of the channels modelling a 100-m and a 200-m UTP-3 cable. | 107 |
| 6.6 | Power spectral density of the radio frequency interference. | 108 |
| 6.7 | Achievable bit rate of the OFDM system and the proposed transceiver using zero-padding and a block linear equalizer with a zero-forcing and a MMSE solution. | 110 |
| 6.8 | Achievable bit rate of the OFDM system and the proposed transceiver using zero-padding and a block linear equalizer with insufficient guard length ($B = 6$). | 112 |
| 6.9 | Symbol mean square error using a one-tap per subcarrier equalizer. | 113 |
| 6.10 | Achievable bit rate of the OFDM system and the proposed transceiver using a one-tap per subcarrier equalizer (approximate zero-forcing solution) with a PR and a non-PR prototype filter. | 115 |

6.11 Time-averaged channel MSE using different cyclic frequencies. 118

6.12 Estimation of the cyclic autocorrelation and the channel coefficients using a
one-cycle and a multiple-cycle approach. 119

6.13 Symbol mean square error of the transceiver using a one-tap equalizer. . . . 121

6.14 Channel coefficient estimation using the inverse iteration method and the
SVD. 122

List of Tables

| | | |
|-----|---|----|
| 2.1 | Implementation of the DFT filter bank transmitter. | 38 |
| 2.2 | Implementation of the DFT filter bank receiver. | 38 |
| 3.1 | Computation of the autocorrelation function using the FFT. | 52 |
| 4.1 | Algorithm for the computation of $\mathbf{v}[n] = \mathbf{E}_{\text{ZF}}\mathbf{w}[n]$ | 61 |
| 4.2 | Algorithm for the computation of $\mathbf{v}[n] = \mathbf{E}_{\text{MMSE}}\mathbf{w}[n]$ | 64 |
| 4.3 | Algorithm for the computation of $\mathbf{D} = \mathbf{C}_{0,0}\mathbf{C}_{0,0}^T$, where $\mathbf{C}_{0,0}$ is Toeplitz and lower triangular. | 65 |
| 4.4 | Algorithm for the computation of $\mathbf{D} = \mathbf{C}_{1,0}\mathbf{C}_{1,0}^T$, where $\mathbf{C}_{1,0}$ is Toeplitz and upper triangular. | 67 |
| 4.5 | Algorithm for the computation of $\hat{\mathbf{x}}[n] = \mathbf{\Lambda}_E\mathbf{y}[n]$ | 73 |
| 4.6 | Proposed equalization schemes for PR DFT filter bank transceivers. | 77 |
| 4.7 | Computational complexity of the zero-padded block linear equalizer and the one-tap equalizer (per frame). | 78 |
| 4.8 | Number of flops of the zero-padded block linear equalizer and the one-tap equalizer with $M = 128$, $K/M = 1.25$, $N/M = 1.375$ and $D/M = 20$ (per frame). | 79 |

| | | |
|-----|--|-----|
| 5.1 | Algorithm for the computation of $\hat{\Phi}_n$ | 93 |
| 5.2 | Blind channel identification algorithm. | 97 |
| 6.1 | Spectral features of several PR prototype filters, obtained via the method proposed in Chapter 3. | 100 |
| 6.2 | Spectral features of the OFDM prototype filters. | 100 |
| 6.3 | International amateur radio frequency bands (below 11 MHz). | 107 |

List of Acronyms

| | |
|-------|------------------------------------|
| AWGN | Additive White Gaussian Noise |
| A/D | Analog-to-digital |
| CSI | Channel State Information |
| DCT | Discrete Cosine Transform |
| DFE | Decision-Feedback Equalizer |
| DFT | Discrete Fourier Transform |
| DMT | Discrete Multitone |
| DSL | Digital Subscriber Line |
| DTFT | Discrete-Time Fourier Transform |
| D/A | Digital-to-analog |
| FDM | Frequency Division Multiplexing |
| FEQ | Frequency-Domain Equalizer |
| FFT | Fast Fourier Transform |
| FIR | Finite Impulse Response |
| flops | floating point operations |
| FMT | Filtered Multitone |
| IDFT | Inverse Discrete Fourier Transform |
| ISI | Intersymbol Interference |

| | |
|------|--|
| MCM | Multicarrier Communication |
| MMSE | Minimum Mean Square Error |
| MSE | Mean Square Error |
| OFDM | Orthogonal Frequency Division Multiplexing |
| PCFB | Principal Component Filter Bank |
| PR | Perfect Reconstruction |
| PSD | Power Spectral Density |
| QAM | Quadrature Amplitude Modulation |
| QPSK | Quadrature Phase-Shift Keying |
| RFI | Radio Frequency Interference |
| SNR | Signal-to-Noise Ratio |
| SVD | Singular Value Decomposition |

List of Important Symbols

| | |
|-----------------|--|
| M | Number of subcarriers |
| K | Upsampling factor |
| P | Least common multiple of M and K |
| D | Prototype filter length |
| Q | Channel length |
| $C(z)$ | Z -transform of the channel coefficients $c[m]$ |
| $\mathbf{C}(z)$ | Channel matrix |
| $G_{k,i}(z)$ | Polyphase components of the transmitting filter bank |
| $\mathbf{G}(z)$ | Polyphase matrix of the transmitting filter bank |
| $S_{i,k}(z)$ | Polyphase components of the receiving filter bank |
| $\mathbf{S}(z)$ | Polyphase matrix of the receiving filter bank |
| \mathbf{W} | DFT matrix |
| $\mathbf{U}(z)$ | Polyphase matrix of the DFT filter bank |
| $F_0(z)$ | Z -transform of the prototype filter $f_0[m]$ |
| $x_i[n]$ | Transmitted symbol |
| σ_x^2 | Symbol power |
| $y_i[n]$ | Received symbol |
| $u[m]$ | Transmitted signal |

| | |
|-------------------------------------|---|
| σ_u^2 | Power of the transmitted signal |
| $r_u[n, \tau]$ | Autocorrelation of the transmitted signal |
| $R_u[k, \tau]$ | Cyclic autocorrelation of the transmitted signal |
| $\mathbf{u}[n]$ | Vector of transmitted samples |
| $v[m]$ | Received signal |
| $r_v[n, \tau]$ | Autocorrelation of the received signal |
| $R_v[k, \tau]$ | Cyclic autocorrelation of the received signal |
| $\mathbf{v}[n]$ | Vector of received samples |
| $\eta[m]$ | Additive noise |
| $\boldsymbol{\eta}[n]$ | Vector of additive noise samples |
| $\boldsymbol{\theta}$ | Vector of real numbers, parametrizing a PR prototype filter |
| $\mathbf{f}_0(\boldsymbol{\theta})$ | Vector of filter coefficients parametrized by $\boldsymbol{\theta}$ |
| $J(\boldsymbol{\theta})$ | Stopband energy of the PR prototype filter |
| B | Guard length |
| \mathbf{E} | Block linear equalizer |
| e_i | Coefficients of the one-tap equalizer |
| $\mathbf{T}(z)$ | Transfer function of the transceiver |
| d | Internal latency (delay) of the transceiver |

Chapter 1

Introduction

An overview of the thesis is presented in this chapter. The general framework is introduced in Section 1.1, where we discuss how filter banks can be employed in digital communications. In Section 1.2, a survey of the relevant literature is given. The objective of the thesis and the research contributions presented throughout this work are then outlined in Section 1.3. Lastly, we present in Section 1.4 a brief overview of the upcoming chapters.

1.1 Filter Banks in Digital Communications

Digital technology has revolutionized our relationship with information. For instance, digital information offers an environment rich in multimedia capabilities, interactive content and customization possibilities towards a specific user. This new environment is beyond anything that could be envisioned with traditional means such as analog broadcasting or printed media. Perhaps more importantly, digital information can easily be shared across the globe by individuals and companies in the blink of an eye. In this new digital age, digital communications have become an integral part of today's life. The constant desire to

increase the transmission speed and robustness against errors is a driving factor that, from an engineering point of view, has contributed to the advancement of digital communication theory. The transmission of digital information still presents many challenges that must be overcome, and the study of novel and improved transmission techniques represents one step forward to further enhance the global digital experience. One such technique, based on the use of modulated filter banks in a multicarrier modulation context, is developed in this work.

1.1.1 Multicarrier Modulation and Filter Bank Transceivers

In order to improve the robustness of communication systems against various impairments, the concept of multicarrier modulation (MCM) was introduced [1, 2]. In MCM systems, the channel bandwidth is divided into several subchannels through the use of narrowband subcarriers. Digital information, represented by a sequence of constellation symbols (e.g. QAM or QPSK symbols), is transmitted in parallel using the available subcarriers. Sending and receiving constellation symbols in parallel offer many advantages. For instance, the duration of each symbol is longer than that of a single-carrier system with an identical symbol rate. We can thus conclude that impairments that are localized in time, such as multipath fading and impulse noise, are less likely to provoke catastrophic errors. Moreover, highly efficient solutions to combat intersymbol interference (ISI) can be derived by appending redundant information to the block of transmitted data. The added redundancy can act as a guard interval that will prevent successive blocks to interfere with each other.

A well known MCM scheme, referred to as orthogonal frequency-division multiplexing (OFDM), relies on the discrete Fourier transform (DFT) to modulate the constellation symbols onto different subcarriers [3]. OFDM-based MCM systems are now becoming more and more ubiquitous with their presence in many wireless and wireline communication

standards. For example, these systems are currently deployed in wireless Internet routers (Wi-Fi) [4, 5], in high-definition television tuners (digital terrestrial television) [6] and in digital subscriber line (DSL) modems [7, 8]. The wide adoption and huge popularity of OFDM can be explained in part by its robustness against ISI, multipath fadings and impulse noise, as explained above. Furthermore, the entire system can be implemented using reasonable computational power since the DFT can be performed very efficiently via the fast Fourier transform (FFT). ISI can also be mitigated at a low computational cost by a combination of additional redundancy in the form of a cyclic prefix and the use of a one-tap frequency domain equalizer [9].

Despite its success story, OFDM suffers from a few, but important, drawbacks. Chiefly among them is the considerable overlap between adjacent subchannels, which leads to a very poor spectral containment, and makes OFDM highly sensitive to narrowband interference [10]. This problem can be remedied by considering alternatives to the OFDM's usage of the DFT. One promising solution consists in using filter banks, i.e. an array of filters arranged in a parallel configuration [11]. Compared to the DFT, filter banks offer a much higher spectral containment.

However, filter banks usually require high computational power to operate and their design generally involves solving complex mathematical optimization problems. These issues can be mitigated by considering *modulated* filter banks instead of unstructured ones. Modulated filter banks rely on modulation techniques, which can be implemented efficiently using fast algorithms such as the FFT, to properly shift the frequency content of a so-called prototype filter [12]. The design of these filter banks is thus considerably simplified since only a single filter has to be designed.

1.1.2 Application to DSL Communications

We consider digital subscriber line (DSL) as the main application for the filter bank based transceiver under study, although many results and ideas presented in this thesis can be applied to other situations (e.g. wireless communications). Many telecommunication companies rely on the DSL technology to offer broadband Internet access points to business or residential customers [13]. As illustrated in Figure 1.1, DSL utilizes standard twisted copper telephone lines (or local loops) to transmit high-bit-rate data, at frequencies well above the voice spectrum. These local loops, typically measuring a few kilometres, connect the so-called central office, which serves a small neighbourhood, to the customer premises. In recent years, optical network units have been deployed in an effort to bring optical fibre links closer to customers. In these cases, the local loop is generally shortened to a few hundred metres. Traditional voice-based telephone services can easily co-exist with DSL by using a duplexing technique (or a splitter) that will keep the voice band separate from the data band.

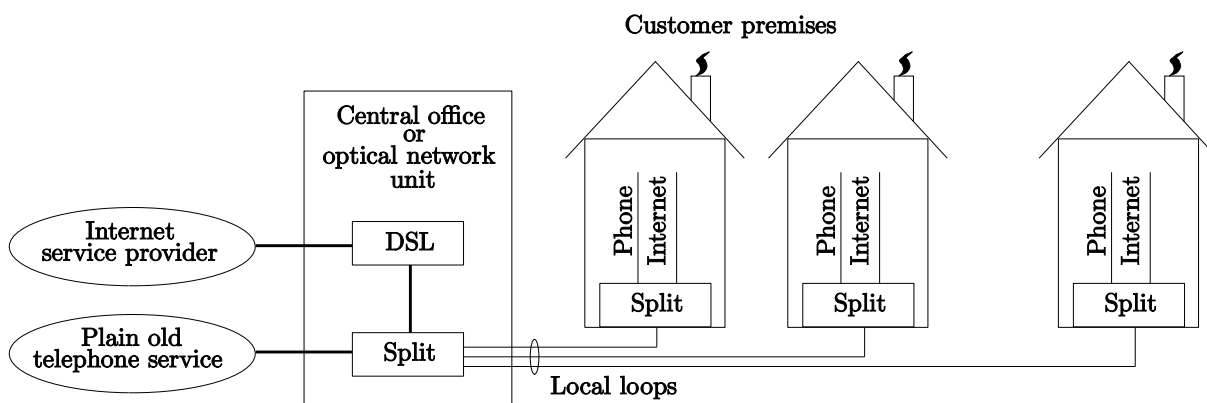


Fig. 1.1 DSL Topology.

Noise in local telephone loops comes from different sources. First, we have to consider the fact that local loops leaving the central office are usually grouped in a large cable [14].

Due to the electromagnetic coupling, the proximity of the local loops to each other gives rise to a crosstalk phenomenon. Crosstalk is often considered as the most severe impairment, but dynamic spectrum management techniques can be employed to mitigate this problem [15]. Other sources of noise include impulse noise, generated by various natural or artificial transient phenomena such as electrostatic discharges, and thermal white noise, caused by the agitation of the electrons in a metallic wire [14]. Finally, radio frequency interference (RFI) is also a significant contaminant. The local loop can indeed serve as an antenna which picks up radio broadcasts in the environment [16]. In DSL, RFI takes the form of a narrowband noise.

1.2 Literature Survey

Traditionally, filter banks and MCM systems have been studied independently from each other. Filter banks were mainly considered in applications like speech coders and echo cancellers, where subband processing can be highly beneficial [17]. MCM systems, however, would rely on transforms like the DFT, which do not require the consideration of filter bank theory [2]. We review in this section the literature that contributed to link MCM and filter banks together. We specifically focus on key contributions that considered the use of modulated filter banks in MCM systems.

1.2.1 Filter Banks for Multicarrier Communications

Vetterli was one of the first to notice that by inverting the analysis and synthesis stages of a subband coder, a filter bank-based multicarrier transceiver could be obtained [18]. As such, the vast literature on filter banks (see e.g. [12] and the references therein) was suddenly available to researchers interested in multicarrier systems. In recent years, filter bank

transceivers have been investigated in many publications. Important milestones include the work of Lin and Phoong on distortion-free unstructured filter bank transceivers which appears in [19]. Instead of considering ISI-free systems, Vaidyanathan *et al.* study in [20] the use of so-called principal component filter banks (PCFB) as a solution to the bit rate maximization problem.

Although both transceivers in [19] and [20] present valuable theoretical breakthroughs, they have important limitations that prevent their use in practice. For instance, to implement the transceiver in [19], one must solve several highly nonlinear optimization problems, a rather difficult task. In [20], the optimality of PCFB may not hold in real conditions, due to certain over-simplifications assumed by the authors. Moreover, both transceivers are channel dependant, meaning that a new filter bank would have to be designed each time the channel varies. This is, in practice, unconceivable due to the complexity of the operations involved. Even if we assume a zero-cost design, the use of such filter banks is computationally expensive because of their unstructured nature, which does not allow an efficient implementation.

To reduce the computational complexity of the filter banks considered in [19, 20], one may consider the use of modulated filters. In this regard, both the cosine function, implemented efficiently using the discrete cosine transform (DCT) [21–27], or the complex exponential, through the use of the DFT and the FFT, can be employed [28–37].

In [21], Tzannes *et al.* have coined the term “discrete wavelet multitone” or its acronym, DWMT, for a multicarrier system based on cosine modulated filter banks that satisfy the perfect reconstruction (PR) property¹. The DWMT system is thoroughly investigated by Sandberg and Tzannes in [23], where it is determined that, to properly combat ISI intro-

¹A pair of filter banks has the perfect reconstruction property if, when connected back-to-back, a signal passing through it would remain unchanged, except for a delay.

duced by the channel, a group of so-called post-combiners must be added after the receiving filter bank. These post-combiners take the form of two-dimensional filters spanning across time and nearby subchannels. They can be derived analytically according to the work of Farhang-Boroujeny and Lin [26]. The necessity of such a scheme can be understood intuitively by noting that, due to the nature of the DCT, only real constellation symbols may be transmitted in DWMT systems. Thus, any phase rotation caused by a non-linear phase channel can only be compensated through a linear combination of the present and past received symbols from different subchannels [22]. Lastly, Farhang-Boroujeny and Lin propose in [25, 27] to simplify the post-combiner structure by employing a modified receiver. Although the computational complexity of the receiver is increased, these authors report that a two-tap per subcarrier equalizer is sufficient to mitigate the ISI, which is considerably less than the number of taps normally required for the proper operation of post-combiners [25, 27].

Cherubini *et al.* investigate in [28–30] the use of DFT modulated filter banks in multicarrier transceivers. The proposed system is referred to as a filtered multitone (FMT) transceiver. Contrary to DWMT transceivers, the prototype filter is not designed such that PR is enforced, and it exploits over-interpolation² to increase the spectral containment [28–30]. Moreover, in FMT, the cancellation of the ISI can be performed without post-combiners, since complex constellation symbols, whose phase can easily be corrected, are employed. Per-subchannel decision-feedback equalizers (DFE) are thus employed [28–30]. These equalizers can be derived analytically according to the work of Benvenuto *et al.* [38], where it is shown that they actually combat both the ISI introduced by the channel and the distortion due to the non-PR nature of the filter banks [38].

²A transmitting filter bank is over-interpolated when the number of output samples, K , is greater than the number of input symbols, M , i.e. when $K > M$.

This work focuses on the use of the DFT filter banks instead of the cosine modulated filter banks for multicarrier modulation. This choice can be explained, in part, by the greater ease of equalization, since no post-combiners are required. We thus now review in the next section the literature relevant to the design of DFT filter bank transceivers.

1.2.2 Design of DFT Filter Bank Transceivers

To implement a DFT filter bank transceiver, the issues of prototype filter design and channel equalization must be addressed. As noted in this section, several solutions have been proposed throughout the years. The design of prototype filters suitable for DFT filter bank multicarrier transceivers has been investigated by many researchers using different approaches [30–37], which can be grouped in two categories:

Near-PR methods. The distortion introduced by the filter banks is explicitly taken into account in near-PR methods, but is not completely eliminated.

Heuristic methods. The distortion is not an explicit factor in heuristic methods. It is assumed to be below an acceptable threshold.

Note that none of these methods yield PR prototype filters.

References advocating the use of heuristic methods include [34–37]. For instance, in [34], Berenguer and Wassel propose to use any general purpose lowpass filter design methods. In [35], Lim *et al.* suggest the use of the window methods [39]. Gao *et al.* consider in [36] the window method and a modified Parks-McClellan algorithm. Finally, Tonello in [37] synthesizes the prototype filter in the frequency domain based on a root-raised-cosine spectrum.

The design techniques presented in [30–33] attempt to minimize the distortion introduced by the filter banks and are hereby referred to as near-PR methods. Specifically,

in [30], Cherubini *et al.* use an iterative least squares algorithm to minimize the stopband energy and the ISI due to the filter banks. Borna and Davidson explore in [32, 33] the tradeoff between the subchannel interference mitigation and the stopband energy of the filter. In particular, the design problem is formulated into a convex optimization problem where the goal is to minimize the stopband energy of the filter while constraining the ISI due to the filter banks to be below a certain threshold. Lastly, Phoong *et al.* derive in [31] an analytical expression for the prototype filter that maximizes the signal-to-interference ratio.

Regardless of how the prototype filter is designed, equalization in DFT filter bank transceivers is commonly performed via per-subchannel DFEs as proposed by Cherubini *et al.* in [28–30]. If we hypothesize that the ISI present at the output of the receiving filter bank is small enough, other schemes are possible such as a one-tap per-subchannel equalizer, which is considered by Tonello and Phoong *et al.* in [37] and [31], respectively. Moreover, if one can afford the bandwidth cost, the received symbols can be equalized by adding guard intervals between each transmitted frame of data. These guard interval will isolate (or “flush”) the channel between each frame, and, thus, effectively cancel interblock ISI. Intrablock ISI is then usually cancelled by a block linear equalizer. Guard intervals in the form of zero-padding are studied in [40] and [41] respectively by Scaglione *et al.* and by Vaidyanathan and Vrcelj.

The acquisition of channel state information (CSI) in DFT filter bank transceivers has been addressed very scarcely in the literature. Cherubini *et al.* suggest in [30] to employ a training procedure similar to the one used in the ADSL standard [7]. To the best of our knowledge, published works which specifically deal with blind estimation techniques for DFT filter bank transceivers are quasi nonexistent. Current techniques are mostly limited

to non-overlapping filter banks³ (e.g. see [42, 43]), and are thus not appropriate for DFT filter bank transceivers.

1.3 Thesis Objectives and Contributions

The main objective of this thesis is to propose a filter bank transceiver suitable for multicarrier systems as an alternative to OFDM. The aim is to provide better spectral containment to combat impairments such as narrowband noise. We specifically focus on DFT filter banks due to their overall low computational complexity and their attractive spectral features which yield a high spectral containment. Unlike earlier works (e.g. [30, 31, 33, 35–37]), we design the DFT filter bank using a novel approach that enforces the PR criterion. PR greatly simplifies the equalization process, since one does not need to worry about any distortion generated by the filter bank itself.

1.3.1 Key Contributions

This thesis presents several key contributions in the field of DFT filter bank transceivers. They can be grouped in three categories and are summarized as follows:

Design of PR prototype filters for DFT filter bank transceivers. A novel method for the design of PR prototype filters suitable for DFT filter bank transceivers is developed. The design problem is formulated as an unconstrained minimization problem where the objective is to minimize the stopband energy of the prototype filter. The minimization process is carried out over a set of real parameters that parametrize the filter coefficients in such a way that PR is achieved. For PR to be theoretically feasible, we consider over-interpolated DFT filter banks, i.e. filter banks where the

³Non-overlapping filter banks employ filters whose length is equal to the number of subcarriers. As such, the filters do not “overlap” from one transmitted frame to the other.

interpolation factor K is greater than the number of subcarriers M ($K > M$). Unlike the somewhat similar parametrization-based method proposed in [44], we do not necessarily assume that K is a multiple of M , i.e. $K = 2M, 3M, \dots$. The flexibility provided by our method in terms of choosing M and K is essential if we want the excess bandwidth ratio K/M to be close to 1, i.e. $K/M \approx 1$, in order to maintain a good bandwidth efficiency. Design examples presented in this thesis show that the spectral containment of the resulting PR DFT filter bank transceiver is much higher than that of an OFDM system. For instance, one particular design with $M = 128$ and $K/M = 1.25$ has a stopband energy which is 14 dB lower than the stopband energy of a conventional OFDM system.

Equalization methods for PR DFT filter bank transceivers. Traditionally, equalization in DFT filter bank transceivers is performed using per-subcarrier DFEs that must mitigate both the distortion due to the presence of non-PR filter banks and the ISI introduced by the channel [30]. By exploiting the PR nature of the proposed DFT filter bank transceiver, we only have to be concerned with the channel ISI, which greatly simplifies the equalization process. We thus consider new equalization schemes for DFT filter bank transceivers that satisfy the PR property. The first method is based on a well-known combination of zero-padding and block linear equalization [40]. The main drawback of this method is its computational complexity, which is even higher than that of the traditional approach, i.e. a group of per-subcarrier DFEs. In order to reduce the computational complexity, we propose a second method which relies on simple per-subcarrier one-tap equalizers. Such an equalizer operates under the assumptions that the number of subcarriers M is high enough so that the subchannel frequency response is approximately flat, and that the stopband energy

of the prototype filter is low so that the interference between adjacent subcarriers is small. As shown in this thesis, these assumptions can easily be satisfied in practice. Moreover, the computational cost of the one-tap equalizer is considerably lower than the cost of the zero-padded block linear equalizer and the cost of per-subchannel DFEs. Performance is evaluated for the two proposed equalization methods by taking into account the signal-to-noise ratio (SNR) of each subcarrier and by measuring the maximum achievable bit rate to satisfy a certain error probability. Results presented in this thesis indicate that the PR DFT filter bank transceiver using either proposed equalization methods outperforms the conventional OFDM transceiver in environments where narrowband noise dominates. Obviously, the one-tap equalizer is preferred due to its low computational requirements.

Blind channel identification in DFT filter bank transceivers. To compute the equalizer coefficients, we first need to estimate the channel impulse response. We propose in this thesis a novel blind method that exploits the inherent cyclostationarity present in over-interpolated DFT filter banks. Blind methods do not require the transmission of a known sequence to identify the channel; they rely instead on the statistical properties of the signal being transmitted. Cyclostationarity and blind channel identification have been previously considered in [43,45], but the methods presented therein are restricted to non-overlapping filter banks and are therefore of little use here. By analyzing the statistical properties of the received signal within a DFT filter bank transceiver, we show that the cyclostationarity can be exploited to derive a homogeneous system of linear equations. The channel coefficients can then be estimated by finding the null space of the aforementioned system using the inverse iteration method. Results presented in this thesis show that the estimated channel coefficients

do indeed converge to their true values. Convergence necessitates a certain number of frames, which is feasible in slowly time-varying channels.

1.3.2 List of Publications

Most results and ideas presented in this thesis have been published by the author in various articles. The list of publications contains the following five references (the relevant chapters or sections of this thesis are indicated in parentheses):

1. F. D. Beaulieu and B. Champagne, “Design of Prototype Filters for Perfect Reconstruction DFT Filter Bank Transceivers”, submitted to *Signal Processing* (journal). (Chapters 3 and 4.)
2. F. D. Beaulieu and B. Champagne, “Blind Channel Equalization for Perfect Reconstruction DFT Filter Bank Transceivers”, submitted to *to be determined*. (Chapter 5.)
3. F. D. Beaulieu and B. Champagne, “One-Tap Equalizer for Perfect Reconstruction DFT Filter Bank Transceivers”, *Proc. URSI Int. Symp. on Signals, Systems and Electronics*, Montreal, Canada, July 2007, pp. 391-394. (Section 4.2.)
4. F. D. Beaulieu and B. Champagne, “MMSE Equalization for Zero Padded Multicarrier Systems with Insufficient Guard Length”, *Proc. IEEE Int. Conf. on Acoustics, Speech, and Signal Processing*, vol. 4, Toulouse, France, May 2006, pp. 377-380. (Section 4.1.)
5. F. D. Beaulieu and B. Champagne, “Multicarrier Modulation using Perfect Reconstruction DFT Filter Bank Transceivers”, *Proc. Int. Conf. on Information, Communication and Signal Processing*, Bangkok, Thailand, Dec. 2005, pp. 111-115. (Chapter 3.)

1.4 Thesis Organization and Notation

This thesis is organized as follows.

Chapter 2 contains the essential background information that will serve as a basis for the subsequent chapters. We present the concept of multicarrier modulation and provide an introduction to the theory of filter banks. The DFT filter bank is then discussed in detail.

In Chapter 3, we propose a method for the design of a PR prototype filter suitable for DFT filter banks. The design problem is expressed as an optimization problem based on the parametrization of the prototype filter. The parametrization is established such that the PR property can always be satisfied.

Chapter 4 investigates the equalization issue in DFT filter bank transceivers. A zero-padding scheme, which preserves the PR property of the transceiver, is first presented. A suboptimal but very computationally simple method, based on the use of single-tap equalizers, is then proposed.

In Chapter 5, we consider the estimation of the channel impulse response using a blind algorithm. The statistical properties of the output signal of a transmitting DFT filter bank is established and proved to be cyclostationary. The cyclostationary property is then exploited to derive a system of linear equations which can be solved to obtain the channel coefficients.

We assess in Chapter 6 the performance of the different methods and algorithms proposed in this thesis. Performance is evaluated through numerous computer-based experiments that simulate real-world DSL deployment conditions. We present examples of PR prototype filter designs, measure the achievable bit rates obtained by the proposed equalization schemes and verify the convergence of the blind channel estimation algorithm.

Finally, Chapter 7 summarizes the results and ideas presented in this thesis. Some possibilities for future research are also discussed.

Notation: Matrices and vectors are written using uppercase and lowercase bold letters, respectively. The $M \times N$ zero matrix is denoted by $\mathbf{0}_{M \times N}$; \mathbf{I}_M denotes the $M \times M$ identity matrix. Subscripts are omitted when they can easily be deduced from the context. We use $[\mathbf{A}]_{i,k}$ to refer to the (i, k) entry of matrix \mathbf{A} , while $[\mathbf{A}]_{i,:}$ and $[\mathbf{A}]_{:,k}$ respectively denote the i -th row and the k -th column of \mathbf{A} . Finally, superscripts $*$, T and H represent complex conjugation, transposition and hermitian transposition, respectively.

Chapter 2

Overview of Multicarrier Modulation and DFT Filter Banks

In this chapter, we establish the theoretical framework of this thesis by reviewing the appropriate background information on multicarrier modulation and DFT filter banks. The theory presented here will provide a basis for the remaining chapters. Specifically, we first give an overview of multicarrier modulation in Section 2.1. We then introduce the theory of filter bank transceivers in Section 2.2. DFT filter banks are discussed in Section 2.3, and, lastly, a summary of this chapter appears in Section 2.4.

2.1 Multicarrier Modulation

We present in this section an outline of the theory of multicarrier modulation (MCM). To illustrate the concept of MCM clearly, we briefly describe one the most widely deployed MCM scheme, namely, OFDM.

2.1.1 Multicarrier Modulation Overview

Unlike traditional communication schemes, MCM utilizes several carriers, commonly referred to as subcarriers, to transmit digital data. In essence, MCM divides the available channel bandwidth into M subchannels through the use of M narrowband subcarriers. Such idea is illustrated in Figure 2.1. The input bit stream is first divided in frames of length β . These bits are then allocated to each subcarrier such that we have a set of β_i bits in the i -th subcarrier, and $\sum_{i=0}^{M-1} \beta_i = \beta$. The number of bits β_i in each subcarriers does not have to be identical, and the overall bit error rate can be improved by loading more bits in subcarriers having higher signal-to-noise ratios (SNR) [46]. Each set of bits is mapped to a complex symbol using, for instance, a QAM or a QPSK constellation [3]. These symbols are then digitally modulated and added together. Each subcarrier is thus responsible for modulating a specific portion of the input bit stream. Lastly, the resulting signal is converted to an analog representation, using, for example, radio-frequency circuitry in the case of wireless communications, or a baseband front end for DSL.

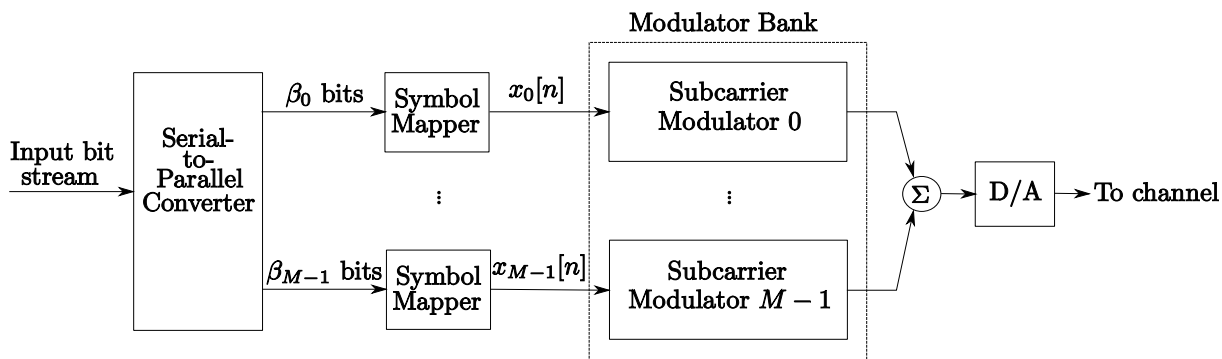


Fig. 2.1 Multicarrier modulator.

On the surface, MCM is very similar to frequency division multiplexing (FDM), but there are important differences. In FDM, different signals belonging to different users are

multiplexed together by shifting their spectrum so that they do not overlap with the others. This usually requires guard bands or sharp filters to ensure that overlapping does not occur. Any overlap would create interferences capable of degrading the performance of the system significantly. In MCM, there is only one data source, corresponding to a single bit stream which is divided among different subcarriers, as explained previously. Overlap in frequency is allowed and, by employing *orthogonal* subcarriers, perfect recovery is still possible.

One of the key advantages of MCM is the increased symbol duration due to the temporal “smearing” offered by the frequency multiplexing. This provides better robustness against impairments such as impulse noise and sudden fades [2]. Compared to MCM systems, the duration of each individual symbol in single carrier systems is effectively shortened by a factor M . Single carrier systems are thus much more vulnerable to impairments that are localized in time.

2.1.2 OFDM and Discrete Multitone

Transmitter and Receiver

OFDM or, equivalently, discrete multitone (DMT), as it is referred in the DSL literature (e.g. [9]), is probably the most well documented MCM system¹. In a nutshell, as illustrated in Figure 2.2, OFDM relies on the inverse discrete Fourier transform (IDFT) to digitally modulate a frame of constellation symbols [9, 47]. Specifically, the modulated symbols are given by

$$u_i[n] = \frac{1}{M} \sum_{k=0}^{M-1} x_k[n] e^{j2\pi ki/M}, \quad i = 0, \dots, M-1.$$

¹In this work, we employ the terms “OFDM” and “DMT” interchangeably.

Inversely, $x_k[n]$ can be retrieved using the DFT, i.e.

$$x_k[n] = \sum_{i=0}^{M-1} u_i[n] e^{-j2\pi ki/M}, \quad i = 0, \dots, M-1. \quad (2.1)$$

In practice, the fast Fourier transform (FFT) algorithm is used to compute the DFT, implying that M is usually a power of 2. For baseband systems like DSL, we require $u_i[n]$ to be real to ensure that a real signal is sent through the physical channel. To satisfy this constraint, we must select $x_i[n] = x_{M-i}^*[n]$ for $i = M/2 + 1, \dots, M-1$, while $x_0[n]$ and $x_{M/2}[n]$ must be real symbols.

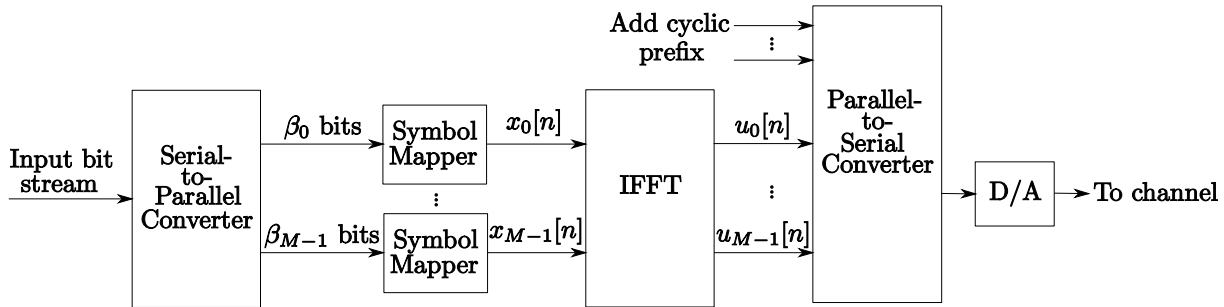


Fig. 2.2 OFDM transmitter.

The presence of a channel between the transmitter and the receiver will destroy the subcarrier orthogonality which could make symbol recovery rather difficult. To maintain orthogonality, a so-called cyclic prefix of length B is concatenated to the time-domain block (a mathematical justification is given later), yielding the following transmitted sequence

$$\{u_{M-B}[n], \dots, u_{M-1}[n], u_0[n], \dots, u_{M-1}[n]\}.$$

After the cyclic prefix has been added, the sequence is converted to an analog signal, via a digital-to-analog (D/A) converter, and sent through the channel.

The OFDM receiver is shown in Figure 2.3. The received signal is first digitally sampled via an analog-to-digital (A/D) converter, and the cyclic prefix is removed. Demodulation is performed using an FFT, and the resulting symbols are equalized by a one-tap frequency-domain equalizer (FEQ), as detailed later. Once these symbols are decoded, the original bit stream can be retrieved.

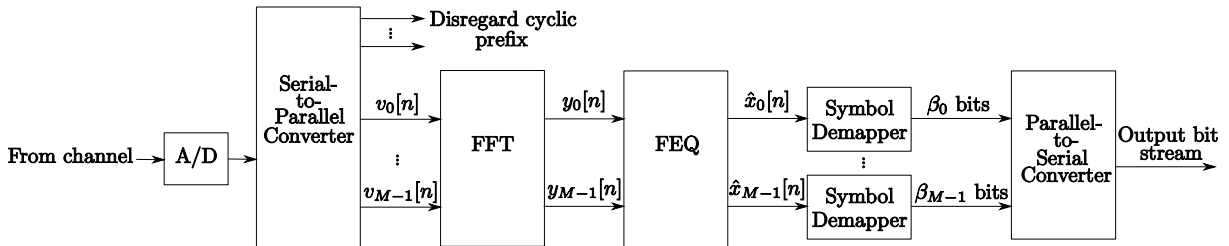


Fig. 2.3 OFDM receiver.

Cyclic Prefix

We will now show how the cyclic prefix can conserve orthogonality in the presence of a channel. Throughout this work, the cascade of the D/A converter, the transmission channel, the additive noise source $\eta(t)$ and the A/D converter is modelled as a discrete-time linear time-invariant filter $C(z)$ with discrete-time additive noise $\eta[m]$, as illustrated in Figure 2.4. Such assumption is reasonable by assuming that the Nyquist criterion is satisfied, i.e. the highest frequency component of the received waveform is at most one-half the sampling frequency of the transceiver. We also assume the use of high quality D/A and A/D circuitry with good anti-aliasing filters. In addition, we suppose that the digital channel $C(z)$ is a Q -tap finite impulse response (FIR) filter, i.e.

$$C(z) = \sum_{m=0}^{Q-1} c[m]z^{-m}, \quad (2.2)$$

and that the coefficients $c[m]$ are real. In situations where the impulse response of the channel is infinite, a shortening filter can be employed to reduce the channel to a finite length [48]. Note that the noise signal $\eta[m]$ may represent a combination of several noise sources. In DSL applications, for instance, $\eta[m]$ could represent the combined effects of crosstalk, impulse noise, thermal noise and/or radio frequency interference (see Section 1.1.2 for an explanation concerning the presence of such noise types in DSL).

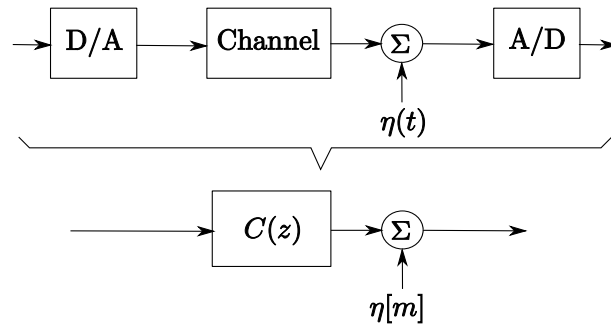


Fig. 2.4 Channel model.

If the length of the cyclic prefix, B , is greater or equal to $Q - 1$, i.e. if $B \geq Q - 1$, then one can verify that, in the absence of noise, the received time-domain sequence can be expressed as

$$v_i[n] = u_i[n] \textcircled{C} c_{\text{ZP}}[i], \quad i = 0, \dots, M - 1, \quad (2.3)$$

where \textcircled{C} denotes circular convolution and $c_{\text{ZP}}[m]$ represents the zero-padded sequence of channel coefficients, i.e.

$$c_{\text{ZP}}[i] = \begin{cases} c[i] & \text{if } 0 \leq i \leq Q - 1 \\ 0 & \text{if } Q \leq i \leq M - 1. \end{cases}$$

Taking the M -point DFT of (2.3) and using (2.1) yield [39]

$$y_k[n] = x_k[n]C_{\text{ZP}}[k], \quad k = 0, \dots, M - 1,$$

where $y_k[n]$ and $C_{\text{ZP}}[k]$ respectively denote the DFT of $v_m[n]$ and $c_{\text{ZP}}[m]$. Assuming that $C_{\text{ZP}}[k] \neq 0$, the transmitted symbols, $x_k[n]$, can be recovered with

$$x_k[n] = \frac{1}{C_{\text{ZP}}[k]} y_k[n]. \quad (2.4)$$

We can now observe that the one-tap FEQ illustrated in Figure 2.3 simply corresponds to the term $1/C_{\text{ZP}}[k]$ that appears in (2.4). In practice, this quantity can be estimated by a blind algorithm or by a training procedure [49].

The transmission scheme described in this section is at the core of some widely deployed telecommunication technologies such as DSL [7, 8], terrestrial digital audio/video broadcasting [6] and various Wi-Fi standards [4, 5]. OFDM benefits from the advantages of MCM at a very low computational cost. The number of flops (floating point operations), defined in this thesis as the total number of real additions and multiplications, required by an OFDM receiver is approximately $5M \log_2 M$, which corresponds to the implementation of the FFT [50]. The cost of implementing the FEQ is negligible for a moderately high M .

2.2 Filter Bank Transceivers

Many schemes suitable for MCM exist, and, despite the popularity of OFDM, there are good reasons to consider alternatives. The theory of filter banks, as explained below, can be used to extend the concept of OFDM into a more general framework, so that different techniques can be considered.

2.2.1 General Concepts

As illustrated in Figure 2.5, a filter bank transceiver consists of two filter banks, one at the transmitting end and the other at the receiving end². A filter bank contains M digital filters arranged in a parallel configuration. These filters are employed in combination with K -fold digital upsamplers³ at the transmitter, denoted by $\uparrow K$, and with K -fold decimators⁴ at the receiver, denoted by $\downarrow K$. To emphasize the multirate nature of the system, we use two time indices, n and m , to denote the time samples corresponding to the low sampling rate (or the symbol rate) and the high sampling rate (or the channel rate), respectively. There exist many types of filter banks depending on how the filters are designed. In Figure 2.5, we assume that the input bit stream is already appropriately partitioned and mapped to constellation symbols $x_0[n], \dots, x_{M-1}[n]$. The symbol demapping devices are also omitted. In practical implementations, to combat intersymbol interference (ISI) due to the presence of a frequency selective channel, the symbols at the output of the receiving filter bank, $y_0[n], \dots, y_{M-1}[n]$, need to be equalized. The equalization scheme is not shown in Figure 2.5, but it will be fully discussed in Chapter 4.

The relationship between M , the number of subcarrier, and K , the upsampling factor, is important. Three situations can occur:

²The transmitting and receiving filter banks are sometimes referred as the synthesis and analysis filter banks, respectively.

³A K -fold upsampler is a device that inserts $K - 1$ zeros between each successive sample of an arbitrary signal $x[n]$. The resulting signal, denoted here by $x_u[m]$, is thus given by

$$x_u[m] = \begin{cases} x[m/K] & \text{if } m/K \text{ is an integer} \\ 0 & \text{otherwise.} \end{cases}$$

⁴A K -fold decimator reduces the sampling rate by selecting one sample for every K successive samples of an arbitrary signal $x[m]$. The resulting signal, denoted here by $x_d[n]$, is thus given by

$$x_d[n] = x[Kn].$$

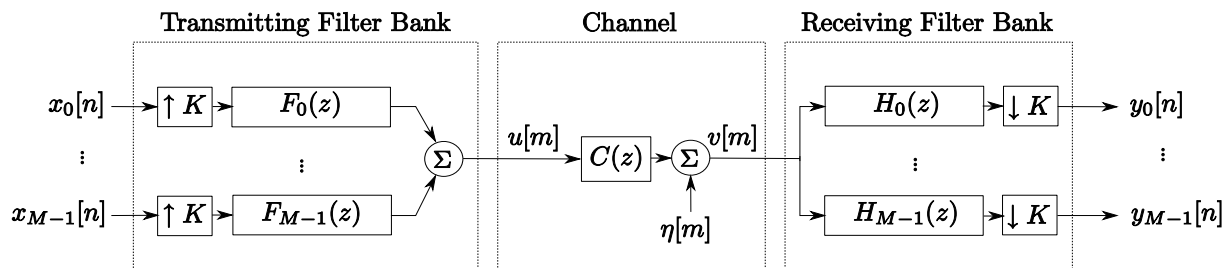


Fig. 2.5 A filter bank transceiver.

1. $K = M$. The transceiver is minimally interpolated, i.e. non-redundant.
2. $K > M$. The transceiver is over-interpolated, i.e. redundant.
3. $K < M$. The transceiver is under-interpolated. In this case, some information is irretrievably lost. This configuration is not suitable for practical applications.

Although redundancy reduces the bandwidth efficiency of the system, it can be very desirable for equalization purposes. For instance, the OFDM transceiver utilizes redundancy (in the form of a cyclic prefix) to equalize an FIR channel. A similar approach can be developed for filter banks, as detailed in Chapters 3 and 4. For this reason, in this work, we focus our attention on over-interpolated transceivers.

So why one should consider filter bank transceivers since OFDM is a proven and widely deployed MCM technique? Essentially, filter banks offer more degrees of freedom which can be exploited to mitigate certain issues associated with OFDM. For instance, OFDM suffers from poor subchannel spectral selectivity since the frequency response of adjacent subchannels overlap significantly with each other, as shown in Figure 2.6, where we illustrate the magnitude response of the filters $F_i(e^{j\omega})$, $i = 0, 1, 2, 3$, corresponding to the OFDM system. The poor spectral selectivity may pose problems in the presence of narrowband noise (e.g., in DSL, the local loop can act as an antenna picking up radio transmissions),

because subchannels adjacent to the narrowband noise will provide a rather poor attenuation. The latter can severely affect performance [10]. In this case, filter banks can be designed to provide much better spectral selectivity [29]. At a more fundamental level, the problem of selecting the optimal transformation that minimizes the bit error rate for a given transmitted power can be considered using the filter bank framework [11].

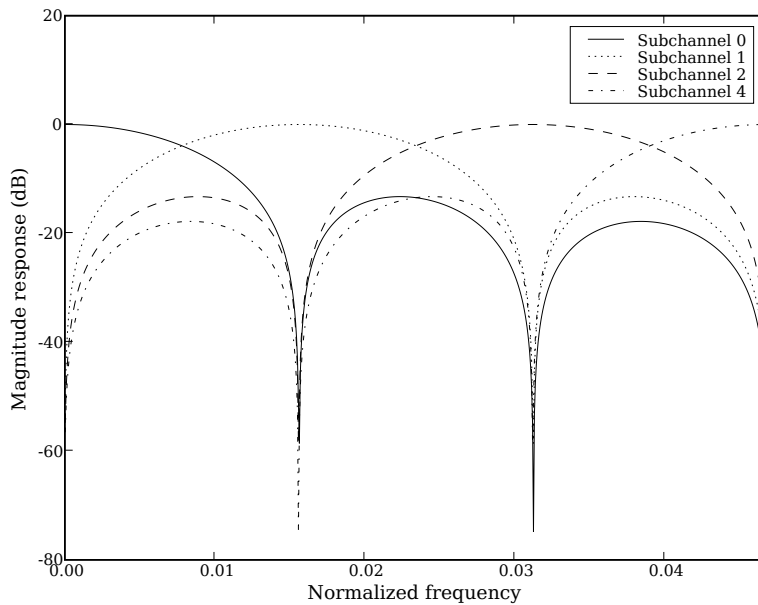


Fig. 2.6 Frequency response of OFDM subchannels for $M = 64$.

2.2.2 Polyphase Representation and Perfect Reconstruction

The polyphase decomposition is a very useful tool for studying various filter bank properties [12]. We will restrict our attention to the class of D -tap FIR filter banks, i.e. we assume

that the filters $F_i(z)$ and $H_i(z)$, $i = 0, \dots, M - 1$, in Figure 2.5 can be written as

$$F_i(z) = \sum_{m=0}^{D-1} f_i[m]z^m$$

$$H_i(z) = \sum_{m=0}^{D-1} h_i[m]z^{-m},$$

where the filter coefficients $f_i[m]$ and $g_i[m]$ can be complex. Note that, for convenience in mathematical analysis, $F_i(z)$ is noncausal. In practice, causality can simply be retrieved by adding a delay of $D - 1$ samples at the transmitter. The K -fold polyphase decompositions of $F_i(z)$ and $H_i(z)$ are given as follows:

$$F_i(z) = \sum_{k=0}^{K-1} z^k G_{k,i}(z^K)$$

$$H_i(z) = \sum_{k=0}^{K-1} z^{-k} S_{i,k}(z^K),$$

where

$$G_{k,i}(z) = \sum_{n=0}^{D/K-1} f_i[Kn + k]z^n \quad (2.5)$$

$$S_{i,k}(z) = \sum_{n=0}^{D/K-1} h_i[Kn + k]z^{-n} \quad (2.6)$$

are the polyphase components of $F_i(z)$ and $H_i(z)$, respectively [12]. We assume, without loss of generality, that D is a multiple of K , as zeros can always be appended to the transmitting and receiving filters. The filter bank transceiver can thus be represented, with the help of the noble identities, as in Figure 2.7 [19, 40, 42, 51]. $\mathbf{G}(z)$ and $\mathbf{S}(z)$ are $K \times M$

and $M \times K$ polyphase filter matrices whose entries⁵ are respectively given by

$$[\mathbf{G}(z)]_{k,i} = G_{k,i}(z) \quad (2.7)$$

$$[\mathbf{S}(z)]_{i,k} = S_{i,k}(z). \quad (2.8)$$

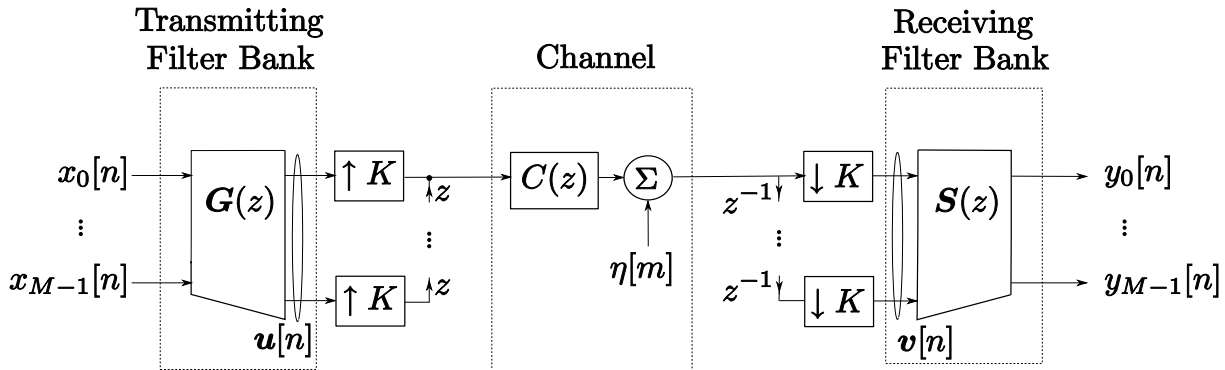


Fig. 2.7 Polyphase representation of a filter bank transceiver.

Assuming an ideal channel (i.e. $C(z) = 1$) and zero noise (i.e. $\eta[m] = 0$), the overall transfer function of the filter bank transceiver, from the transmitter to the receiver, is equal to

$$\mathbf{R}_0(z) \triangleq \mathbf{S}(z)\mathbf{G}(z). \quad (2.9)$$

For errorless data transmission, the transfer function should be equal to the $M \times M$ identity matrix, i.e. $\mathbf{R}_0(z) = \mathbf{I}_M$. A system satisfying the above property is called a *perfect reconstruction* (or PR) system. Note that OFDM, essentially composed of an IFFT/FFT pair, is a PR system. PR systems are very important because they allow perfect data transmission in ideal conditions. In practice, even in the presence of a non-ideal channel, the PR property can be exploited to simplify equalization, as discussed in Chapter 4. PR

⁵Each entry corresponds to an FIR filter represented by its Z -transform.

systems can be designed using *paraunitary* matrices. By definition, a paraunitary matrix $\mathbf{G}(z)$ satisfies the following relation [12]:

$$\tilde{\mathbf{G}}(z)\mathbf{G}(z) = \mathbf{I}_M, \quad (2.10)$$

where the tilde represents paraconjugation, i.e.

$$\tilde{\mathbf{G}}(z) = \mathbf{G}^H(1/z^*).$$

For such systems, the receiving filter bank is set to $\mathbf{S}(z) = \tilde{\mathbf{G}}(z)$.

If we consider a non-ideal channel, that is, we no longer assume that $C(z) = 1$, the transfer function of the transceiver (2.9) becomes

$$\mathbf{R}(z) \triangleq \mathbf{S}(z)\mathbf{C}(z)\mathbf{G}(z), \quad (2.11)$$

where $\mathbf{C}(z)$ is the $K \times K$ channel matrix, which results from cascading the decimators, advance elements, $C(z)$, upsamplers and delay elements (see Figure 2.7). $\mathbf{C}(z)$ can be obtained by using the so-called polyphase identity [12]. In fact, we can show that, assuming $Q < K - 1$, the channel matrix can be decomposed as follows [40]

$$\mathbf{C}(z) = \mathbf{C}_0 + \mathbf{C}_1 z^{-1}, \quad (2.12)$$

where

$$\mathbf{C}_0 \triangleq \begin{bmatrix} c[0] & 0 & \dots & 0 & 0 \\ \vdots & c[0] & & & \\ c[Q-1] & \vdots & & \vdots & \vdots \\ 0 & c[Q-1] & \ddots & & \\ & 0 & & 0 & \\ \vdots & \vdots & & c[0] & 0 \\ 0 & 0 & & c[1] & c[0] \end{bmatrix}$$

and

$$\mathbf{C}_1 \triangleq \begin{bmatrix} 0 & \dots & 0 & c[Q-1] & \dots & & c[1] \\ 0 & \dots & & 0 & c[Q-1] & \dots & c[2] \\ \vdots & & & & & \ddots & \vdots \\ 0 & & \dots & & & 0 & c[Q-1] \\ 0 & & \dots & & & & 0 \\ \vdots & & & & & & \vdots \\ 0 & & \dots & & & & 0 \end{bmatrix}.$$

Note that \mathbf{C}_0 and \mathbf{C}_1 are respectively a lower triangular Toeplitz matrix and an upper triangular Toeplitz matrix, each of dimension $K \times K$. The condition on Q (i.e. $Q < K - 1$) is not very restrictive as it is almost always satisfied in real-world applications. For instance, in VDSL, we have $K = 4096$, and the number of channel taps is usually much lower than that. Using (2.12), the transceiver in Figure 2.7 can now be entirely represented via polynomial matrices, as illustrated in Figure 2.8, where we define the noise vector $\boldsymbol{\eta}[n]$ as follows:

$$\boldsymbol{\eta}[n] \triangleq \left[\eta[Kn] \quad \eta[Kn+1] \quad \dots \quad \eta[Kn+K-1] \right]^T.$$

Note that the system now operates at a single sampling rate, i.e. the symbol rate, but it uses vector quantities instead of scalar ones.

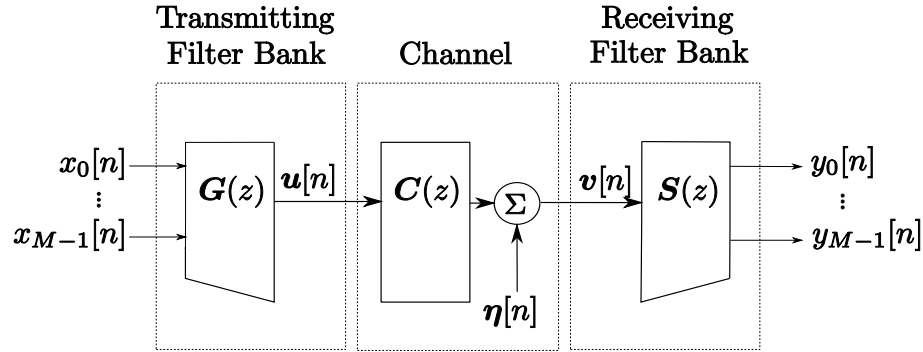


Fig. 2.8 Polynomial matrix representation of a filter bank transceiver.

2.3 DFT Filter Banks

Filter bank transceivers using the general form illustrated in Figure 2.5 are characterized by a high computational power requirement and are difficult to implement since $2M$ filters need to be designed. The use of modulated filter banks can solve these problems. Instead of having M different filters for each subcarrier, a modulated filter bank employs only one filter, a so-called prototype filter, and a modulation function $p_i[m]$ to shift the signal in frequency. The prototype filter is denoted by $F_0(z)$ or $H_0(z)$ depending whether the filter bank is located at the transmitting end or at the receiving end, respectively. This scheme is illustrated in Figure 2.9 for $F_i(z)$; $H_i(z)$ could be expressed similarly. Compared to unstructured filter banks, modulated filter banks necessitate the design of only one filter and allow efficient implementations by using a fast transform such as the FFT, as explained below.

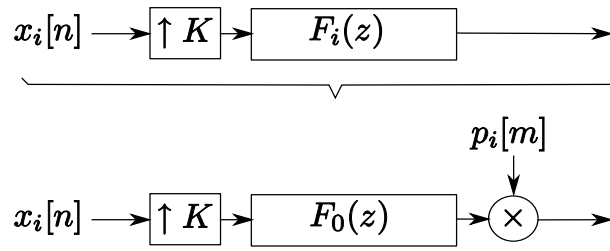


Fig. 2.9 Modulated filter.

2.3.1 DFT Modulation

When the modulation function $p_i[m]$ is a complex exponential, i.e. if the impulse responses of the filters $F_i(z)$ and $H_i(z)$ are given by

$$f_i[m] = e^{j2\pi im/M} f_0[m] \quad (2.13)$$

$$h_i[m] = e^{-j2\pi im/M} h_0[m], \quad (2.14)$$

the corresponding modulated filter bank is termed a DFT filter bank. As is it commonly assumed, e.g. see [30–37], we limit our attention to real prototype filter coefficients. However, due to the complex modulation function, $f_i[m]$ and $h_i[m]$, $i = 1, \dots, M - 1$, are still complex quantities. By letting $W \triangleq e^{-j2\pi/M}$, (2.13) and (2.14) can be re-written in the Z -domain as

$$F_i(z) = F_0(zW^i)$$

$$H_i(z) = H_0(zW^{-i}).$$

DFT filter banks are a “direct” generalization of OFDM. In fact, if both $F_0(z)$ and $H_0(z)$ are M -tap rectangular filters, i.e. if $f_0[m] = h_0[m] = 1$ for $m = 0, \dots, M - 1$, the transceiver

becomes a simple IFFT/FFT pair like the one in Figures 2.2 and 2.3.

In the case of DFT filter banks, the polyphase matrix $\mathbf{G}(z)$ can be factorized as described here, using the ideas presented in [52]. Such factorization will be used in this chapter to derive an efficient implementation of the DFT filter bank. It will also prove to be useful in obtaining various theoretical results in subsequent chapters of this thesis. Let us assume that D is a multiple of both M and K , i.e. $D = k_1M = k_2K$ for k_1, k_2 integers, and let $\mathbf{g}_i(z)$ be the i -th column of the $K \times M$ matrix $\mathbf{G}(z)$. From (2.5) and (2.7), $\mathbf{g}_i(z)$ can be expressed as

$$\mathbf{g}_i(z) = \tilde{\mathbf{L}}_0(z)\mathbf{f}_i, \quad (2.15)$$

where $\tilde{\mathbf{L}}_0(z)$ is a $K \times D$ matrix given by

$$\tilde{\mathbf{L}}_0(z) \triangleq \begin{bmatrix} \mathbf{I}_K & z\mathbf{I}_K & \dots & z^{\frac{D}{K}-1}\mathbf{I}_K \end{bmatrix},$$

and

$$\mathbf{f}_i \triangleq \begin{bmatrix} f_i[0] & \dots & f_i[D-1] \end{bmatrix}^T.$$

Using the fact that $f_i[m]$ is a modulated filter and $W^{M+d} = W^d$, we can write

$$\mathbf{f}_i = \mathbf{\Lambda}_f \mathbf{L}_1^T \begin{bmatrix} W^{-0i} \\ \vdots \\ W^{-(M-1)i} \end{bmatrix}, \quad (2.16)$$

where

$$\mathbf{\Lambda}_f \triangleq \text{diag}(f_0[0], \dots, f_0[D-1]), \quad (2.17)$$

and \mathbf{L}_1 is an $M \times D$ matrix defined as

$$\mathbf{L}_1 \triangleq \underbrace{\begin{bmatrix} \mathbf{I}_M & \mathbf{I}_M & \dots & \mathbf{I}_M \end{bmatrix}}_{D/M \text{ times}}. \quad (2.18)$$

From (2.15) and (2.16), $\mathbf{G}(z)$ can thus be factorized as follows:

$$\mathbf{G}(z) = \begin{bmatrix} \mathbf{g}_0(z) & \dots & \mathbf{g}_{M-1}(z) \end{bmatrix} = \tilde{\mathbf{L}}_0(z) \mathbf{\Lambda}_f \mathbf{L}_1^T \mathbf{W}^*, \quad (2.19)$$

where \mathbf{W} is the DFT matrix, i.e. $[\mathbf{W}]_{i,k} \triangleq W^{ik}$. Moreover, by defining

$$\mathbf{U}(z) \triangleq \mathbf{L}_1 \mathbf{\Lambda}_f \mathbf{L}_0(z), \quad (2.20)$$

$\mathbf{G}(z)$ can conveniently be expressed as

$$\mathbf{G}(z) = \tilde{\mathbf{U}}(z) \mathbf{W}^*. \quad (2.21)$$

Based on (2.21), a DFT filter bank transceiver with $\mathbf{S}(z) = \tilde{\mathbf{G}}(z)$ can be represented as shown in Figure 2.10.

2.3.2 Implementation and Computational Complexity

The DFT filter bank transceiver can be implemented efficiently based on the factorization obtained in (2.19). As reported in [52], the transmitter and the receiver can be implemented as illustrated in Figures 2.11 and 2.12, respectively. To obtain a causal expression for the transmitter, we consider the addition of a delay component to the polyphase matrix $\mathbf{G}(z)$, as shown in Figure 2.11. Tables 2.1 and 2.2 describe the implementation in

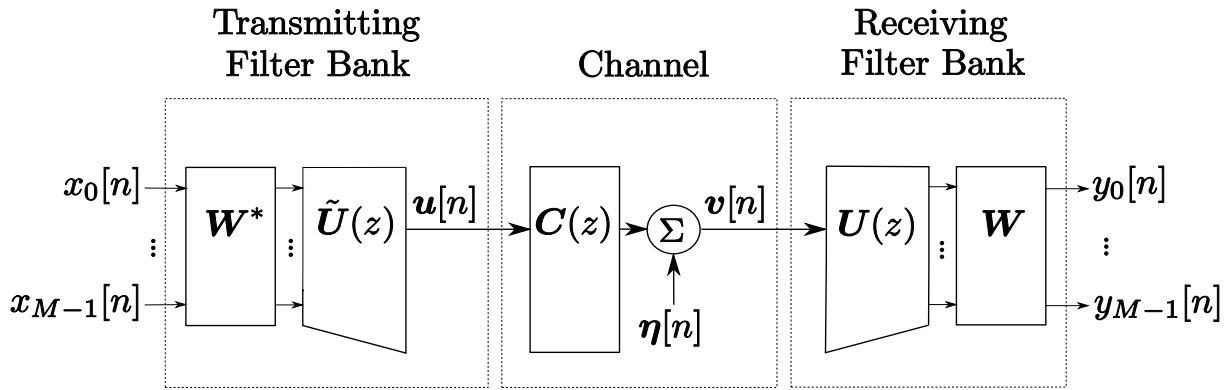


Fig. 2.10 DFT filter bank transceiver with $\mathbf{S}(z) = \tilde{\mathbf{G}}(z)$.

a step-by-step layout. The amount of flops required by each operation is also specified. Both the receiver and the transmitter necessitate approximately $5M \log_2 M + 2D$ flops per transmitted frame or received frame. Recall that the OFDM transmitter and receiver can be implemented using $5M \log_2 M$ flops. Overall, if we leave aside the equalization part, the main difference between the computational complexity of OFDM and that of the DFT filter bank transceiver linearly depends on the prototype filter length, D . In DFT filter bank transceivers, we typically employ long prototype filters [30]. For instance, assuming that $D = 20M$ and $M = 128$, we can determine that the receiving DFT filter bank requires 1.57 times more flops than the OFDM receiver (without taking into account equalization, which will be considered in Chapter 4). The small increase in computational complexity can largely be compensated by the gain in performance as shown in Chapter 6. Note that the design of the prototype filter $F_0(z)$ is addressed in Chapter 3.

2.4 Chapter Summary

In this chapter, we have presented the necessary background information to provide an appropriate theoretical basis for the remaining chapters of this thesis. The concept of

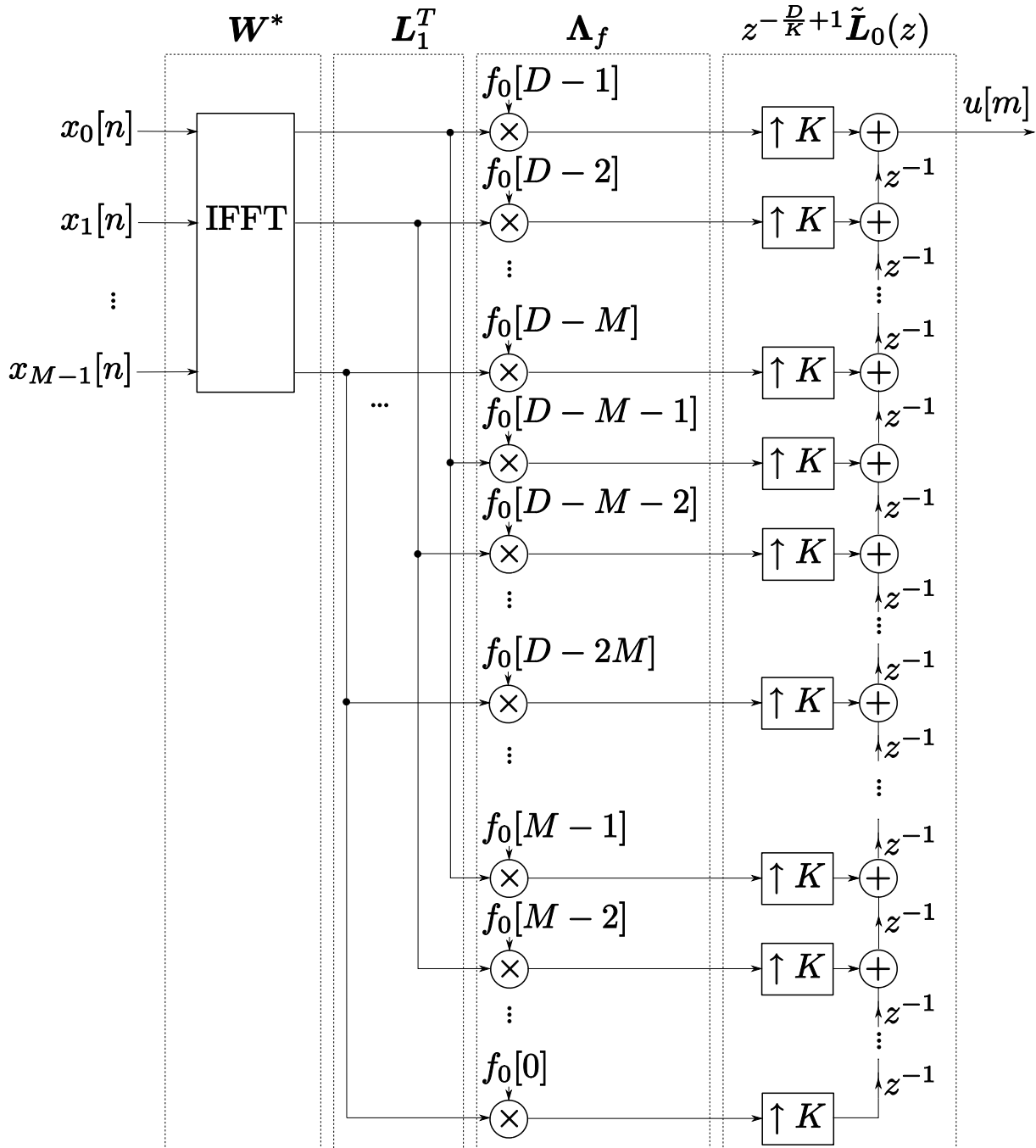


Fig. 2.11 Implementation of the DFT filter bank transmitter.

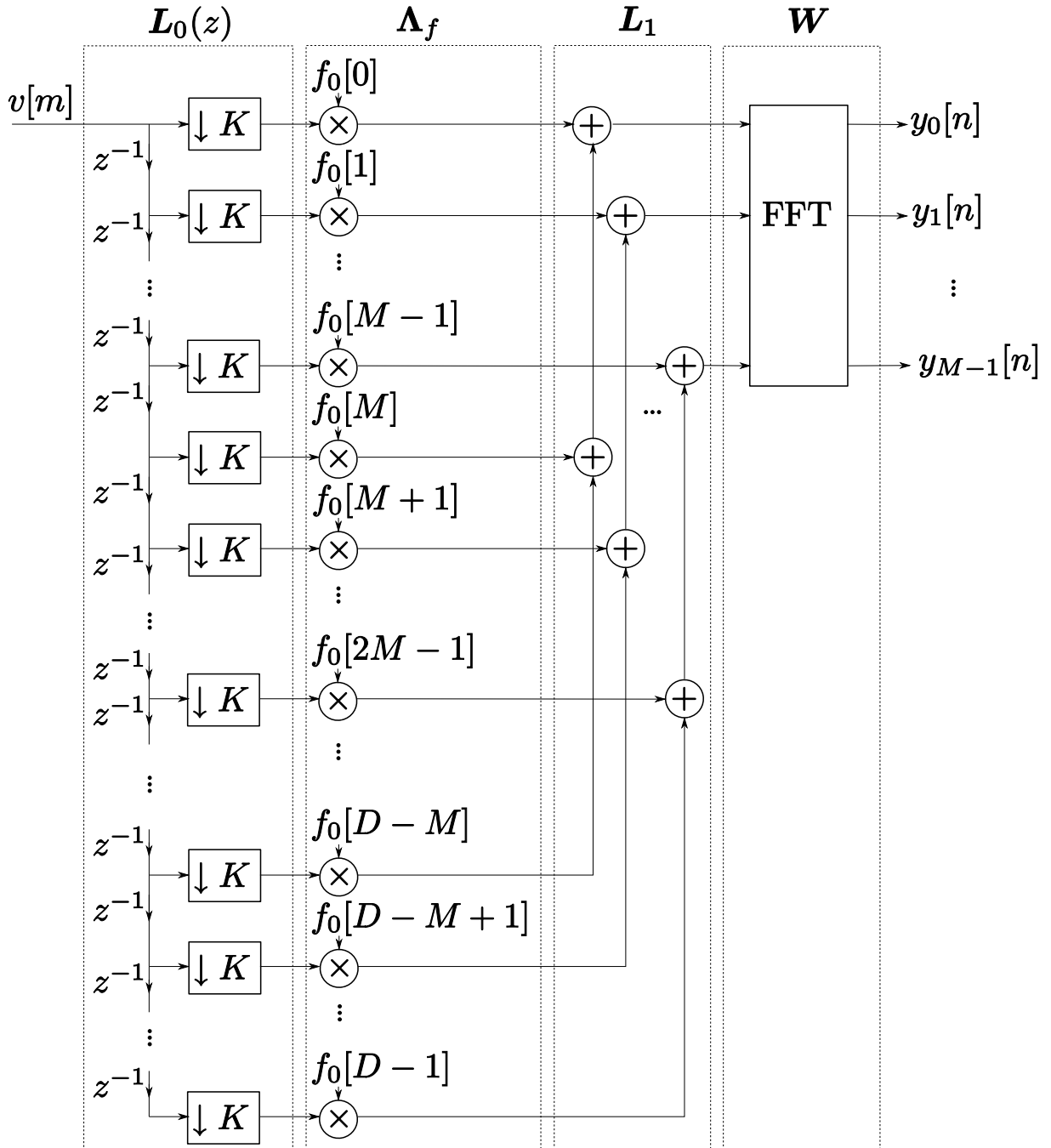


Fig. 2.12 Implementation of the DFT filter bank receiver.

| Instructions | Flops (per iter.) |
|---|-------------------|
| 1: Let $\{r[l]\}_{l=0}^{D-1}$ be an internal shift register initialized to zero. | |
| 2: For $n = 0, 1, 2, \dots$ | |
| 3: Compute $\{X_i[n]\}_{i=0}^{M-1}$ the M -point FFT of $\{x_i[n]\}_{i=0}^{M-1}$. | $5M \log_2 M$ |
| 4: Let $r[l] \leftarrow r[l] + X_{(l \bmod K)}[n] f_0[D-1-l]$ for $l = 0, \dots, D-1$. | $2D$ |
| 5: Let the output vector be given by $\mathbf{u}[n] = [r[K-1] \ \dots \ r[0]]^T$. | |
| 6: Shift in K zeros in $r[\cdot]$, i.e. $r[l] \leftarrow r[l+K]$ for $l = 0, \dots, D-K-1$ and $r[l] \leftarrow 0$ for $l = D-K, \dots, D-1$. | |
| 7: end for | |

Table 2.1 Implementation of the DFT filter bank transmitter.

| Instructions | Flops (per iter.) |
|--|-------------------|
| 1: Let $\{r[l]\}_{l=0}^{D-1}$ be an internal shift register initialized to zero. | |
| 2: For $n = 0, 1, 2, \dots$ | |
| 3: Shift in the input vector $\mathbf{v}[n]$ in $r[\cdot]$, i.e. $r[l] \leftarrow r[l-K]$ for $l = D-1, \dots, K$ and $r[l] \leftarrow [\mathbf{v}[n]]_l$ for $l = K-1, \dots, 0$. | |
| 4: Let $Y_l[n] \leftarrow r[k] f_0[k]$ for $l = 0, \dots, D-1$. | D |
| 5: Let $Y_i[n] \leftarrow Y_i[n] + Y_{i+lM}[n]$ for $i = 0, \dots, M-1$ and $l = 1, \dots, D/M-1$. | D |
| 6: Compute $\{y_i[n]\}_{i=0}^{M-1}$ the M -point IFFT of $\{Y_i[n]\}_{i=0}^{M-1}$. | $5M \log_2 M$ |
| 7: end for | |

Table 2.2 Implementation of the DFT filter bank receiver.

MCM was first introduced, and, as an example, the OFDM transceiver was presented. Filter bank transceivers and the polyphase representation were then introduced. Finally, we showed how a DFT filter bank can use the DFT to modulate a prototype filter. The implementation of such a filter bank was also discussed.

Chapter 3

Design of Perfect Reconstruction

DFT Filter Banks

The purpose of this chapter is to present a method to design a prototype filter such that the resulting DFT filter bank is characterized by the PR property and has good spectral properties, i.e. a flat passband and a low stopband energy. In Section 3.1, we show that the prototype filter coefficients can be parametrized in such a way that the PR property is always satisfied. In Section 3.2, the design method is formulated into an optimization problem, where the goal is to minimize the stopband energy of the prototype filter. The optimization problem is applied to the parametrized prototype filter coefficients, and the PR property is thus automatically satisfied. Lastly, results presented in this chapter are summarized in Section 3.3.

3.1 Parametrization of the Prototype Filter

We define in this section the necessary mathematical relations to parametrize the prototype filter coefficients $f_0[m]$ such that the transmitting polyphase matrix $\mathbf{G}(z)$ is paraunitary and, thus, characterized by the PR property. The design of the prototype filter itself is addressed in Section 3.2. The parametrization requires that D , the prototype filter length, be a multiple of P , where P is defined as the least common multiple of M and K . We also define the quantities J and L as $J \triangleq P/M$ and $L \triangleq P/K$, respectively.

3.1.1 The Two-Step Parametrization Method

From (2.10), since $\mathbf{W}\mathbf{W}^* = \mathbf{I}_M$, one can observe that the paraunitaryness of $\mathbf{G}(z)$ can be guaranteed by letting $\mathbf{U}(z)$ to be paraunitary. The matrix $\mathbf{U}(z)$, defined in (2.20), exhibits a particular structure. Each entry of $\mathbf{U}(z)$, denoted by $U_{i,k}(z)$, $i = 0, \dots, M-1$, $k = 0, \dots, K-1$, is given by (see the appendix for a proof):

$$U_{i,k}(z) = z^{-\alpha_{i,k}} G_{\beta_{i,k}}(z^L), \quad (3.1)$$

where $G_{\beta_{i,k}}(z)$ is the P -fold polyphase component of $f_0[m]$, i.e.

$$G_{\beta_{i,k}}(z) \triangleq \sum_{n=0}^{D/P-1} f_0[Pn + \beta_{i,k}] z^{-n},$$

$\beta_{i,k} \triangleq \alpha_{i,k}K + k$, and $\alpha_{i,k} \in \{0, \dots, L-1\}$ is an integer that depends on (i, k) . As specified in the appendix, $\alpha_{i,k}$ must satisfy the congruence relation¹

$$\alpha_{i,k}K + k \equiv i \pmod{M}. \quad (3.2)$$

Note that $\alpha_{i,k}$ may — or may not — exist depending on the given (i, k) . When $\alpha_{i,k}$ does not exist, we have $U_{i,k}(z) = 0$.

As an aside, let us now prove the critical importance of over-interpolation, i.e. having $K > M$, for the PR property to be feasible in a DFT filter bank. When $M = K$ (implying that $P = M$ and $L = 1$), (3.2) can only be satisfied for $i = k$, in which case we have $\alpha_{i,k} = 0$. The matrix $\mathbf{U}(z)$ is thus diagonal with the following entries:

$$U_{i,i}(z) = G_i(z), \quad i = 0, \dots, M-1.$$

To satisfy the PR property, i.e. $\mathbf{U}(z)\tilde{\mathbf{U}}(z) = \mathbf{I}_M$, we must have

$$G_i(z)\tilde{G}_i(z) = 1,$$

which is only possible if $f_0[m] = 1$ for $m = 0, \dots, M-1$. Accordingly, the only possible choice for $\mathbf{U}(z)$ is the identity matrix \mathbf{I}_M . This situation is that of OFDM, where the “prototype filter” is a rectangular window. Overlapping non-rectangular windows, such as the ones in DFT filter banks, can have the PR property only if over-interpolation is allowed.

The parametrization of $f_0[m]$ is based on the idea that if we can generate a polyphase matrix $\mathbf{U}(z; \boldsymbol{\theta})$ which is paraunitary, then we can find the parametrized filter coefficients

¹We say that two integers a and b are congruent modulo M , denoted here by $a \equiv b \pmod{M}$, if and only if $a - b$ is divisible by M .

$f_0[m; \boldsymbol{\theta}]$ via the relation in (3.1). We thus proceed in two steps:

1. From a vector of parameters $\boldsymbol{\theta} \in \mathbb{R}^S$, we compute a polyphase matrix $\mathbf{U}(z; \boldsymbol{\theta})$ such that it is paraunitary and obeys the structure in (3.1). This operation can be represented by the mapping p , which is defined as

$$p : \mathbb{R}^S \longrightarrow \mathcal{U}; \boldsymbol{\theta} \mapsto \mathbf{U}(z; \boldsymbol{\theta}),$$

where \mathcal{U} is the set of all $M \times K$ paraunitary matrices which comply with the form outlined in (3.1).

2. Using the relation in (3.1), we obtain the filter coefficients $f_0[m; \boldsymbol{\theta}]$ by inspecting the entries of $\mathbf{U}(z; \boldsymbol{\theta})$. Formally, this relation can be represented by the mapping q , given by

$$q : \mathcal{U} \longrightarrow \mathbb{R}^D; \mathbf{U}(z; \boldsymbol{\theta}) \mapsto \mathbf{f}_0(\boldsymbol{\theta}),$$

where $\mathbf{f}_0(\boldsymbol{\theta})$ denotes the vector of the parametrized filter coefficients, i.e.

$$\mathbf{f}_0(\boldsymbol{\theta}) = \left[f_0[0; \boldsymbol{\theta}] \quad \dots \quad f_0[D-1; \boldsymbol{\theta}] \right]^T,$$

In short, the filter coefficients are obtained via the composition of the mappings p and q , i.e.

$$\mathbf{f}_0(\boldsymbol{\theta}) = q \circ p(\boldsymbol{\theta}).$$

Once a suitable polyphase matrix $\mathbf{U}(z; \boldsymbol{\theta})$ has been obtained via Step 1, finding the corresponding filter coefficients, i.e. Step 2, is straightforward. The proper mapping is given by (3.1). However, Step 1 requires a less direct approach, as summarized here. An arbitrary paraunitary matrix, which we denote by $\mathbf{V}(z; \boldsymbol{\theta})$, can be parametrized using a dyadic-

based factorization [53]. Unfortunately, the entries of such matrix will not correspond to the proper polyphase components as given in (3.1). While preserving its paraunitaryness, $\mathbf{V}(z; \boldsymbol{\theta})$ must thus be transformed so that its entries are compatible with those of $\mathbf{U}(z; \boldsymbol{\theta})$. The exact relation between $\mathbf{V}(z; \boldsymbol{\theta})$ and $\mathbf{U}(z; \boldsymbol{\theta})$ depends on whether M and K are coprime or not. Both situations are considered below.

3.1.2 Parametrization of the Polyphase Matrix for M and K Coprime

Let us first consider the case where M and K are coprime, i.e. we have $L = M$ and $J = K$. We first compute a $L \times J$ paraunitary matrix $\mathbf{V}(z; \boldsymbol{\theta})$ using the following dyadic-based factorization [12, 53]:

$$\mathbf{V}(z; \boldsymbol{\theta}) = \prod_{l=0}^{D/P-3} \mathbf{A}(z; \boldsymbol{\theta}_l) \prod_{l=D/P-2}^{D/P+J-4} \mathbf{B}(\boldsymbol{\theta}_l) \quad (3.3)$$

where

$$\begin{aligned} \boldsymbol{\Gamma} &= \begin{bmatrix} \mathbf{I}_L & \mathbf{0}_{L \times (J-L)} \end{bmatrix}, \\ \mathbf{A}(z; \boldsymbol{\theta}_l) &= \mathbf{I}_J - \frac{\boldsymbol{\theta}_l \boldsymbol{\theta}_l^T}{\boldsymbol{\theta}_l^T \boldsymbol{\theta}_l} + z^{-1} \frac{\boldsymbol{\theta}_l \boldsymbol{\theta}_l^T}{\boldsymbol{\theta}_l^T \boldsymbol{\theta}_l}, \\ \mathbf{B}(\boldsymbol{\theta}_l) &= \mathbf{I}_J - 2 \frac{\boldsymbol{\theta}_l \boldsymbol{\theta}_l^T}{\boldsymbol{\theta}_l^T \boldsymbol{\theta}_l}, \end{aligned}$$

and $\boldsymbol{\theta}_l$ are J -length vectors given by

$$\boldsymbol{\theta}_l = \begin{bmatrix} 1 & \theta_{l(J-1)} & \theta_{l(J-1)+1} & \dots & \theta_{l(J-1)+J-2} \end{bmatrix}^T.$$

The entries of $\boldsymbol{\theta}_l$ are taken from the vector of parameters $\boldsymbol{\theta} = \begin{bmatrix} \theta_0 & \dots & \theta_{S-1} \end{bmatrix}^T$ with $S = (D/P + J - 3)(J - 1)$. When M and K are coprime, we can observe that, regardless of i and k , there always exists an integer $\alpha_{i,k} \in \{0, \dots, L - 1\}$ such that (3.2) is satisfied.

In this case, each entry of $\mathbf{U}(z)$ is non-zero. However, we cannot simply let $\mathbf{U}(z; \boldsymbol{\theta})$ to be equal to the paraunitary matrix $\mathbf{V}(z; \boldsymbol{\theta})$ due to the terms $z^{-\alpha_{i,k}}$ and z^L in (3.1). In general, the structure of $\mathbf{U}(z; \boldsymbol{\theta})$ is not compatible with that of $\mathbf{V}(z; \boldsymbol{\theta})$. We thus have to transform $\mathbf{V}(z; \boldsymbol{\theta})$ such that the paraunitaryness is preserved and its entries can be mapped directly to those given in (3.1).

In order to find a suitable transformation for $\mathbf{V}(z; \boldsymbol{\theta})$, as proposed in [54], we consider two paraunitary matrices $\mathbf{D}_0(z)$ and $\mathbf{D}_1(z)$ such that

$$\begin{aligned} \mathbf{D}_0(z) &= \text{diag} \left(\begin{bmatrix} z^{\alpha_{0,0}} & z^{\alpha_{1,0}} & \dots & z^{\alpha_{L-1,0}} \end{bmatrix} \right) \\ \mathbf{D}_1(z) &= \text{diag} \left(\begin{bmatrix} z^{\alpha_{0,0}} & z^{\alpha_{0,1}} & \dots & z^{\alpha_{0,J-1}} \end{bmatrix} \right). \end{aligned}$$

By pre-multiply and post-multiplying $\mathbf{U}(z)$ by $\mathbf{D}_0(z)$ and $\mathbf{D}_1(z)$, respectively, we can show that

$$[\mathbf{D}_0(z)\mathbf{U}(z)\mathbf{D}_1(z)]_{i,k} = z^{\bar{\alpha}_{i,k}} G_{\beta_{i,k}}(z^L),$$

where $\bar{\alpha}_{i,k} = \alpha_{i,0} + \alpha_{0,k} - \alpha_{i,k}$. Let us consider two expressions derived from (3.2), where we respectively let $(i, k) = (0, k)$ and $(i, k) = (i, 0)$. Using the properties of congruences [55], adding these two expressions together and subtracting from it the relation (3.2) yield

$$(\alpha_{i,0} + \alpha_{0,k} - \alpha_{i,k})J \equiv 0 \pmod{L}.$$

The above expression indicates that $\bar{\alpha}_{i,k}$ can only take two different values, 0 or L , since we have $0 \leq \alpha_{i,k} \leq L - 1$ for all i and k . Based on this information, we note that the entries of $\mathbf{D}_0(z)\mathbf{U}(z)\mathbf{D}_1(z)$ are solely given in terms of z^L . Hence, we can now let

$$\mathbf{D}_0(z)\mathbf{U}(z; \boldsymbol{\theta})\mathbf{D}_1(z) = \mathbf{V}(z^L; \boldsymbol{\theta}),$$

or, equivalently,

$$\mathbf{U}(z; \boldsymbol{\theta}) = \tilde{\mathbf{D}}_0(z) \mathbf{V}(z^L; \boldsymbol{\theta}) \tilde{\mathbf{D}}_1(z). \quad (3.4)$$

Since $\mathbf{V}(z; \boldsymbol{\theta})$ is paraunitary, then so is $\mathbf{U}(z; \boldsymbol{\theta})$, as the product of two paraunitary matrices preserves paraunitaryness [12].

In essence, we have shown that the first step of the parametrization, i.e. to obtain a proper paraunitary matrix $\mathbf{U}(z; \boldsymbol{\theta})$, first consists in generating a generic paraunitary matrix $\mathbf{V}(z; \boldsymbol{\theta})$ via the dyadic-based factorization given in (3.3). As shown in (3.4), we then apply a transformation to $\mathbf{V}(z; \boldsymbol{\theta})$ to make its entries compatible with those of $\mathbf{U}(z; \boldsymbol{\theta})$. Once $\mathbf{U}(z; \boldsymbol{\theta})$ has been obtained, we may easily carry out the second step of the parametrization by retrieving the filter coefficients via the mapping (3.1).

3.1.3 Parametrization of the Polyphase Matrix for M and K Non-Coprime

When M and K are not coprime, it is not always possible to find an integer $\alpha_{i,k}$ which satisfies (3.2) for a given (i, k) . Hence, $\mathbf{U}(z)$ will have zero and non-zero entries. It turns out that the paraunitaryness of $\mathbf{U}(z)$ is equivalent to the paraunitaryness of $L \times J$ submatrices $\mathbf{U}_l(z)$, $l = 0, \dots, K/J - 1$, of $\mathbf{U}(z)$ [54]. These submatrices are constructed as follows:

$$\mathbf{U}_l(z) = \begin{bmatrix} U_{l,l}(z) & \cdots & U_{l,l+(J-1)\frac{K}{J}} \\ U_{l+\frac{M}{L},l}(z) & \cdots & U_{l+\frac{M}{L},l+(J-1)\frac{K}{J}} \\ \vdots & \ddots & \vdots \\ U_{l+(L-1)\frac{M}{L},l}(z) & \cdots & U_{l+(L-1)\frac{M}{L},l+(J-1)\frac{K}{J}} \end{bmatrix}, \quad (3.5)$$

where each entry is given by (3.1).

Notice that, for any entry of $\mathbf{U}_l(z)$, the congruence relation (3.2) can be written as

$$\alpha_{i,k}K + l + k\frac{K}{J} \equiv l + i\frac{M}{L} \pmod{M},$$

which is equivalent to

$$\alpha_{i,k}J + k \equiv i \pmod{M},$$

since, by definition, $K/J = M/L$. By comparing the above expression with (3.2), we may conclude that the distribution of the term $\alpha_{i,k}$ in the $L \times J$ matrix $\mathbf{U}_l(z)$ is identical to the one found in the coprime case. Hence, the same transformation as in (3.4) can be used, and we can write

$$\mathbf{U}_l(z; \boldsymbol{\theta}) = \tilde{\mathbf{D}}_0(z) \mathbf{V}_l(z^L; \boldsymbol{\theta}) \tilde{\mathbf{D}}_1(z), \quad (3.6)$$

where $\mathbf{V}_l(z^L; \boldsymbol{\theta})$ is a $L \times J$ paraunitary matrix, generated via the same dyadic-based factorization used in the coprime case.

The procedure to obtain $\mathbf{f}_0(\boldsymbol{\theta})$ can now be generalized as follows. Initially, the factorization theorem of paraunitary matrices, i.e. (3.3), is used to generate K/J matrices $\mathbf{V}_l(z; \boldsymbol{\theta})$. These matrices are then mapped to $\mathbf{U}_l(z; \boldsymbol{\theta})$ via the transformation shown in (3.6). Finally, we retrieve the filter coefficients by inspecting each entry of $\mathbf{U}_l(z; \boldsymbol{\theta})$, using the information contained in (3.5) and in (3.1).

3.2 Prototype Filter Design

In this section, we use the parametrization of the filter coefficients described in Section 3.1 to propose a design methodology for PR DFT filter banks with good spectral containment.

3.2.1 Optimization Problem

In order to provide good spectral containment, among all parameter vectors $\boldsymbol{\theta}$, it is desirable to select the one that minimizes the stopband energy of $f_0[m; \boldsymbol{\theta}]$. The prototype filter design problem can thus be cast as the following unconstrained optimization problem:

$$\boldsymbol{\theta}_0 = \arg \min_{\boldsymbol{\theta}} J(\boldsymbol{\theta}), \quad (3.7)$$

where the cost function, $J(\boldsymbol{\theta})$, corresponds to the stopband energy of the prototype filter. The stopband energy can be expressed as

$$J(\boldsymbol{\theta}) = \int_{\omega_s}^{2\pi - \omega_s} |F_0(e^{j\omega}; \boldsymbol{\theta})|^2 d\omega, \quad (3.8)$$

where $F_0(e^{j\omega}; \boldsymbol{\theta})$ represents the discrete-time Fourier transform (DTFT) of $f_0[m; \boldsymbol{\theta}]$, i.e.

$$F_0(e^{j\omega}; \boldsymbol{\theta}) = \sum_{m=0}^{D-1} f_0[m; \boldsymbol{\theta}] e^{-j\omega m},$$

and ω_s denotes the stopband frequency, which is given by

$$\omega_s = \frac{\pi}{M}.$$

Note that this approach is similar to the one suggested in [19] for unstructured filter banks. Thanks to the parametrization of $f_0[m]$, one is certain that $f_0[m; \boldsymbol{\theta}]$ will always yield a PR prototype filter regardless of the outcome of the minimization process. It is not necessary to constrain the passband of the prototype filter to be flat to obtain a good frequency response. Due to the paraunitaryness of $\mathbf{G}(z)$, one can show, using the power complementary property, that the passband region of $|F_0(e^{j\omega}; \boldsymbol{\theta})|^2$ will be constant, even if the cost function

does not explicitly take this into account [12].

Minimization of the cost function can be carried out using the BFGS algorithm, which is appropriate for solving large-scale nonlinear unconstrained optimization problems [56]. In such nonlinear problems, the convergence towards a global minimum cannot be guaranteed. To find a “good” minimum, the algorithm should be run several times with a different set of initial values, and the solution yielding the lowest minimum should be kept. To implement the BFGS algorithm, we use in this work the L-BFGS-B (Bound constrained² Limited memory BFGS) software [57, 58]. The required gradient of the cost function, $\nabla J(\boldsymbol{\theta})$, can be approximated numerically using the standard difference-based approach. The i -th entry of the gradient is thus obtained as follows:

$$[\nabla J(\boldsymbol{\theta})]_i \approx \frac{J(\boldsymbol{\theta} + \epsilon \mathbf{e}_i) - J(\boldsymbol{\theta})}{\epsilon},$$

where ϵ is a small positive real number, and \mathbf{e}_i is an all-zero vector, except at the i -th entry where it is one.

3.2.2 Computation of the Stopband Energy

The cost function in (3.8) can be evaluated without resorting to approximate numerical integration methods. The main idea is to consider the autocorrelation of the impulse response of the prototype filter [59], defined for $-D + 1 \leq \tau \leq D - 1$ as

$$r_f[\tau; \boldsymbol{\theta}] \triangleq \sum_{m=0}^{D-1} f_0[m; \boldsymbol{\theta}] f_0[m + \tau; \boldsymbol{\theta}]. \quad (3.9)$$

²Despite its name, L-BFGS-B is also suitable for unconstrained problem, like the one in (3.7).

Using basic properties of the DTFT [39], the cost function can be re-written in terms of the autocorrelation function as follows:

$$J(\boldsymbol{\theta}) = \int_{\omega_s}^{2\pi-\omega_s} R_f(e^{j\omega}; \boldsymbol{\theta}) d\omega, \quad (3.10)$$

where $R_f(e^{j\omega}; \boldsymbol{\theta})$ is the DTFT of $r_f[\tau; \boldsymbol{\theta}]$, i.e.

$$R_f(e^{j\omega}; \boldsymbol{\theta}) = \sum_{\tau=-D+1}^{D-1} r_f[\tau; \boldsymbol{\theta}] e^{-j\omega\tau}. \quad (3.11)$$

Finally, substituting (3.11) in (3.10) and carrying out the integral yields

$$J(\boldsymbol{\theta}) = \sum_{\tau=0}^{D-1} b[\tau] r_f[\tau; \boldsymbol{\theta}], \quad (3.12)$$

where

$$b[\tau] = \begin{cases} 1 - \omega_s/\pi & \text{if } \tau = 0 \\ -\frac{2}{\pi\tau} \sin(\tau\omega_s) & \text{if } \tau = 1, \dots, D-1 \\ 0 & \text{elsewhere.} \end{cases}$$

The stopband energy can thus be computed analytically via a finite sum, as shown in (3.12).

Computing the stopband energy of $f_0[m; \boldsymbol{\theta}]$ can be a costly operation if one implements (3.9) and (3.12) directly. In fact, even if we take into account the symmetry of $r_f[\tau; \boldsymbol{\theta}]$, i.e. $r_f[-\tau; \boldsymbol{\theta}] = r_f[\tau; \boldsymbol{\theta}]$, its computation requires $2D^2$ flops (floating point operations). For a 512-tap filter, this amounts to 0.52 Mflops, which makes the optimization problem a relatively time-consuming and a resource-demanding process. Instead, we can carry out the computation in the frequency domain, as described in Table 3.1. The main idea is to use the Plancherel theorem [39] to compute (3.12) using the FFTs of $b[\tau]$ and $r_f[\tau; \boldsymbol{\theta}]$.

If we consider again a 512-tap filter, the FFT-based method necessitates 0.05 Mflops, a reduction by almost a factor of 10 compared to the direct approach. Computing the stopband energy via the FFT thus decreases the computational burden of the optimization problem significantly.

Table 3.1 Computation of the autocorrelation function using the FFT.

| Instructions | Flops |
|---|-----------------|
| 1: Let $D' = 2^E$, where $E = \lceil \log_2 D \rceil + 1$. | Negligible |
| 2: Let $B[k]$ be the D' -point FFT of $b[\tau]$ (This can be computed offline). | |
| 3: Compute $F_0[k]$, the D' -point FFT of $f_0[m; \boldsymbol{\theta}]$, by zero-padding the sequence. | $5D' \log_2 D'$ |
| 4: Let $H[k] = F_0[k] ^2$ for $k = 0, \dots, D' - 1$. | $3D'$ |
| 5: Compute $J(\boldsymbol{\theta}) = \frac{1}{D'} \sum_{k=0}^{D'-1} B[k]H^*[k]$ | $2D'$ |

3.3 Chapter Summary

We have developed in this chapter a method to design prototype filters suitable for PR DFT filter banks. The proposed method can be summarized as illustrated in Figure 3.1. Essentially, we use an optimization algorithm to minimize the stopband energy of the prototype filter. The optimization algorithm operates on a vector of parameters $\boldsymbol{\theta}$ which effectively parametrizes the prototype filter such that it is characterized by the PR property. The stopband energy is evaluated based on the autocorrelation coefficients of the filter, and is computed using an efficient FFT-based method.

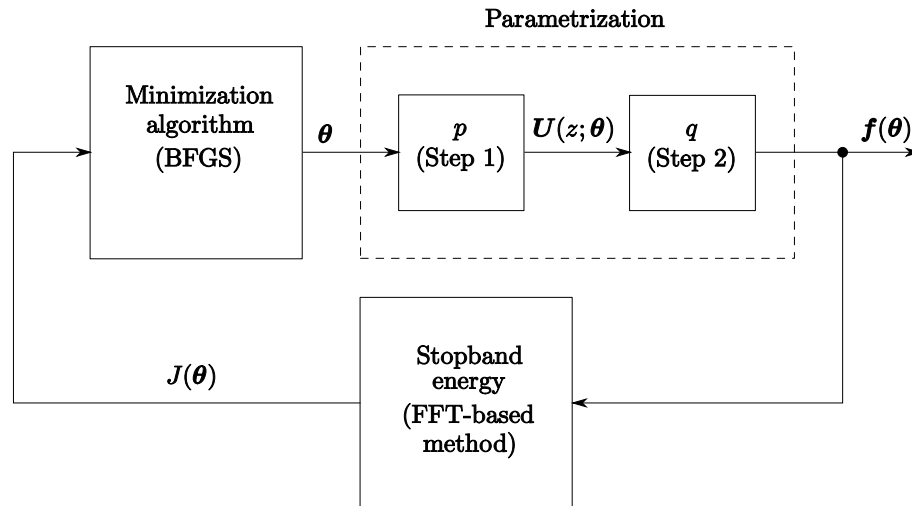


Fig. 3.1 Outline of the prototype filter design process.

Chapter 4

Channel Equalization Techniques

Many schemes have been proposed to equalize the received symbols in a DFT filter bank transceiver. Systems employing non-PR DFT filter banks usually rely on a set of decision feedback equalizers (DFEs) which compensate for the channel perturbations and the distortions introduced by the filter banks [28–30, 38]. In PR DFT filter bank transceivers, symbol equalization is simplified since only the channel perturbations must be mitigated. In this case, a more appropriate equalization scheme should not attempt to compensate for the filter banks' presence and should solely focus on the channel-induced perturbations, i.e. intersymbol interference (ISI) and additive noise.

With the use of PR DFT filter banks, we can thus consider a new equalization strategy which is normally not possible with traditional non-PR ones. The idea is to take advantage of the fact that when the transmitting and receiving filter banks are connected back-to-back, the resulting ISI is nil, thanks to the PR property. To exploit this simple fact, we can envision two different types of equalizer architectures: one that will equalize the channel before the receiving filter bank (referred to as a “pre-equalizer”) and one that will equalize the channel after the receiving filter bank (referred to as a “post-equalizer”). Both

equalization architectures have their own advantages and disadvantages as briefly discussed below.

With the pre-equalizer architecture, the received signal is equalized before being processed by the receiving filter bank. This can be accomplished by appending a block of zeros to each frame of modulated symbols, whose purpose is to “flush” the channel between each transmitted frame, and by employing a block linear transform to remove the residual interference within each frame. Such scheme is referred to as a *zero-padded block linear equalizer* and was previously studied in [40, 41]. Here, we consider its use and evaluate its performance in a PR DFT filter bank context. The zero-padded block linear equalizer presents the advantage of being able to extend the PR property of the filter banks to the entire transceiver¹ even in the presence of a non-ideal channel. However, it can be computationally expensive to implement.

When the post-equalizer architecture is considered, the received signal is equalized after the receiving filter bank. In this case, if we suppose that the subchannels are sufficiently narrow (in the sense that the bandwidth of each subchannel is very small compared to the total bandwidth used by the transceiver), we may then assume that the constellation symbols sent in each subchannel are merely scaled by a complex coefficient. A simple equalizer, employing a single tap for each subchannel, may thus be used to properly equalize the received symbols. Such equalizer is referred to as a *one-tap equalizer*. This method is very attractive due to its low computational cost. As mentioned above, however, certain conditions in terms of spectral properties must be met to guarantee a proper performance. Note that using a one-tap equalizer in DFT filter bank transceivers was considered in previous works (see e.g. [31, 37]), but a non-PR context was assumed. Here we study the

¹That is, the transceiver system (i.e. the cascade of the transmitting filter bank, channel, equalizer and receiving filter bank) can be characterized by the PR property, i.e. it can be completely ISI-free.

use and performance of a one-tap equalizer for DFT filter bank transceivers satisfying the PR property.

This chapter is organized as follows. In Section 4.1, the zero-padded block linear equalizer, based on the “pre-equalizer” architecture, is presented. The second equalization scheme, a simple one-tap equalizer which employs the “post-equalizer” architecture, is then described in Section 4.2. In both cases, the channel state information is assumed to be known. We discuss the performance of the proposed equalization schemes in Section 4.3, where we derive expressions for the computational complexity and the resulting subchannel SNR for each method. Finally, a brief conclusion appears in Section 4.4.

4.1 Zero-Padded Block Linear Equalizer

To combat ISI, one possible scheme, as shown in Figure 4.1, involves appending a block of B zeros to the modulated time-domain samples and employing a $K \times N$, $N \triangleq K + B$, block linear equalizer \mathbf{E} to remove the remaining ISI [40, 41]. We first observe that an $N \times N$ polynomial channel matrix $\mathbf{C}(z)$ can be defined as in (2.12), i.e.

$$\mathbf{C}(z) = \mathbf{C}_0 + \mathbf{C}_1 z^{-1}.$$

Similarly the noise vector $\boldsymbol{\eta}[n]$ can be expressed as

$$\boldsymbol{\eta}[n] = \begin{bmatrix} \eta[Nn] & \eta[Nn + 1] & \dots & \eta[Nn + N - 1] \end{bmatrix}^T.$$

As in Chapter 2, we use $K \times 1$ vectors $\mathbf{u}[n]$ and $\mathbf{v}[n]$ to denote the modulator output and the demodulator input, respectively. Hence, we may write

$$\mathbf{v}[n] = \mathbf{E} \left(\mathbf{C}_0 \begin{bmatrix} \mathbf{u}[n] \\ \mathbf{0}_{B \times 1} \end{bmatrix} + \mathbf{C}_1 \begin{bmatrix} \mathbf{u}[n-1] \\ \mathbf{0}_{B \times 1} \end{bmatrix} + \boldsymbol{\eta}[n] \right). \quad (4.1)$$

The derivation of \mathbf{E} is addressed in the following sections.

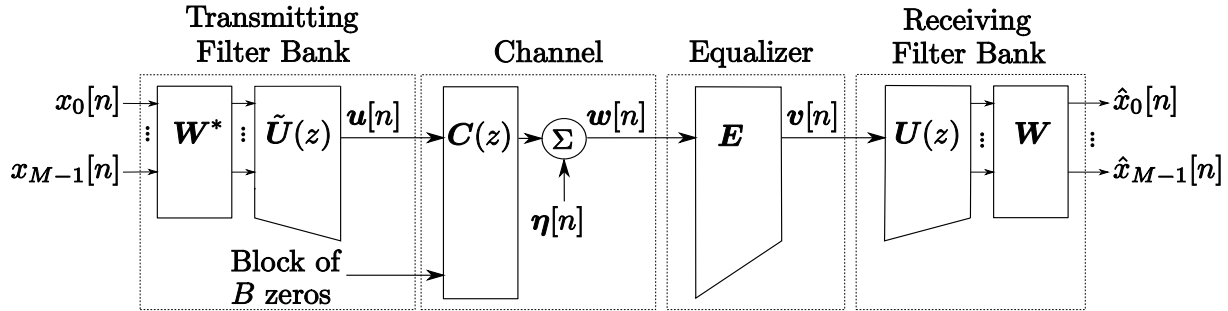


Fig. 4.1 A zero-padded DFT filter bank transceiver.

4.1.1 Zero-Forcing Solution

One of the most common approaches to equalizer design is the well-known zero-forcing solution, denoted here as \mathbf{E}_{ZF} . Such equalizer ignores the presence of noise completely (i.e. $\boldsymbol{\eta}[n] = \mathbf{0}_{N \times 1}$) and enforces $\mathbf{v}[n] = \mathbf{u}[n]$. In other words, in the absence of noise, the zero-forcing equalizer allows the transceiver to be characterized by the PR property, even in the presence of a channel. To find a suitable \mathbf{E}_{ZF} , let us partition \mathbf{C}_0 and \mathbf{C}_1 as

$$\mathbf{C}_l = \begin{bmatrix} \mathbf{C}_{l,0} & \mathbf{C}_{l,1} \end{bmatrix}, \quad l = 0, 1, \quad (4.2)$$

where $\mathbf{C}_{l,0}$ is a $N \times K$ matrix and $\mathbf{C}_{l,1}$ is a $N \times B$ matrix. Equation (4.1) then becomes

$$\begin{aligned} \mathbf{v}[n] &= \mathbf{E}_{\text{ZF}} \left(\begin{bmatrix} \mathbf{C}_{0,0} & \mathbf{C}_{0,1} \end{bmatrix} \begin{bmatrix} \mathbf{u}[n] \\ \mathbf{0}_{B \times 1} \end{bmatrix} + \begin{bmatrix} \mathbf{C}_{1,0} & \mathbf{C}_{1,1} \end{bmatrix} \begin{bmatrix} \mathbf{u}[n-1] \\ \mathbf{0}_{B \times 1} \end{bmatrix} \right) \\ &= \mathbf{E}_{\text{ZF}} (\mathbf{C}_{0,0} \mathbf{u}[n] + \mathbf{C}_{1,0} \mathbf{u}[n-1]) \end{aligned} \quad (4.3)$$

Under the condition that $B \geq Q-1$, where Q is the channel length (see (2.2)), the rightmost term in (4.3) vanishes² since $\mathbf{C}_{1,0} = \mathbf{0}$, i.e.

$$\mathbf{v}[n] = \mathbf{E}_{\text{ZF}} \mathbf{C}_{0,0} \mathbf{u}[n]. \quad (4.4)$$

A zero-forcing solution can be found by using the pseudo-inverse (denoted by the superscript †), i.e.

$$\mathbf{E}_{\text{ZF}} = \mathbf{C}_{0,0}^\dagger. \quad (4.5)$$

Since $\mathbf{C}_{0,0}$ is full rank, a property inherited from its Toeplitz nature [50], the pseudo-inverse can be computed explicitly and is given by

$$\mathbf{C}_{0,0}^\dagger = (\mathbf{C}_{0,0}^T \mathbf{C}_{0,0})^{-1} \mathbf{C}_{0,0}^T.$$

$\mathbf{C}_{0,0}^\dagger$ is then a left inverse of $\mathbf{C}_{0,0}$, i.e. $\mathbf{C}_{0,0}^\dagger \mathbf{C}_{0,0} = \mathbf{I}_K$. It is important to emphasize the fact that the interference caused by the previous block, $\mathbf{u}[n-1]$, can only be mitigated provided that the number of trailing zeros B is greater than or equal to $Q-1$. In this case, the PR property can be achieved, provided that noise is negligible.

Taking into account that $\mathbf{C}_{0,0}$ is full rank, we can use, in practice, the QR factoriza-

²Recall that \mathbf{C}_1 is an upper triangular Toeplitz matrix with $[0 \ \dots \ 0 \ c[Q-1] \ \dots \ c[1]]$ as its first row.

tion instead of the pseudo-inverse, which is a much better alternative from a numerical robustness point of view [50]. The QR factorization of $\mathbf{C}_{0,0}$ is given by

$$\mathbf{C}_{0,0} = \mathbf{Q} \begin{bmatrix} \mathbf{R}_0 \\ \mathbf{0}_{(N-K) \times K} \end{bmatrix},$$

where \mathbf{Q} is an $N \times N$ orthogonal matrix and \mathbf{R}_0 is a $K \times K$ non-singular upper triangular matrix; it can be used to find $\mathbf{v}[n]$ as follows.

Let $\mathbf{w}[n]$ be the equalizer input (see Figure 4.1), given by

$$\mathbf{w}[n] = \mathbf{C}(z)\mathbf{u}[n] + \boldsymbol{\eta}[n].$$

To compute the equalizer output, i.e.

$$\mathbf{v}[n] = \mathbf{E}_{\text{ZF}}\mathbf{w}[n],$$

we proceed in two steps. The first step is to compute $\mathbf{w}'_0[n]$,

$$\begin{bmatrix} \mathbf{w}'_0[n] \\ \times \end{bmatrix} = \mathbf{Q}^T \mathbf{w}[n],$$

where $\mathbf{w}'_0[n]$ is a $K \times 1$ vector partition of $\mathbf{Q}^T \mathbf{w}[n]$. Note that we do not need to compute the remaining $N - K$ entries of $\mathbf{Q}^T \mathbf{w}[n]$. The received signal $\mathbf{v}[n]$ can then be obtained by solving the following triangular system:

$$\mathbf{R}_0 \mathbf{v}[n] = \mathbf{w}'_0[n]$$

via backward substitutions [50]. The procedure outlined above is summarized in Table 4.1. The amount of flops for each step of the algorithm is also given. If the channel is time-invariant, the QR factorization (Step 1 in Table 4.1) has to be computed only once. However, Steps 2 and 3 must be performed for each received frame, an operation requiring $2KN + K^2$ flops. Note that there exist fast algorithms to compute the QR factorization of $\mathbf{C}_{0,0}$ due to its particular structure [60].

| Instructions | Flops |
|---|-----------------|
| 1: Compute the QR factorization of $\mathbf{C}_{0,0}$, i.e. $\mathbf{C}_{0,0} = \mathbf{Q} \begin{bmatrix} \mathbf{R}_0 \\ \mathbf{0} \end{bmatrix}$. | $2K^2(N - K/3)$ |
| 2: Evaluate $\mathbf{w}'_0[n]$, given by $\begin{bmatrix} \mathbf{w}'_0[n] \\ \times \end{bmatrix} = \mathbf{Q}^T \mathbf{w}[n]$. | $2KN$ |
| 3: Solve $\mathbf{R}_0 \mathbf{v}[n] = \mathbf{w}'_0[n]$ using back substitutions. | K^2 |

Table 4.1 Algorithm for the computation of $\mathbf{v}[n] = \mathbf{E}_{ZF} \mathbf{w}[n]$.

As the presence of noise is not taken into account in the zero-forcing solution, performance can be suboptimal in high-noise environments. Such drawback is addressed in the following section, where the MMSE solution is considered.

4.1.2 MMSE Solution

In order to compensate for noise, we develop in this section the zero-padded block linear MMSE equalizer, denoted here as \mathbf{E}_{MMSE} . If noise is no longer ignored, we can write, from (4.1)

$$\begin{aligned} \mathbf{v}[n] &= \mathbf{E}_{MMSE} (\mathbf{C}_{0,0} \mathbf{u}[n] + \mathbf{C}_{1,0} \mathbf{u}[n-1] + \boldsymbol{\eta}[n]) \\ &= \mathbf{E}_{MMSE} (\mathbf{C}_{0,0} \mathbf{u}[n] + \boldsymbol{\eta}[n]) \quad \text{if } B \geq Q - 1, \end{aligned} \tag{4.6}$$

where $\mathbf{C}_{0,0}$ and $\mathbf{C}_{1,0}$ are the matrix partitions defined in (4.2). In (4.6), we assume that $\mathbf{C}_{1,0} = \mathbf{0}$, but the case where the guard length is insufficient (i.e. $B < Q - 1$) can also be

considered as shown later. The goal of the MMSE approach is to find a linear transformation such that the average power of the error vector $\mathbf{e}[n]$, given by

$$\mathbf{e}[n] = \mathbf{v}[n] - \mathbf{u}[n] \quad (4.7)$$

$$= \mathbf{E}_{\text{MMSE}} (\mathbf{C}_{0,0} \mathbf{u}[n] + \boldsymbol{\eta}[n]) - \mathbf{u}[n], \quad (4.8)$$

is minimized. Here, the average power of the error, denoted by \mathcal{P} , is given by

$$\mathcal{P} = \mathcal{E} (\text{tr} (\mathbf{e}[n] \mathbf{e}^T[n])), \quad (4.9)$$

where \mathcal{E} and tr respectively denote the expectation and trace operators. The minimization problem can be solved by finding the stationary points of the error power surface, i.e. by solving

$$\frac{\partial \mathcal{P}}{\partial \mathbf{E}_{\text{MMSE}}} = \mathbf{0}. \quad (4.10)$$

Using the matrix differentiation rules in [61], if we substitute (4.7) and (4.9) into (4.10), we can solve for \mathbf{E}_{MMSE} and obtain

$$\mathbf{E}_{\text{MMSE}} = \mathbf{R}_u \mathbf{C}_{0,0}^T \mathbf{B}^{-1}, \quad (4.11)$$

where

$$\mathbf{B} = \mathbf{C}_{0,0} \mathbf{R}_u \mathbf{C}_{0,0}^T + \mathbf{R}_\eta$$

and \mathbf{R}_u , \mathbf{R}_η , are the autocorrelation matrices of $\mathbf{u}[n]$ and $\boldsymbol{\eta}[n]$, respectively, i.e.

$$\begin{aligned}\mathbf{R}_u &= \mathcal{E}\mathbf{u}[n]\mathbf{u}^T[n], \\ \mathbf{R}_\eta &= \mathcal{E}\boldsymbol{\eta}[n]\boldsymbol{\eta}^T[n].\end{aligned}$$

In practice, we assume that $\mathbf{u}[n]$ contains uncorrelated samples, i.e.

$$\mathbf{R}_u = \sigma_u^2 \mathbf{I}_K, \quad (4.12)$$

where σ_u^2 denotes the power of the transmitted signal. As it will be noted in Chapter 5, (4.12) is not entirely true since the filter bank output signal is cyclostationary, so that \mathbf{R}_u is in fact a diagonal matrix with non-identical entries given by (5.4). However, (4.12) is an acceptable approximation for the application considered here. The matrix inverse in (4.11) involves symmetric and positive definite matrices. Thus, the equalizer output,

$$\mathbf{v}[n] = \sigma_u^2 \mathbf{C}_{0,0}^T \mathbf{B}^{-1} \mathbf{w}[n],$$

can be obtained efficiently using the Cholesky decomposition of \mathbf{B} , i.e. $\mathbf{B} = \mathbf{L}\mathbf{L}^T$, where \mathbf{L} is a lower triangular matrix. In practice, backward substitutions [50] can be employed to successively solve the following systems:

$$\begin{aligned}\mathbf{L}\mathbf{w}'[n] &= \mathbf{w}[n], \\ \mathbf{L}^T \mathbf{w}''[n] &= \mathbf{w}'[n].\end{aligned}$$

Once these steps have been performed, $\mathbf{v}[n]$ can be obtained by computing

$$\mathbf{v}[n] = \sigma_u^2 \mathbf{C}_{0,0}^T \mathbf{w}''[n].$$

This procedure is summarized in Table 4.2.

| Instructions | Flops |
|--|--|
| 1: Form $\mathbf{B} = \sigma_u^2 \mathbf{C}_{0,0} \mathbf{C}_{0,0}^T + \mathbf{R}_\eta$. | $\frac{7}{2}N^2 - NK + \frac{1}{2}K^2$ |
| 2: Compute the Cholesky factorization of \mathbf{B} , i.e. $\mathbf{B} = \mathbf{L}\mathbf{L}^T$. | $\frac{1}{3}N^3$ |
| 3: Solve $\mathbf{B}\mathbf{w}''[n] = \mathbf{L}\mathbf{L}^T\mathbf{w}''[n] = \mathbf{w}[n]$ using back substitutions. | $2N^2$ |
| 4: Evaluate $\mathbf{v}[n] = \mathbf{E}_{\text{MMSE}}\mathbf{w}[n] = \sigma_u^2 \mathbf{C}_{0,0}^T \mathbf{w}''[n]$. | $2NK$ |

Table 4.2 Algorithm for the computation of $\mathbf{v}[n] = \mathbf{E}_{\text{MMSE}}\mathbf{w}[n]$.

Notice that the product $\mathbf{C}_{0,0}\mathbf{C}_{0,0}^T$ in Table 4.2 involves highly structured matrices (being both Toeplitz and triangular) and can be computed very efficiently using the algorithm that we propose in Table 4.3. If the structure of $\mathbf{C}_{0,0}$ is disregarded, about $2N^2K$ flops would be required for such operation, whereas the algorithm in Table 4.3 necessitates $\frac{3}{2}N^2 - NK + \frac{1}{2}K^2$ flops (if $N = K$, this amounts to N^2 flops). Note that further optimizations are possible since $\mathbf{C}_{0,0}$ has lower bandwidth $Q - 1$. The complexity of the algorithm in Table 4.2 is thus dominated by the Cholesky factorization which requires $\frac{1}{3}N^3$ flops [50]. In comparison, an implementation using the LU factorization and without the algorithm in Table 4.3 would involve $\frac{2}{3}N^3 + 2N^2K$ flops. In cases where the channel is time-invariant, the Cholesky factorization needs to be computed once, and only Steps 3 and 4 in Table 4.2 have to be performed to equalize a received frame. The latter necessitates a total of $2N^2 + 2NK$ flops.

| Instructions | Flops |
|--|-----------------------|
| 1: Let $\mathbf{D}_0 = \mathbf{C}_{0,0}(:, 1)\mathbf{C}_{0,0}^T(:, 1)$ | $\frac{1}{2}N^2$ |
| 2: $\mathbf{D} = \mathbf{D}_0$ | |
| 3: for $i = 2 : K$ | |
| 4: for $j = i : N$ | |
| 5: $\mathbf{D}(i, j) = \mathbf{D}(j, i) = \mathbf{D}(i, j) + \mathbf{D}(i - 1, j - 1)$ | $NK - \frac{1}{2}K^2$ |
| 6: end for | |
| 7: end for | |
| 8: for $i = K + 1 : N$ | |
| 9: for $j = i : N$ | |
| 10: $\mathbf{D}(i, j) = \mathbf{D}(j, i) = \mathbf{D}(i, j) + \mathbf{D}(i - 1, j - 1) - \mathbf{D}_0(i - K, j - K)$ | $(N - K)^2$ |
| 11: end for | |
| 12: end for | |

Table 4.3 Algorithm for the computation of $\mathbf{D} = \mathbf{C}_{0,0}\mathbf{C}_{0,0}^T$, where $\mathbf{C}_{0,0}$ is Toeplitz and lower triangular.

4.1.3 MMSE with Insufficient Guard Length

So far, we have assumed that the duration of the guard interval (or trailing zeros) must be longer than the channel impulse response for the proposed equalizer to operate properly. This may pose problems in applications where the channel impulse response is long because an important fraction of the available bandwidth will have to be reserved for equalization purposes. The MMSE equalizer can easily be modified to compensate for the additional interference when the guard length is insufficient, i.e. if $Q - 1 > B$. This modified equalizer is hereby termed as the modified MMSE equalizer.

If the guard interval is insufficient, then $\mathbf{C}_{1,0}$ is not longer an all-zero matrix and (4.6) becomes

$$\mathbf{v}[n] = \mathbf{E}'_{\text{MMSE}} (\mathbf{C}_{0,0}\mathbf{u}[n] + \mathbf{C}_{1,0}\mathbf{u}[n - 1] + \boldsymbol{\eta}[n]), \quad (4.13)$$

where $\mathbf{E}'_{\text{MMSE}}$ denotes the modified MMSE equalizer. The error signal (4.7) is thus now

given by

$$\mathbf{e}[n] = \mathbf{v}[n] - \mathbf{u}[n] \quad (4.14)$$

$$= \mathbf{E}'_{\text{MMSE}} (\mathbf{C}_{0,0}\mathbf{u}[n] + \mathbf{C}_{1,0}\mathbf{u}[n-1] + \boldsymbol{\eta}[n]) - \mathbf{u}[n], \quad (4.15)$$

and we can solve for $\mathbf{E}'_{\text{MMSE}}$ if we substitute (4.14) and (4.9) into (4.10), where the differentiation is now carried out with respect to $\mathbf{E}'_{\text{MMSE}}$ instead of \mathbf{E}_{MMSE} . This yields

$$\mathbf{E}'_{\text{MMSE}} = \sigma_u^2 \mathbf{C}_{0,0}^T \mathbf{B}_M^{-1}, \quad (4.16)$$

where

$$\mathbf{B}_M = \sigma_u^2 (\mathbf{C}_{0,0} \mathbf{C}_{0,0}^T + \mathbf{C}_{1,0} \mathbf{C}_{1,0}^T) + \mathbf{R}_\eta. \quad (4.17)$$

As in the previous section, we assume here that $\mathbf{u}[n]$ is white, i.e. $\mathcal{E}\mathbf{u}[n]\mathbf{u}^T[n] = \sigma_u^2 \mathbf{I}$. The modified MMSE equalizer found in (4.16) is similar in form to the one derived in (4.11), except that imperfect ISI mitigation (due to insufficient guard length) is now taken into account via the term $\mathbf{C}_{1,0} \mathbf{C}_{1,0}^T$.

The modified MMSE equalizer given by (4.16) can be implemented efficiently via the algorithm proposed in Table 4.2, where Step 1 has to be updated to account for the term $\mathbf{C}_{1,0} \mathbf{C}_{1,0}^T$ that appears in (4.17). Since the matrix $\mathbf{C}_{1,0}$ is Toeplitz and upper triangular, computing $\mathbf{C}_{1,0} \mathbf{C}_{1,0}^T$ can be carried out in K^2 flops via the algorithm given in Table 4.4, meaning that the overall complexity of the modified MMSE equalizer is still constrained by the Cholesky factorization, which needs $\frac{1}{3}N^3$ flops. For time-invariant channels, the Cholesky factorization becomes irrelevant as it must only be computed once, and the implementation then requires $2N^2 + 2NK$ flops per frame (see Steps 3 and 4 in Table 4.2). Note that the efficient equalizer implementation proposed in [62], based on the use of cir-

culant matrices, cannot be exploited here. Indeed, such technique requires “extending” the Toeplitz matrix $\mathbf{C}_{0,0}$ into a circulant structure and can only be applied in situations where the guard length is sufficiently long (i.e. $B \geq Q - 1$).

| Instructions | Flops |
|---|------------------|
| 1: Let $\mathbf{D}_0 = \mathbf{C}_{1,0}^T(1, K : -1 : 2)\mathbf{C}_{1,0}(1, K : -1 : 2)$ | $\frac{1}{2}K^2$ |
| 2: $\mathbf{D} = \mathbf{0}_{N \times N}$ | |
| 3: $\mathbf{D}(1 : K - 1, K - 1) = \mathbf{D}(K - 1, 1 : K - 1) = \mathbf{D}_0(:, K - 1)$ | |
| 4: for $i = K - 2 : -1 : 1$ | |
| 5: for $j = i : -1 : 1$ | |
| 6: $\mathbf{D}(i, j) = \mathbf{D}(j, i) = \mathbf{D}_0(i, j) + \mathbf{D}(i + 1, j + 1)$ | $\frac{1}{2}K^2$ |
| 7: end for | |
| 8: end for | |

Table 4.4 Algorithm for the computation of $\mathbf{D} = \mathbf{C}_{1,0}\mathbf{C}_{1,0}^T$, where $\mathbf{C}_{1,0}$ is Toeplitz and upper triangular.

4.2 One-Tap Equalizer

As an alternative to the use of zero-padding combined with block linear equalization, one may consider a simple one-tap per subcarrier equalizer, as illustrated in Figure 4.2. Compared to the previous method, the one-tap equalizer does not require additional bandwidth to accommodate the transmission of extra zeros and the computational complexity is minimal, requiring only one complex multiplication (or 6 flops) per subcarrier once the equalizer coefficients are obtained, exactly like in OFDM/DMT. For this one-tap equalizer to operate properly, however, the prototype filter $F_0(z)$ used in the transmitting and receiving filter banks must exhibit “good” spectral characteristics, i.e. a narrow passband, a sharp transition band and a high out-of-band rejection. Under these conditions, it is shown in this section that each subchannel can then be modelled as a simple complex gain which, in turn, can be compensated by a single tap.

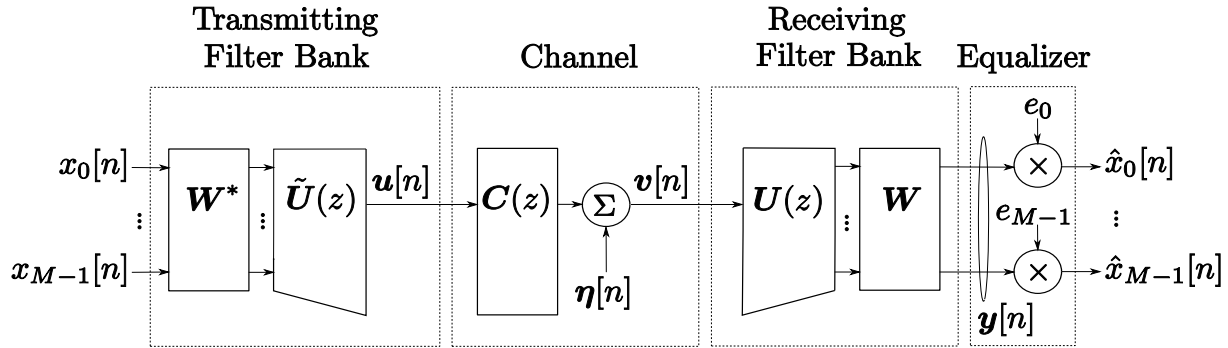


Fig. 4.2 Polyphase representation of a DFT filter bank transceiver with a one-tap per subcarrier equalizer.

4.2.1 Intrablock and Interblock ISI

In order to justify the use of a single tap per subcarrier for channel equalization, we must first distinguish between two types of ISI, namely, intrablock ISI and interblock ISI. To define these two types of ISI, let us consider the noise-free transfer function of the system shown in Figure 4.2, i.e.

$$\mathbf{T}_0(z) = \mathbf{\Lambda}_E \mathbf{R}(z), \quad (4.18)$$

where $\mathbf{\Lambda}_E = \text{diag}(e_0, \dots, e_{M-1})$ represents the one-tap equalizer, and $\mathbf{R}(z)$ represents the combined effect of the transmitting filter bank, channel and receiving filter bank. The latter can be expressed as

$$\mathbf{R}(z) \triangleq z^{-D/K+1} \mathbf{W} \mathbf{U}(z) \mathbf{C}(z) \tilde{\mathbf{U}}(z) \mathbf{W}^*, \quad (4.19)$$

where we recall from Chapter 2 that M is the number of subcarriers, K is the upsampling factor, D is the prototype filter length, $\mathbf{C}(z)$ is the channel matrix (given in (2.12)), $\mathbf{U}(z)$ is the polyphase matrix of the DFT filter bank (defined in (2.20)), and \mathbf{W} is the DFT

matrix. Note that we have added a delay of

$$d \triangleq D/K - 1$$

in (4.19) to make the transmitter causal. This delay represents the inherent processing latency caused by the filter banks. By expanding (4.19) and substituting the proper expressions for $\mathbf{C}(z)$ and $\mathbf{U}(z)$, we can show that the maximum degree of $\mathbf{R}(z)$ is $2D/K - 1$. $\mathbf{R}(z)$ can thus be written as

$$\mathbf{R}(z) = \sum_{l=0}^{2D/K-1} \mathbf{R}[l]z^{-l}.$$

Interblock ISI is present in the system when the symbols from a previous block interfere with those of the current received block or, in other terms, when $\mathbf{R}[l] \neq \mathbf{0}$ for $l \neq d$. Intrablock ISI occurs when an off-diagonal entry of the matrix $\mathbf{R}[d]$ is not zero, i.e. when the symbols within a block interfere with each other across different subchannels. Thus, to achieve the PR property with a one-tap equalizer, i.e. $\mathbf{T}_0(z) = z^{-d}\mathbf{I}_M$, a system must be free of intrablock and interblock ISI. As explained below, two conditions must be satisfied to eliminate intrablock and interblock ISI.

Intrablock ISI: First, we note that if the stopband energy of the prototype filter $F_0(z)$ is sufficiently low, the intrablock ISI should also be very low, or negligible. This can be observed by considering the non-polyphase representation of the transceiver, as shown in Figure 4.3. The DTFT of the i -th output of the receiving filter bank, denoted by $Y_i(e^{j\omega}) \triangleq \sum_n y_i[n]e^{-j\omega n}$, can be written as

$$Y_i(e^{j\omega}) = [\tilde{F}_i(e^{j\omega})C(e^{j\omega}) \sum_{l=0}^{M-1} F_l(e^{j\omega})X_l(e^{j\omega K})]_{\downarrow K}, \quad (4.20)$$

where $F_i(e^{j\omega}) \triangleq \sum_{m=0}^{D-1} f_i[m]e^{j\omega m}$ is the DTFT of the i -th transmitting filter, $C(e^{j\omega}) \triangleq$

$\sum_{m=0}^{Q-1} c[m]e^{-j\omega m}$ is the DTFT of the channel coefficients, and $X_l(e^{j\omega}) \triangleq \sum_n x_l[n]e^{-j\omega n}$ is the DTFT of the l -th input signal. In (4.20), we use the symbol $[\cdot]_{\downarrow K}$ to denote the DTFT of a K -fold decimated signal, i.e. we have [12]:

$$[D(e^{j\omega})]_{\downarrow K} \triangleq \frac{1}{K} \sum_{k=0}^{K-1} D(e^{j(\omega-2\pi k)/K}).$$

If the stopband energy of $F_l(e^{j\omega})$ is zero, i.e. if $F_l(e^{j\omega}) = 0$ for $|\omega - \frac{2\pi l}{M}| > \frac{\pi}{M}$, then (4.20) becomes

$$\begin{aligned} Y_i(e^{j\omega}) &= (\tilde{F}_i(e^{j\omega})C(e^{j\omega})F_i(e^{j\omega})X_i(e^{j\omega K}))|_{\downarrow K} \\ &= (\tilde{F}_i(e^{j\omega})C(e^{j\omega})F_i(e^{j\omega}))|_{\downarrow K}X_i(e^{j\omega}), \end{aligned} \quad (4.21)$$

where the last step is a direct application of the noble identities [12]. Since $Y_i(e^{j\omega})$ does not depend on any $X_l(e^{j\omega})$, $l \neq i$, the output signal is effectively free of intrablock ISI.

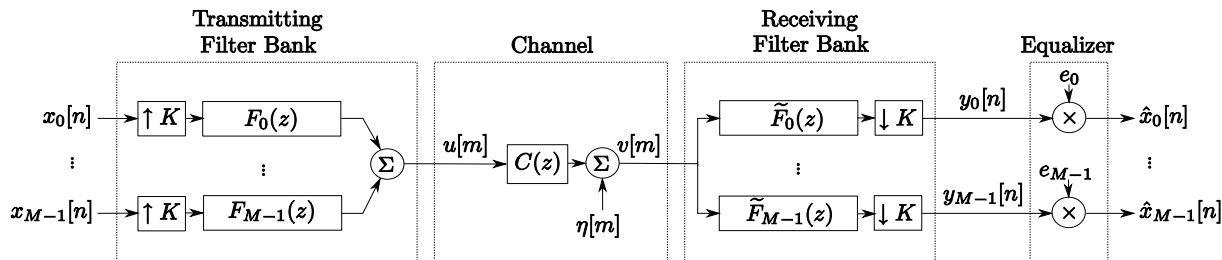


Fig. 4.3 Alternate (non-polyphase) representation of the DFT filter bank transceiver with a one-tap per subcarrier equalizer.

Interblock ISI: In addition, if the number of subcarriers M is large, then the subchannel frequency response should be almost flat as depicted in Figure 4.4. In turn, this would make the interblock ISI very small. In this case, the expression $\tilde{F}_i(e^{j\omega})C(e^{j\omega})F_i(e^{j\omega})$ in (4.21) can indeed be approximated as $C(e^{j\frac{2\pi i}{M}})\tilde{F}_i(e^{j\omega})F_i(e^{j\omega})$. By using the PR property of

the filter bank, (4.21) can then be simplified as follows:

$$\begin{aligned} Y_i(e^{j\omega}) &= C(e^{j\frac{2\pi i}{M}}) \left[\tilde{F}_i(e^{j\omega}) F_i(e^{j\omega}) \right]_{\downarrow K} X_i(e^{j\omega}) \\ &= C(e^{j\frac{2\pi i}{M}}) X_i(e^{j\omega}), \end{aligned} \quad (4.22)$$

since $\left[\tilde{F}_i(e^{j\omega}) F_i(e^{j\omega}) \right]_{\downarrow K} = 1$ for all ω . In (4.22), $X_i(e^{j\omega})$ is now scaled by a mere complex coefficient, $C(e^{j\frac{2\pi i}{M}})$.

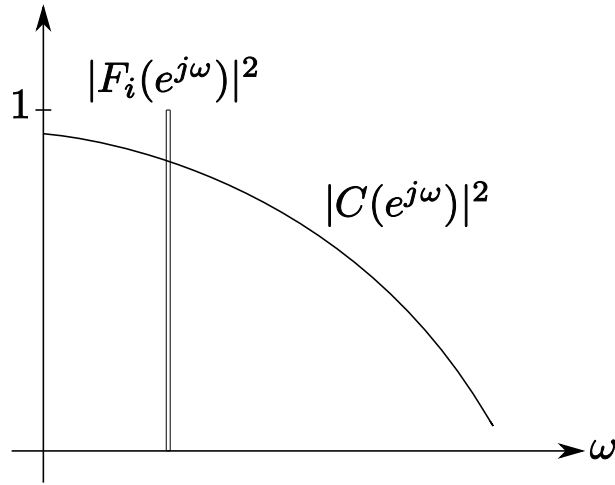


Fig. 4.4 Subchannel frequency response for a large M .

Under the two abovementioned conditions, the structure of a one-tap per subchannel equalizer is thus sufficient to perfectly recover the transmitted symbols under a noise-free environment.

Even though we employ PR DFT filter banks, i.e. we have $\mathbf{W}\mathbf{U}(z)\tilde{\mathbf{U}}(z)\mathbf{W}^* = \mathbf{I}_M$, we need to emphasize the fact that $\mathbf{T}_0(z)$ in (4.18) does not generally satisfy the PR property, due to the term $\mathbf{C}(z)$ in (4.19), i.e. the channel. PR filter banks are still an asset since we do not have to cope with any distortion originating from the filter banks themselves, as indicated by (4.22). Non-PR filter banks would contribute to interblock ISI,

making the subchannel frequency response non-flat and a one-tap per subchannel equalizer unsuitable [38]. In practice, the overall system is characterized by the near-PR property, i.e. $\mathbf{T}_0(z) \approx z^{-d}\mathbf{I}_M$, as no filter can exhibit a perfect stopband attenuation and an infinitely narrow passband. A tradeoff between intraband and interband ISI must thus be considered during the design process of the filter banks, as a prototype filter with very narrow passband would consequently suffer from a weak stopband attenuation, and vice-versa.

4.2.2 Zero-Forcing and MMSE Solutions

As previously stated, to ensure proper ISI cancellation, the one-tap equalizer operates under the assumptions that the number of subcarriers must be high enough (so that the subchannel frequency response is approximately flat) and that the stopband energy of the prototype filter is low (so that the interference between adjacent subcarriers is small). From (4.22), a zero-forcing approach yields

$$e_i^{\text{ZF}} = \frac{1}{C(e^{j\frac{2\pi i}{M}})}. \quad (4.23)$$

We can efficiently obtain $C(e^{j\frac{2\pi i}{M}})$ by performing the M -point FFT of the channel impulse response, $c[m]$. The overall implementation of the one-tap zero-forcing equalizer is described in Table 4.5, where we use $\mathbf{y}[n]$ to denote the output vector of the receiving filter bank (see Figure 4.2). If the channel is time invariant, then only Step 3 of the proposed algorithm, which requires a total of $6M$ flops, needs to be carried out repetitively. Otherwise, assuming we need to update the coefficients of the equalizer every time a frame of data is received, the computational complexity is bounded by the FFT, an operation necessitating $5M \log_2 M$ flops.

A MMSE approach is also possible. In this case, under the assumption that intrablock

| Instructions | Flops |
|---|---------------|
| 1: Compute $C[i]$, the M -point FFT of $c[m]$ | $5M \log_2 M$ |
| 2: Let $\mathbf{\Lambda}_E = \text{diag}(e_0, \dots, e_{M-1})$, where $e_i = 1/C[i]$ | $5M$ |
| 3: Evaluate $\hat{\mathbf{x}}[n] = \mathbf{\Lambda}_E \mathbf{y}[n]$ | $6M$ |

Table 4.5 Algorithm for the computation of $\hat{\mathbf{x}}[n] = \mathbf{\Lambda}_E \mathbf{y}[n]$.

and interblock ISI are negligible, we note that the received signal can be expressed as

$$\hat{x}_i[n] = C(e^{j\frac{2\pi i}{M}})e_i x_i[n-d] + e_i \zeta_i[n], \quad (4.24)$$

where $\zeta_i[n] \triangleq [\zeta[n]]_i$ is the noise term after demodulation. The latter can be written as

$$\zeta[n] = \mathbf{W} \sum_{l=0}^{D/K-1} \mathbf{U}[l] \boldsymbol{\eta}[n-l], \quad (4.25)$$

where $\mathbf{U}[l]$ denotes the inverse Z -transform of $\mathbf{U}(z)$, i.e. we assume that $\mathbf{U}(z)$ can be expressed as $\mathbf{U}(z) = \sum_{l=0}^{D/K-1} \mathbf{U}[l] z^{-l}$. To minimize the output mean square error, i.e. $\mathcal{E}|\hat{x}_i[n] - x_i[n-d]|^2$, we solve the following expression for e_i :

$$\frac{\partial \mathcal{E}|\hat{x}_i[n] - x_i[n-d]|^2}{\partial e_i^*} = 0, \quad (4.26)$$

where the partial derivative is defined as (note that e_i is complex) [63]

$$\frac{\partial \mathcal{E}|\hat{x}_i[n] - x_i[n-d]|^2}{\partial e_i^*} \triangleq \frac{1}{2} \left(\frac{\partial \mathcal{E}|\hat{x}_i[n] - x_i[n-d]|^2}{\partial \Re(e_i)} + j \frac{\partial \mathcal{E}|\hat{x}_i[n] - x_i[n-d]|^2}{\partial \Im(e_i)} \right).$$

Substituting (4.24) in (4.26) and solving for e_i yields

$$e_i^{\text{MMSE}} = \frac{C^*(e^{j\frac{2\pi i}{M}}) \sigma_{x_i}^2}{|C(e^{j\frac{2\pi i}{M}})|^2 \sigma_{x_i}^2 + \sigma_{\zeta_i}^2}, \quad (4.27)$$

where $\sigma_{x_i}^2 \triangleq \mathcal{E}|x_i[n]|^2$ and $\sigma_{\zeta_i}^2 \triangleq \mathcal{E}|\zeta_i[n]|^2$. In practice, the one-tap MMSE equalizer can be implemented by replacing Step 2 of the algorithm in Table 4.5 with (4.27). The overall computational complexity remains unchanged as the FFT is still the dominating operation (if M is large) and the last step still requires $6M$ flops, whether a zero-forcing or a MMSE solution is selected.

4.2.3 Optimal Solution for Non-Ideal Prototype Filters

The zero-forcing and MMSE solutions respectively found in (4.23) and (4.27) rely on an approximation based on the use of ideal prototype filters. According to (4.22), the transmitted symbols are then merely scaled by a complex coefficient. In the non-ideal case, the situation is more complicated since the received signal is expressed as

$$\hat{x}_i[n] = e_i y_i[n] + e_i \zeta_i[n], \quad (4.28)$$

where

$$y_i[n] = \sum_{l=0}^{2D/K-1} \sum_{k=0}^{M-1} [\mathbf{R}[l]]_{i,k} x_k[n-l], \quad (4.29)$$

and $\zeta_i[n]$ is the i -th entry of the demodulated noise vector $\boldsymbol{\zeta}[n]$ in (4.25). In the presence of a non-ideal prototype filter, the one-tap equalizer coefficients that minimize the mean square error, denoted here by e_i^{MMSE} , can be found by substituting (4.28) in (4.26) and by solving the resulting expression. We then obtain

$$e_i^{\text{MMSE}} = \frac{\mathcal{E} y_i^*[n] x_i[n-d]}{\mathcal{E} |y_i[n]|^2 + \sigma_{\zeta_i}^2}. \quad (4.30)$$

If we now take into account that $y_i[n]$ is given by (4.29), (4.30) becomes

$$e_i^{\prime\text{MMSE}} = \frac{[\mathbf{R}[d]]_{i,i}^* \sigma_{x_i}^2}{\sum_{k=0}^{M-1} \sigma_{x_k}^2 \sum_{l=0}^{2D/K-1} \left| [\mathbf{R}[l]]_{i,k} \right|^2 + \sigma_{\zeta_i}^2}. \quad (4.31)$$

In order to compute $e_i^{\prime\text{MMSE}}$, we note that the matrix $\mathbf{R}[l]$ must be given explicitly.

To find an expression for $\mathbf{R}[l]$, let us first express $\mathbf{U}(z)$, the polyphase matrix of the DFT filter bank, as a sum of matrices. Based on (2.20), $\mathbf{U}(z)$ can equivalently be written as

$$\mathbf{U}(z) = \begin{bmatrix} \mathbf{U}[0] & \dots & \mathbf{U}[D/K - 1] \end{bmatrix} \mathbf{L}_0(z) = \sum_{l=0}^{D/K-1} \mathbf{U}[l] z^{-l}. \quad (4.32)$$

From (2.20) and (4.32), we note that the $M \times K$ matrices $\mathbf{U}[l]$, $l = 0, \dots, D/K - 1$, representing the inverse Z -transform of $\mathbf{U}(z)$, can be given as partitions of $\mathbf{L}_1 \mathbf{\Lambda}_f$, i.e.

$$\begin{bmatrix} \mathbf{U}[0] & \dots & \mathbf{U}[D/K - 1] \end{bmatrix} = \mathbf{L}_1 \mathbf{\Lambda}_f,$$

where \mathbf{L}_1 and $\mathbf{\Lambda}_f$ are defined in (2.18) and in (2.17), respectively. As an example, let $M = 2$, $K = 3$ and $D = 6$. The expression above can then be written as

$$\mathbf{L}_1 \mathbf{\Lambda}_f = \begin{bmatrix} f_0[0] & 0 & f_0[2] & 0 & f_0[4] & 0 \\ 0 & f_0[1] & 0 & f_0[3] & 0 & f_0[5] \end{bmatrix},$$

which implies that $\mathbf{U}[0]$ and $\mathbf{U}[1]$ are respectively given by

$$\mathbf{U}[0] = \begin{bmatrix} f_0[0] & 0 & f_0[2] \\ 0 & f_0[1] & 0 \end{bmatrix},$$

and

$$\mathbf{U}[1] = \begin{bmatrix} 0 & f_0[4] & 0 \\ f_0[3] & 0 & f_0[5] \end{bmatrix}.$$

Substituting (4.32) and (2.12) in (4.19) yields

$$\mathbf{R}(z) = \mathbf{W} \left(\sum_{p=0}^{D/K-1} \mathbf{U}[p]z^{-p} \right) (\mathbf{C}_0 + \mathbf{C}_1z^{-1}) \left(\sum_{q=0}^{D/K-1} \mathbf{U}^T[D/K - 1 - q]z^{-q} \right) \mathbf{W}^* \quad (4.33)$$

$$= \sum_{l=0}^{2D/K-1} \mathbf{R}[l]z^{-l}. \quad (4.34)$$

By re-arranging (4.33) appropriately, $\mathbf{R}[l]$ can thus be expressed as

$$\mathbf{R}[l] = \mathbf{W} \left(\sum_{p=0}^{D/K} \mathbf{U}[l-p] (\mathbf{C}_0\mathbf{U}^T[D/K-p-1] + \mathbf{C}_1\mathbf{U}^T[D/K-p]) \right) \mathbf{W}^*, \quad (4.35)$$

with $\mathbf{U}[l] = \mathbf{0}$ for $l < 0$ and $l > D/K - 1$. With the help of (4.35), a proper numerical expression for $\mathbf{R}[l]$ can now be obtained, which, in turn, can be used to compute $e_i^{\prime\text{MMSE}}$ according to (4.31).

In terms of computational complexity, computing $e_i^{\prime\text{MMSE}}$ requires much more flops than e_i^{ZF} or e_i^{MMSE} , due to the numerous matrix operations involved in (4.35). As a rough approximation, if we assume that $D \gg M$ and $D \gg K$, the computation necessitates about $2MD(2K + M)$ flops³. However, regardless of the chosen method to obtain e_i , equalization itself can always be performed in $6M$ flops. In situations where the channel coefficients do not change (or change slowly) over time, it would be preferable to use the solution for non-ideal filters found in (4.31), since the high cost of computing the equalizer coefficients

³This is the number of flops necessary to compute the expression in parenthesis in (4.35) using a “brute force” approach which does not take into account that some operations can be omitted due to the fact that $\mathbf{U}[l] = \mathbf{0}$ for $l < 0$ and $l > D/K - 1$.

would eventually become irrelevant. Otherwise, the use of the approximate zero-forcing solution or the approximate MMSE solution (i.e. (4.23) or (4.27), respectively) would be more appropriate.

4.3 Performance of the Proposed Equalizers

The different equalization schemes and solutions proposed in this chapter are summarized in Table 4.6. We may observe that, under certain conditions, some solutions can become equivalent to other solutions. For instance, if noise is ignored or set to zero (i.e. if $\mathbf{R}_\eta = \mathbf{0}$ or $\sigma_{\eta_i}^2 = 0$), then the MMSE solutions of the one-tap scheme and the zero-padded block linear one correspond to the respective zero-forcing solutions. Similarly, the modified MMSE solution of the zero-padded block linear scheme becomes identical to the MMSE solution if the guard interval has sufficient length (i.e. if $B \geq Q - 1$), since, in this case, we have $\mathbf{C}_{1,0}\mathbf{C}_{1,0}^T = \mathbf{0}$.

| Equalization scheme | Solution | Expression |
|---------------------|-------------------------|---|
| | Zero-forcing (ZF) | $\mathbf{E}_{\text{ZF}} = (\mathbf{C}_{0,0}^T \mathbf{C}_{0,0})^{-1} \mathbf{C}_{0,0}^T$ |
| Zero-padded | MMSE | $\mathbf{E}_{\text{MMSE}} = \sigma_u^2 \mathbf{C}_{0,0}^T (\sigma_u^2 \mathbf{C}_{0,0} \mathbf{C}_{0,0}^T + \mathbf{R}_\eta)^{-1}$ |
| | Modified MMSE | $\mathbf{E}'_{\text{MMSE}} = \sigma_u^2 \mathbf{C}_{0,0}^T (\sigma_u^2 (\mathbf{C}_{0,0} \mathbf{C}_{0,0}^T + \mathbf{C}_{1,0} \mathbf{C}_{1,0}^T) + \mathbf{R}_\eta)^{-1}$ |
| One-tap | Approx. solution (ZF) | $e_i^{\text{ZF}} = \frac{1}{C(e^{j\frac{2\pi i}{M}})}$ |
| | Approx. solution (MMSE) | $e_i^{\text{MMSE}} = \frac{C^*(e^{j\frac{2\pi i}{M}}) \sigma_{x_i}^2}{ C(e^{j\frac{2\pi i}{M}}) ^2 \sigma_{x_i}^2 + \sigma_{\zeta_i}^2}$ |
| | Optimal solution | $e_i^{\prime\text{MMSE}} = \frac{[\mathbf{R}[d]]_{i,i}^* \sigma_{x_i}^2}{\sum_{k=0}^{M-1} \sigma_{x_k}^2 \sum_{l=0}^{2D/K-1} [\mathbf{R}[l]]_{i,k} ^2 + \sigma_{\zeta_i}^2}$ |

Table 4.6 Proposed equalization schemes for PR DFT filter bank transceivers.

In the rest of this section, we analyze the performance of the proposed equalizers. We will focus our analysis on two aspects: the computational complexity and the resulting

subchannel SNR.

4.3.1 Computational Complexity

The computational complexity of each method is given in Table 4.7. The computational cost is divided in two categories: the computation of the equalizer coefficients (i.e. obtaining \mathbf{E} or e_i) and the equalization properly speaking (i.e. computing the equalized signals provided that \mathbf{E} or e_i is given). Obviously, in environments where the channel is time-invariant or slowly time-varying, only the equalization complexity will matter in the long run. In this case, depending on the application, the equalizer coefficients could even be computed offline.

| Equalization scheme | Solution | Coefficient computation (flops) | Equalization (flops) |
|---------------------|-------------------------|---------------------------------|----------------------|
| Zero-padded | Zero-forcing (ZF) | $2K^2(N - K/3)$ | $K^2 + 2NK$ |
| | MMSE | $N^3/3$ | $2N^2 + 2NK$ |
| | Modified MMSE | $N^3/3$ | $2N^2 + 2NK$ |
| One-tap | Approx. solution (ZF) | $5M \log_2 M$ | $6M$ |
| | Approx. solution (MMSE) | $5M \log_2 M$ | $6M$ |
| | Optimal solution | $2MD(2K + M)$ | $6M$ |

Table 4.7 Computational complexity of the zero-padded block linear equalizer and the one-tap equalizer (per frame).

As pointed out in the previous section, one of the biggest advantages of the one-tap scheme is its low computational complexity (except for the computation of the optimal solution e_i^{MMSE}). For instance, let us consider a system with $M = 128$, $K/M = 1.25$, $N/M = 1.375$ and $D/M = 20$. These are typical values which will be employed in various computer experiments presented in Chapter 6. Using these values, we show in Table 4.8 the actual number of flops needed per received frame of data. We note that there is indeed a significant difference in terms of computational complexity between the zero-padded block linear equalizer and the one-tap one. The number of flops required by the latter is more

than two orders of magnitude lower than the former.

| Equalization scheme | Solution | Coefficient computation (Mflops) | Equalization (Mflops) |
|---------------------|-------------------------|----------------------------------|-----------------------|
| Zero-padded | Zero-forcing (ZF) | 2.28 | 0.082 |
| | MMSE | 1.82 | 0.118 |
| | Modified MMSE | 1.82 | 0.118 |
| One-tap | Approx. solution (ZF) | 4.5×10^{-3} | 0.77×10^{-3} |
| | Approx. solution (MMSE) | 4.5×10^{-3} | 0.77×10^{-3} |
| | Optimal solution | 293.6 | 0.77×10^{-3} |

Table 4.8 Number of flops of the zero-padded block linear equalizer and the one-tap equalizer with $M = 128$, $K/M = 1.25$, $N/M = 1.375$ and $D/M = 20$ (per frame).

4.3.2 Subchannel SNR

Here, we assess the performance of the proposed equalizers by deriving an expression for the subchannel SNR at the receiver end. The subcarrier SNR can be used to compute the theoretical achievable bit rate, a highly meaningful performance metric. The exact relationship between the subcarrier SNR and the achievable bit rate will be discussed in Chapter 6⁴.

To obtain the subcarrier SNR, which we denote by SNR_i , $i = 0, \dots, M - 1$, we consider the transfer functions of the signal and noise, respectively represented by $\mathbf{T}(z)$ and $\mathbf{P}(z)$, where

$$\mathbf{T}(z) = \sum_{l=0}^{2D/K-1} \mathbf{T}[l]z^{-l},$$

and

$$\mathbf{P}(z) = \sum_{l=0}^{D/K-1} \mathbf{P}[l]z^{-l}.$$

⁴See (6.1) and (6.2) specifically.

The expressions for $\mathbf{T}[l]$ and $\mathbf{P}[l]$ will vary depending on the equalization scheme, i.e. whether we use a one-tap equalizer or a zero-padded block linear one. Assuming that $\mathbf{T}[l]$ and $\mathbf{P}[l]$ are properly given, the SNR of the i -th subchannel can be computed as follows:

$$\text{SNR}_i = \frac{\sigma_{x_i}^2 \left[\sum_{l=0}^{2D/K-1} \mathbf{T}[l] \mathbf{T}^H[l] \right]_{i,i}}{\left[\sum_{l=0}^{D/K-1} \mathbf{P}[l] \mathbf{R}_\eta \mathbf{P}^H[l] \right]_{i,i}}, \quad (4.36)$$

where $\sigma_{x_i}^2$ is the signal input power in the i -th subchannel and \mathbf{R}_η is the noise autocorrelation matrix. This equation is valid regardless of the equalization scheme, provided that $\mathbf{T}[l]$ and $\mathbf{P}[l]$ are chosen accordingly. Expressions for $\mathbf{T}[l]$ and $\mathbf{P}[l]$ are provided below for each equalization scheme.

One-tap equalizer: When the one-tap equalizer is employed, $\mathbf{T}[l]$, which we refer in this case by $\mathbf{T}_0[l]$, is given by

$$\mathbf{T}_0[l] = \mathbf{\Lambda}_E \mathbf{R}[l],$$

where $\mathbf{\Lambda}_E$ represents any one of the solutions developed for the one-tap equalizer (see Table 4.6), and $\mathbf{R}[l]$ is defined in (4.35). Concerning the noise transfer function, by inspecting Figure 4.2, we note that $\mathbf{P}[l]$ can be expressed as

$$\mathbf{P}_0[l] = \mathbf{\Lambda}_E \mathbf{W} \mathbf{U}[l].$$

The subchannel SNR can now be easily computed by substituting $\mathbf{T}_0[l]$ and $\mathbf{P}_0[l]$ for $\mathbf{T}[l]$ and $\mathbf{P}[l]$, respectively, in (4.36), yielding

$$\text{SNR}_i = \frac{\sigma_{x_i}^2 \left[\sum_{l=0}^{2D/K-1} \mathbf{R}[l] \mathbf{R}^H[l] \right]_{i,i}}{\left[\mathbf{W} \left(\sum_{l=0}^{D/K-1} \mathbf{U}[l] \mathbf{R}_\eta \mathbf{U}^H[l] \right) \mathbf{W}^* \right]_{i,i}}.$$

We note that the equalizer coefficients Λ_E do not appear in the expression above. Hence, the subchannel SNR does not depend on the chosen solution for the one-tap equalizer. However, the equalizer coefficients will have an impact on the bit error rate and on the symbol mean square error as discussed in Chapter 6.

Zero-padded block linear equalizer: The signal and noise transfer functions for the zero-padded block linear scheme are similar to the one-tap ones. The only difference comes from the fact that equalization is performed before demodulation and that a block of zeros is appended to the transmitted signal (see Figure 4.1). Based on (4.35), which was developed for the one-tap equalizer, we can show that, when a zero-padded block linear scheme is employed, $\mathbf{T}[l]$, denoted here by $\mathbf{T}_1[l]$, can be written as

$$\mathbf{T}_1[l] = \mathbf{W} \left(\sum_{p=0}^{D/K} \mathbf{U}[l-p] \mathbf{E} (\mathbf{C}_0 \mathbf{Q}[p] + \mathbf{C}_1 \mathbf{Q}[p-1]) \right) \mathbf{W}^*,$$

where \mathbf{E} is one of the possible solutions for the block linear equalizer (see Table 4.6), and

$$\mathbf{Q}[p] = \begin{bmatrix} \mathbf{U}^T[D/K - p - 1] \\ \mathbf{0}_{B \times M} \end{bmatrix}.$$

As for $\mathbf{P}[l]$, it can be expressed as

$$\mathbf{P}_1[l] = \mathbf{W} \mathbf{U}[l] \mathbf{E}.$$

The subchannel SNR of the system using the zero-padded block linear equalizer can be found by substituting $\mathbf{T}_1[l]$ and $\mathbf{P}_1[l]$ for $\mathbf{T}[l]$ and $\mathbf{P}[l]$, respectively, in (4.36). Contrary to the one-tap equalizer, the subchannel SNR depends on the coefficients of the block linear equalizer.

We have thus derived in this section an expression which can be used to compute the subchannel SNR of a DFT filter bank transceiver employing either a one-tap equalizer or a zero-padded block linear one. A thorough comparison of the two proposed equalization schemes based on the subchannel SNR and a simulated communication environment is presented in Chapter 6.

4.4 Chapter Summary

In this chapter, we have presented two equalization schemes suitable for PR DFT filter bank transceivers. The first method employs zero-padding and a block linear transform to mitigate ISI. It is capable of completely removing ISI, provided that the guard interval (or the trailing zeros) is longer than the channel impulse response. The second method exploits the spectral characteristics of the prototype filter to derive a simple one-tap per subchannel equalizer. This scheme does not require the transmission of extra zeros and is computationally less demanding than the first method. Finally, the computational complexity and the resulting subchannel SNR of the two proposed schemes have been determined analytically.

Chapter 5

Blind Channel Identification

We have assumed in Chapter 4 that the impulse response of the channel was known for equalization purposes. In practical implementations, however, such information must be obtained using estimation techniques. We present in this chapter an estimation technique which operates blindly. Blind techniques do not require the transmission of a known sequence and rely solely on the statistical properties of the transmitted signal to identify the channel.

In this chapter, we show that the inherent redundancy added by the DFT filter bank proposed in Chapter 3, which was then exploited for PR purposes, can also be used for blind channel identification. In fact, as we will prove here, the redundancy introduces cyclostationarity in transmitted signal. We can exploit this statistical property to build a homogeneous system of linear equations whose solution corresponds to the unknown channel coefficients. The channel coefficients can then be estimated by finding the least squares solution of the aforementioned system.

Using cyclostationarity in a multicarrier modulation context to blindly estimate the channel impulse response has previously been studied in [43, 45, 66]. In [43], it is proved

that the multirate nature of filter banks naturally leads to a transmitted signal which is cyclostationary. However, subsequent analysis on cyclostationarity-based blind identification is restricted to the case of non-overlapping filter banks, and cannot be applied to the filter bank considered in this work. In [45,66], a blind technique is investigated which relies on the cyclostationarity introduced by the cyclic prefix of an OFDM transceiver¹. The technique proposed in [45,66] is based on the use of a pair of *cyclic frequencies*² to derive a system of linear equations which can be solved to estimate the channel impulse response.

The blind estimation technique proposed in this chapter is based on the one given in [45], but there are significant differences. First, by using results presented in [43], the algorithm described in [45] is modified to exploit the cyclostationarity generated by a DFT filter bank transmitter. The method is also extended to take into account multiple pairs of cyclic frequencies, instead of a single pair, for the computation of the channel coefficients. Finally, we propose an efficient method to obtain the channel coefficients based on the so-called inverse iteration algorithm [50]. The proposed identification method, combined with the one-tap equalizer developed in Section 4.2, provides a simple, yet powerful, solution to the equalization issue in PR DFT filter bank transceivers.

This chapter is organized as follows. In Section 5.1, we show that the redundancy added by the proposed PR DFT filter bank introduces cyclostationarity in the transmitted signal. This statistical property is then exploited in Section 5.2 to derive a system of linear equations which can be solved to estimate the channel coefficients. Finally, results presented in this chapter are summarized in Section 5.3.

¹See Section 2.1.2 for a discussion on OFDM and the cyclic prefix.

²As discussed later in this chapter, the cyclic frequencies correspond to the frequency indices of the Fourier series representation of the cyclostationary signal's autocorrelation function.

5.1 Cyclostationarity and Redundant Filter Banks

The redundancy introduced by a transmitting PR DFT filter bank with $K > M$ has important consequences on the statistical properties of the output signal. We prove in this section that the output signal of such filter bank is wide-sense cyclostationary. This property is preserved as the signal is sent through a channel and is contaminated by an additive white noise.

5.1.1 General Considerations on Cyclostationarity

Cyclostationarity arises when a stochastic process is characterized by periodically time-varying statistical properties. For channel identification purposes, we only need to be concerned with second-order statistical properties. When higher-order statistics are disregarded, cyclostationarity is instead referred to as wide-sense cyclostationarity.

In more specific terms, let $x[n]$ be a zero-mean discrete-time stochastic process and let

$$r_x[n, \tau] \triangleq \mathcal{E}x[n]x^*[n + \tau]$$

be its autocorrelation function, where the variable τ represents the discrete-time lag. Then, $x[n]$ is wide-sense cyclostationary if and only if $r_x[n, \tau]$ is periodic with period K (K being a non-negative integer) with respect to the time index n [64], i.e.

$$r_x[n + K, \tau] = r_x[n, \tau], \quad n, \tau \in \mathcal{Z}.$$

Due to its periodic nature, $r_x[n, \tau]$ can also be expressed via a Fourier series representation.

We can thus write

$$r_x[n, \tau] = \sum_{k=0}^{K-1} R_x[k, \tau] e^{j2\pi kn/K},$$

where $R_x[k, \tau]$, $k = 0, \dots, K-1$, denote the Fourier coefficients, which are given by

$$R_x[k, \tau] = \frac{1}{K} \sum_{n=0}^{K-1} r_x[n, \tau] e^{-j2\pi kn/K}.$$

In this context, $R_x[k, \tau]$ is termed as the cyclic autocorrelation function, and the elements of the set $\{0, 1/K, \dots, (K-1)/K\}$ can be referred to as the cyclic frequencies [64]. Note that with $K = 1$, $x[n]$ becomes a wide-sense stationary process as the autocorrelation function $r_x[n, \tau]$ would remain constant with respect to its time argument n . In subsequent sections of this chapter, *we refer to wide-sense cyclostationary simply as cyclostationary*.

5.1.2 Statistical Properties of the DFT Filter Bank Transceiver

We show here that the signals $u[m]$ and $v[m]$,

$$u[m] = \sum_{i=0}^{M-1} \sum_{l=-\infty}^{\infty} x_i[l] f_0[m - lK] e^{j2\pi i(m-lK)/M}, \quad (5.1)$$

$$v[m] = \sum_{l=-\infty}^{\infty} u[l] c[m - l] + \eta[m], \quad (5.2)$$

respectively representing the transmitter output and the receiver input (see Figure 4.3), are both cyclostationary. As detailed in the next section, the cyclostationarity will be exploited to derive a blind channel identification algorithm.

We first assume that the transmitted symbols $x_0[n], \dots, x_{M-1}[n]$ are uncorrelated, i.e.

$$\mathcal{E}(x_i[n] x_{i'}^*[n']) = \sigma_x^2 \delta[i - i'] \delta[n - n'], \quad (5.3)$$

where σ_x^2 is the symbol average power. The cyclostationarity of $u[m]$ in (5.1) can be established by considering its autocorrelation $r_u[m, \tau]$, defined as

$$r_u[m, \tau] \triangleq \mathcal{E}(u[m]u^*[m + \tau]).$$

Using (5.3) and (5.1), we find that

$$r_u[m, \tau] = \sigma_x^2 M \delta[\tau] \sum_{l=-\infty}^{\infty} f_0^2[m - lK]. \quad (5.4)$$

According to (5.4), we thus have $r_u[m + K, \tau] = r_u[m, \tau]$ for all integers m and τ . Therefore $u[m]$ is cyclostationary with a period of K . Similarly, we can show that $v[m]$ is also cyclostationary by proving that its autocorrelation function, i.e. $r_v[m, \tau] \triangleq \mathcal{E}(v[m]v^*[m + \tau])$, is periodic with respect to the argument m . Indeed, using (5.2), we have

$$r_v[m, \tau] = \sum_{l=-\infty}^{\infty} \sum_{l'=-\infty}^{\infty} r_u[l, l' - l] c[m - l] c[m + \tau - l'] + r_\eta[m, \tau], \quad (5.5)$$

where

$$r_\eta[m, \tau] \triangleq \mathcal{E}(\eta[m]\eta[m + \tau])$$

is the noise autocorrelation and is assumed to be white, i.e. $r_\eta[m, \tau] = \sigma_\eta^2 \delta[\tau]$. Since $r_u[l, l' - l] = 0$ for $l' \neq l$, (5.5) can be simplified as follows:

$$r_v[m, \tau] = \sum_{l=-\infty}^{\infty} c[m - l] c[m - l + \tau] r_u[l, 0] + \sigma_\eta^2 \delta[\tau].$$

Finally, if we let $q = m - l$, we obtain

$$r_v[m, \tau] = \sum_{q=0}^{Q-1} c[q]c[q + \tau]r_u[m - q, 0] + \sigma_\eta^2\delta[\tau]. \quad (5.6)$$

Note that the sum in (5.6) is finite, since, by definition, $c[q] = 0$ for $q < 0$ or $q > Q - 1$. From (5.6), one can easily conclude that $v[m]$ is cyclostationary as $r_u[m, \tau]$ is periodic in m with period K .

Let us now consider the cyclic autocorrelation of $u[m]$ and $v[m]$, denoted by $R_u[k, \tau]$ and $R_v[k, \tau]$, respectively. Using (5.4), the cyclic autocorrelation function of $u[m]$ is obtained as

$$\begin{aligned} R_u[k, \tau] &\triangleq \frac{1}{K} \sum_{m=0}^{K-1} r_u[m, \tau] e^{-j2\pi km/K} \\ &= \frac{\sigma_x^2 M}{K} \delta[\tau] \sum_{m=0}^{K-1} e^{-j2\pi km/K} \sum_{l=-\infty}^{\infty} f_0^2[m - lK], \end{aligned} \quad (5.7)$$

whereas, using (5.6), that of $v[m]$ can be expressed as

$$\begin{aligned} R_v[k, \tau] &\triangleq \frac{1}{K} \sum_{m=0}^{K-1} r_v[m, \tau] e^{-j2\pi km/K} \\ &= R_u[k, 0] \sum_{q=0}^{Q-1} c[q]c[q + \tau] e^{-j2\pi kq/K} + \sigma_\eta^2 \delta[\tau] \delta[k]. \end{aligned} \quad (5.8)$$

As specified in the next section, the cyclic autocorrelation functions (5.7) and (5.8) will prove to be key elements for blind channel identification.

5.2 Channel Identification

The presence of a cyclostationary signal at the channel output will be exploited here to build a homogeneous system of linear equations whose solution corresponds to the channel coefficients. In practice, we show that the system of equations can be represented by a matrix, and the channel coefficients can be estimated by tracking its null space.

5.2.1 Homogeneous System of Linear Equations

To derive a system of linear equations, we must first cancel one of the terms $c[q]$ or $c[q + \tau]$ in (5.8). In order to do so, let us take the Z -transform of $R_v[k, \tau]$ with respect to τ , i.e.

$$\begin{aligned} S_v(k, z) &\triangleq \sum_{\tau=-\infty}^{\infty} R_v[k, \tau] z^{-\tau} \\ &= R_u[k, 0] C(z^{-1} e^{j2\pi k/K}) C(z) + \sigma_\eta^2 \delta[k]. \end{aligned} \quad (5.9)$$

To derive (5.9), we have successively used the following Z -transform properties: the convolution property³, the exponential multiplication property and the time-reversal property [65].

We now assume that $k \neq 0$, which effectively cancels out the noise term $\sigma_\eta^2 \delta[k]$ in (5.9).

Let \mathcal{K} denote the following set of integers:

$$\mathcal{K} = \{1, 2, \dots, K - 1\}.$$

Then, from (5.9) we can write

$$S_v(-k, z) = R_u^*[k, 0] C(z^{-1} e^{-j2\pi k/K}) C(z), \quad (5.10)$$

³Note that $\sum_{q=0}^{Q-1} c[q]c[q+\tau]e^{-j2\pi kq/K} = c[\tau]*(c[-\tau]e^{j2\pi k\tau/K})$, where $*$ denotes the convolution operator with respect to τ .

where $k \in \mathcal{K}$. Note that for $k > 0$, we have $R_u[-k, 0] = R_u^*[k, 0]$ and $R_v[-k, \tau] = R_v^*[k, \tau]$. We may then cancel the effect of the term $c[q]$ in (5.8) by considering the quotient formed by (5.9) and (5.10) for $k \neq 0$:

$$\frac{S_v(k, z)}{S_v(-k, z)} = \frac{R_u[k, 0]C(z^{-1}e^{j2\pi k/K})}{R_u^*[k, 0]C(z^{-1}e^{-j2\pi k/K})}. \quad (5.11)$$

By re-arranging (5.11) and taking the inverse Z -transform of the resulting expression, we obtain a linear equation with respect to $c[\tau]$ only:

$$(R_u^*[k, 0]R_v[k, -\tau] * e^{j2\pi k\tau/K} - R_u[k, 0]R_v^*[k, -\tau] * e^{-j2\pi k\tau/K}) c[\tau] = 0, \quad (5.12)$$

where $*$ denotes the convolution operator with respect to τ .

We can express (5.12) in a matrix form by representing the convolution operation as a matrix multiplication. Let us define a convolution matrix $\mathbf{R}_v[k]$ as a $(3Q - 2) \times Q$ lower triangular Toeplitz matrix with the following entries:

$$\mathbf{R}_v[k] \triangleq \begin{bmatrix} R_v[k, Q-1] & 0 & \dots & 0 \\ \vdots & R_v[k, Q-1] & \ddots & 0 \\ R_v[k, -Q+1] & \vdots & & \vdots \\ 0 & R_v[k, -Q+1] & \ddots & 0 \\ 0 & 0 & & R_v[k, Q-1] \\ \vdots & \vdots & \ddots & \vdots \\ 0 & 0 & & R_v[k, -Q+1] \end{bmatrix}. \quad (5.13)$$

Then (5.12) can be expressed as

$$\mathbf{\Phi}[k]\mathbf{c} = \mathbf{0}, \quad (5.14)$$

where

$$\mathbf{c} \triangleq \begin{bmatrix} c[0] & \dots & c[Q-1] \end{bmatrix}^T,$$

$$\mathbf{\Phi}[k] \triangleq R_u^*[k, 0] \mathbf{R}_v[k] \mathbf{D}^*[k] - R_u[k, 0] \mathbf{R}_v^*[k] \mathbf{D}[k] \quad (5.15)$$

and

$$\mathbf{D}[k] \triangleq \text{diag} (1, e^{-j2\pi k/K}, \dots, e^{-j2\pi k(Q-1)/K}).$$

To solve (5.14) for other solutions than the trivial one (i.e. $\mathbf{c} = \mathbf{0}$), the null space of $\mathbf{\Phi}[k]$ must be found. Note that, in practice, we need to estimate $\mathbf{\Phi}[k]$, and (5.14), which represents an overdetermined system, becomes a least squares problem. This problem can be solved by computing the SVD of $\mathbf{\Phi}[k]$, i.e.

$$\mathbf{U}^H \mathbf{\Phi}[k] \mathbf{V} = \text{diag}(\sigma_0, \dots, \sigma_{Q-1});$$

the solution then corresponds to the space spanned by the last column of \mathbf{V} [50]. Alternatively, the solution is also given by the eigenvector corresponding to the smallest eigenvalue of $\mathbf{\Phi}^H[k] \mathbf{\Phi}[k]$ [66]. As with other blind methods, \mathbf{c} can only be identified up to a gain ambiguity [43].

The expression obtained in (5.14) can be referred to as a “one-cycle” scheme [45] since only one frequency cycle is involved. We can easily extend (5.14) to take into account more than one frequency cycle. For instance, let $k_0, \dots, k_{R-1} \in \mathcal{K}$ and let us consider the system of equations

$$\mathbf{\Phi} \mathbf{c} = \mathbf{0}, \quad (5.16)$$

where

$$\mathbf{\Phi} = \begin{bmatrix} \mathbf{\Phi}^T[k_0] & \dots & \mathbf{\Phi}^T[k_{R-1}] \end{bmatrix}^T. \quad (5.17)$$

It can be hoped that by using multiple frequency cycles, the solution will yield a greater accuracy. Solving (5.16) can be very demanding in terms of computational resources since R times more equations than in (5.14) need to be considered. However, as explained in the next section, we can exploit the structure of Φ to solve (5.16) efficiently.

5.2.2 Channel Coefficients Estimation

As discussed in the previous section, we need to estimate Φ to solve (5.16), since the channel is unknown and $R_v[k, \tau]$, $k = k_0, \dots, k_{R-1}$, cannot be evaluated directly. Finding the channel coefficients then becomes a least squares problem which can be solved by computing the SVD or the eigenvalue / eigenvector decomposition. However, such decompositions are typically very expensive in terms of computational resources.

In this section, we look at solutions to estimate Φ and to address the high computational cost associated with the computation of the least squares solution. The estimation problem can be solved by obtaining an approximation of $R_v[k, \tau]$, $k = k_0, \dots, k_{R-1}$, based on the received samples, $v[m]$. We can deal with the computational problem by employing the so-called inverse iteration method [50, 67]. These solutions are detailed below.

We denote the estimates of $r_v[m, \tau]$, $R_v[k, \tau]$, $\mathbf{R}_v[k]$, $\Phi[k]$, Φ , and \mathbf{c} , at time index n , corresponding to the $(n + 1)$ -th frame of received data, by $\hat{r}_v^n[m, \tau]$, $\hat{R}_v^n[k, \tau]$, $\hat{\mathbf{R}}_v^n[k]$, $\hat{\Phi}_n[k]$, $\hat{\Phi}_n$, and $\hat{\mathbf{c}}[n]$, respectively. $\hat{R}_v^n[k, \tau]$ can be obtained by taking the K -point FFT of $\hat{r}_v^n[m, \tau]$ (see (5.8)), and the autocorrelation function can be estimated by the following recursive relation:

$$\hat{r}_v^n[m, \tau] = \alpha \hat{r}_v^{n-1}[m, \tau] + (1 - \alpha)v[m + (n - 1)K]v[m + (n - 1)K + \tau], \quad (5.18)$$

where $0 < \alpha < 1$ is the forgetting factor. $\hat{\Phi}_n$ can then be formed according to (5.13), (5.15)

and (5.17). Note that $R_u[k, 0]$ is known *a priori* and can be computed using (5.7). This procedure is summarized in Table 5.1, where the computational complexity of each step is also given. The overall computational complexity is approximately $32RQ^2$, which mainly corresponds to Step 6 in Table 5.1, i.e. the computation of $\hat{\Phi}_n[k]$, for $k = k_0, \dots, k_{R-1}$. The computational complexity is thus directly linked to the number of frequency cycles, R , and the number of taps used to model the channel $C(z)$, Q . Note that $\hat{\Phi}_n[k]$ is a complex matrix, and we assume in Table 5.1 that complex multiplications and complex additions require 6 flops and 2 flops, respectively.

| Instructions | Flops (per iter.) |
|--|-------------------|
| 1: Let $\hat{r}_v^0[m, \tau] = r_u[m, \tau]$ (see (5.4)). | |
| 2: For each received frame of data, i.e. $n = 0, 1, \dots$ | |
| 3: Obtain $\hat{r}_v^n[m, \tau]$ via (5.18). | $6QK$ |
| 4: Compute $R_v[k, \tau]$ as the K -point FFT of $r_v[m, \tau]$. | $5K \log_2 K$ |
| 5: Form $\hat{R}_v^n[k]$ according to (5.13). | |
| 6: Compute $\hat{\Phi}_n[k]$, for $k = k_0, \dots, k_{R-1}$, via (5.15). | $32RQ^2$ |
| 7: Form $\hat{\Phi}_n$ according to (5.16). | |
| 8: end for | |

Table 5.1 Algorithm for the computation of $\hat{\Phi}_n$.

To find $\hat{c}[n]$, we need to track the least squares solution of $\hat{\Phi}_n \hat{c}[n] = \mathbf{0}$, or, equivalently, to track the eigenvector corresponding to the smallest eigenvalue of $\hat{\Phi}_n^H \hat{\Phi}_n$. Since we are only interested in one eigenvector, it would be a waste of resources to compute a full eigenvalue / eigenvector decomposition. Here, the eigenvalue of interest (i.e. $\lambda = 0$) and its corresponding eigenvector, $\hat{c}[n]$, can be efficiently updated via the inverse iteration

method [67]:

$$\mathbf{z}[n] = (\hat{\Phi}_n^H \hat{\Phi}_n)^{-1} \hat{\mathbf{c}}[n-1] \quad (5.19)$$

$$\hat{\mathbf{c}}[n] = \mathbf{z}[n] / \|\mathbf{z}[n]\|_2. \quad (5.20)$$

To compute $\mathbf{z}[n]$ in (5.19), we could either compute the LU factorization of $\hat{\Phi}_n^H \hat{\Phi}_n$ and solve the resulting triangular systems via backward substitutions, or we could split (5.19) in two equations by considering the following systems:

$$\hat{\Phi}_n^H \mathbf{z}'[n] = \hat{\mathbf{c}}[n-1] \quad (5.21)$$

$$\hat{\Phi}_n \mathbf{z}[n] = \mathbf{z}'[n]. \quad (5.22)$$

The latter approach is described in this section. It has the advantage of avoiding the need to explicitly compute $\hat{\Phi}_n^H \hat{\Phi}_n$, but it necessitates finding the QR factorization of $\hat{\Phi}_n$. Note that the computational complexity of the LU-based method and the QR-based one is approximately the same.

On the one hand, (5.21) is an undetermined system with possibly many solutions. On the other hand, (5.22) is an overdetermined system with generally no solution. As shown here, there exists, however, one solution to (5.22) if $\mathbf{z}'[n]$ is the minimum norm solution of (5.21). Let us partition $\hat{\Phi}_n$ and $\mathbf{z}'[n]$ as follows:

$$\hat{\Phi}_n = \begin{bmatrix} \hat{\Phi}_n^0 \\ \hat{\Phi}_n^1 \end{bmatrix},$$

$$\mathbf{z}'[n] = \begin{bmatrix} z'_0[n] \\ z'_1[n] \end{bmatrix},$$

where $\hat{\Phi}_n^0$ and $\hat{\Phi}_n^1$ respectively are $Q \times Q$ and $(T - Q) \times Q$ matrices, $T \triangleq R(3Q - 2)$, while $\mathbf{z}'_0[n]$ and $\mathbf{z}'_1[n]$ are Q -length and $(T - Q)$ -length vectors, respectively. Equation (5.22) can thus be written as the following set of two equations:

$$\hat{\Phi}_n^0 \mathbf{z}[n] = \mathbf{z}'_0[n] \quad (5.23)$$

$$\hat{\Phi}_n^1 \mathbf{z}[n] = \mathbf{z}'_1[n]. \quad (5.24)$$

From (5.23), a candidate solution of (5.22) is

$$\mathbf{z}[n] = (\hat{\Phi}_n^0)^{-1} \mathbf{z}'_0[n], \quad (5.25)$$

which can be obtained efficiently by back substitutions since $\hat{\Phi}_n^0$ is square triangular [50]. In fact, $\mathbf{z}[n]$ as given above is a solution of (5.22) if and only if (5.24) can be satisfied, i.e.

$$\hat{\Phi}_n^1 (\hat{\Phi}_n^0)^{-1} \mathbf{z}'_0[n] = \mathbf{z}'_1[n]. \quad (5.26)$$

Such condition can be fulfilled by considering the minimum norm solution of (5.21), which is given by [50]

$$\begin{bmatrix} \mathbf{z}'_0[n] \\ \mathbf{z}'_1[n] \end{bmatrix} = \begin{bmatrix} \mathbf{Q}_{00}[n] \\ \mathbf{Q}_{10}[n] \end{bmatrix} \mathbf{R}_0[n]^{-H} \hat{\mathbf{c}}[n - 1],$$

or, equivalently, as the following set of equations:

$$\mathbf{z}'_0[n] = \mathbf{Q}_{00}[n] \mathbf{R}_0[n]^{-H} \hat{\mathbf{c}}[n - 1] \quad (5.27)$$

$$\mathbf{z}'_1[n] = \mathbf{Q}_{10}[n] \mathbf{R}_0[n]^{-H} \hat{\mathbf{c}}[n - 1], \quad (5.28)$$

where $\mathbf{Q}_{00}[n]$, $\mathbf{Q}_{10}[n]$ and $\mathbf{R}_0[n]$ are matrix partitions of the QR factorization of $\hat{\Phi}_n$, i.e.

$$\begin{bmatrix} \hat{\Phi}_n^0 \\ \hat{\Phi}_n^1 \end{bmatrix} = \begin{bmatrix} \mathbf{Q}_{00}[n] & \mathbf{Q}_{01}[n] \\ \mathbf{Q}_{10}[n] & \mathbf{Q}_{11}[n] \end{bmatrix} \begin{bmatrix} \mathbf{R}_0[n] \\ \mathbf{0} \end{bmatrix} = \begin{bmatrix} \mathbf{Q}_{00}[n] \\ \mathbf{Q}_{10}[n] \end{bmatrix} \mathbf{R}_0[n].$$

The QR factorization can also be expressed as

$$\hat{\Phi}_n^0 = \mathbf{Q}_{00}[n] \mathbf{R}_0[n] \quad (5.29)$$

$$\hat{\Phi}_n^1 = \mathbf{Q}_{10}[n] \mathbf{R}_0[n]. \quad (5.30)$$

By substituting (5.27), (5.28), (5.29) and (5.30) in (5.26), one may verify that the minimum norm solution of (5.21) allows (5.25) to be a valid solution of (5.22).

The complete blind identification algorithm is summarized in Table 5.2. The number of flops required by one iteration of the algorithm is approximately $24RQ^3 - \frac{8}{3}Q^3 + 32RQ^2 + 16Q^2$, and thus essentially depends on the number of taps modelling the channel and on the number of frequency cycles. Note that if $R = 1$ (one-cycle scheme), the number of flops is about $21Q^3 + 48Q^2$. The critical operations in terms of computational complexity are the computation of $\hat{\Phi}_n$ and its QR decomposition.

5.3 Chapter Summary

In this chapter, we have proposed a blind channel identification algorithm, which relies on the cyclostationary property of the modulated signal. This property is inherently induced by the transmitting DFT filter bank. An homogeneous system of linear equations can then be solved to obtain an approximation of the channel coefficients. Solving the system is achieved by tracking its least squares solution, an operation which can be performed

| Instructions | Flops (per iter.) |
|---|---------------------------|
| 1: Let $\hat{\mathbf{c}}[0] = [1 \ 0 \ \dots \ 0]^T$. | |
| 2: For each received frame of data, i.e. $n = 0, 1, \dots$ | |
| 3: Form $\hat{\mathbf{\Phi}}_n = \begin{bmatrix} \hat{\mathbf{\Phi}}_n^0 \\ \hat{\mathbf{\Phi}}_n^1 \end{bmatrix}$ (see Table 5.1). | $32RQ^2$ |
| 4: Compute the QR decomposition of $\hat{\mathbf{\Phi}}_n$, i.e. $\hat{\mathbf{\Phi}}_n = \begin{bmatrix} \mathbf{Q}_{00}[n] & \mathbf{Q}_{01}[n] \\ \mathbf{Q}_{10}[n] & \mathbf{Q}_{11}[n] \end{bmatrix} \begin{bmatrix} \mathbf{R}_0[n] \\ \mathbf{0} \end{bmatrix}$. | $24RQ^3 - \frac{8}{3}Q^3$ |
| 5: Solve $\mathbf{R}_0^H[n] \mathbf{z}_0''[n] = \hat{\mathbf{c}}[n-1]$ for $\mathbf{z}_0''[n]$ via back substitutions. | $4Q^2$ |
| 6: Compute $\mathbf{z}_0'[n] = \mathbf{Q}_{00}[n] \mathbf{z}_0''[n]$ (minimum norm solution). | $8Q^2$ |
| 7: Solve $\hat{\mathbf{\Phi}}_n^0 \mathbf{z}[n] = \mathbf{z}_0'[n]$ for $\mathbf{z}[n]$ via back substitutions. | $4Q^2$ |
| 8: Update $\hat{\mathbf{c}}[n]$, i.e. $\hat{\mathbf{c}}[n] = \mathbf{z}[n] / \ \mathbf{z}[n]\ _2$. | $6Q$ |
| 9: end for | |

Table 5.2 Blind channel identification algorithm.

efficiently via the inverse iteration method. The proposed method is fully described in Tables 5.1 and 5.2. Combined with the one-tap equalizer derived in Section 4.2, we now have a complete equalization solution.

Chapter 6

Computer Simulations and Experimental Results

To determine the pertinence and relevancy of the research contributions described in the previous chapters, this chapter presents numerous computer simulations and experimental results. We first show in Section 6.1 several design examples of PR prototype filters using the method proposed in Chapter 3. The spectral characteristics of the resulting filters are compared with non-PR ones and OFDM systems. We then consider in Section 6.2 the various equalization techniques that are described in Chapter 4. In particular, we look at the achievable bit rates of transceivers using a zero-padding scheme and a one-tap per subcarrier equalizer. In Section 6.3, we look at the blind channel identification technique presented in Chapter 5. The error between the estimated channel coefficients and the real ones is measured, and the merits of the proposed algorithm are discussed. Finally, a brief summary of this chapter is given in Section 6.4.

6.1 Design of Perfect Reconstruction Prototype Filters

6.1.1 Design Examples

We first attempt to design a PR prototype filter using the steps outlined in Chapter 3. Various combinations of M , the number of subcarriers, K , the upsampling factor, and D , the prototype filter length, are considered. The frequency responses of the resulting filters are illustrated in Figure 6.1 for $M = 64$ and in Figure 6.2 for $M = 128$. The stopband energy and the attenuation of the first sidelobe of these filters, representing important spectral features, are given in Table 6.1. Note that we normalize the total energy of the filters to 30 dBm. For reference purposes, the spectral features of the corresponding OFDM prototype filters are given in Table 6.2.

| M | K/M | D/M | Stopband energy (dBm) | Attenuation of the first sidelobe (dB) |
|-----|-------|-------|--------------------------|---|
| 64 | 1.125 | 18 | 23 | -26 |
| 64 | 1.125 | 27 | 15 | -38 |
| 64 | 1.25 | 20 | 12 | -40 |
| 64 | 1.25 | 30 | 6.9 | -50 |
| 128 | 1.125 | 18 | 26 | -29 |
| 128 | 1.125 | 27 | 23 | -25 |
| 128 | 1.25 | 20 | 15 | -43 |
| 128 | 1.25 | 30 | 10 | -49 |

Table 6.1 Spectral features of several PR prototype filters, obtained via the method proposed in Chapter 3.

| M | Stopband energy (dBm) | Attenuation of the first sidelobe (dB) |
|-----|--------------------------|---|
| 64 | 24 | -13 |
| 128 | 24 | -13 |

Table 6.2 Spectral features of the OFDM prototype filters.

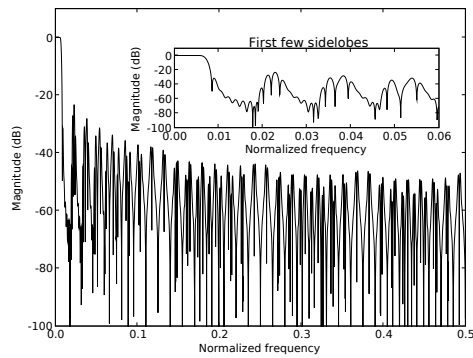
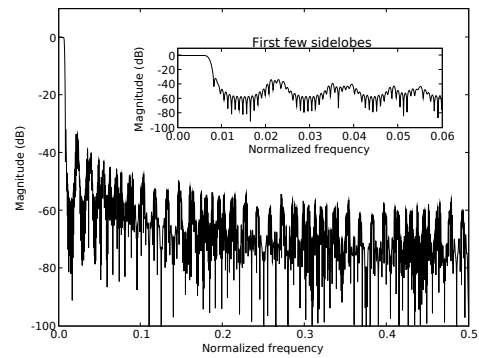
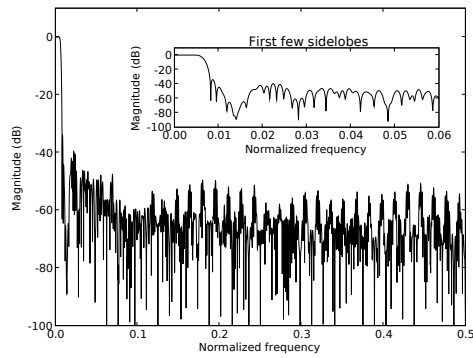
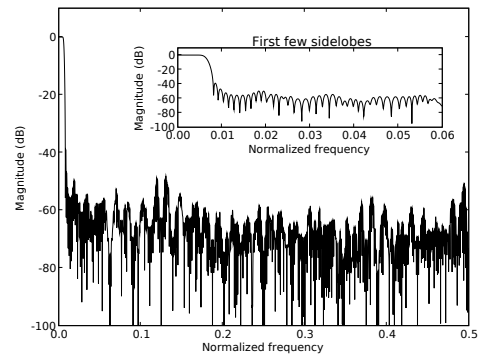
(a) $M = 64$, $K/M = 1.125$ and $D/M = 18$.(b) $M = 64$, $K/M = 1.125$ and $D/M = 27$.(c) $M = 64$, $K/M = 1.25$ and $D/M = 20$.(d) $M = 64$, $K/M = 1.25$ and $D/M = 30$.

Fig. 6.1 Frequency responses of PR DFT filter bank prototype filters with $M = 64$.

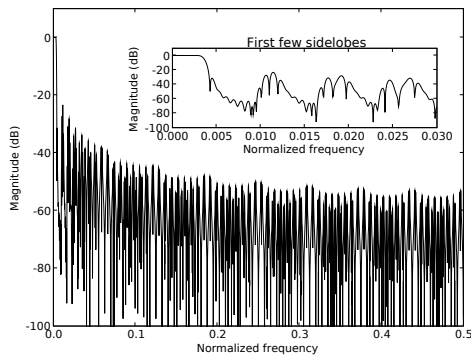
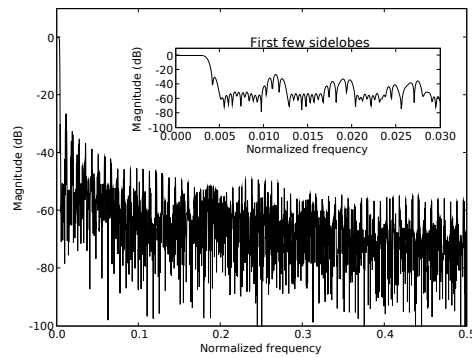
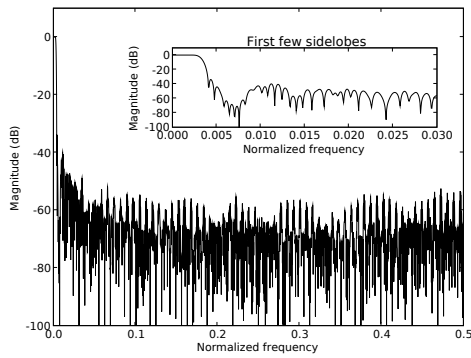
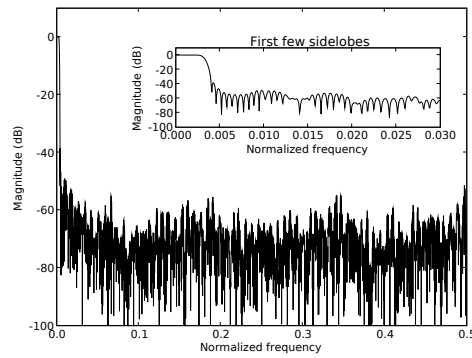
(a) $M = 128$, $K/M = 1.125$ and $D/M = 18$.(b) $M = 128$, $K/M = 1.125$ and $D/M = 27$.(c) $M = 128$, $K/M = 1.25$ and $D/M = 20$.(d) $M = 128$, $K/M = 1.25$ and $D/M = 30$.

Fig. 6.2 Frequency responses of PR DFT filter bank prototype filters with $M = 128$.

From Table 6.1, we can conclude that, for a given number of subcarriers M , better spectral features are obtained if the upsampling factor K and the length of the prototype filter D are increased. However, one must be careful as a higher K will reduce the bandwidth efficiency of the system. Likewise, a higher D will introduce more latency in the system and increase its computational complexity. These factors must be balanced carefully in order to maintain a low latency, a low computational complexity, and a high bandwidth efficiency while benefiting from good spectral features.

6.1.2 Comparison with OFDM and Other Non-PR Design

Figure 6.3 shows the frequency responses of an OFDM prototype filter with $M = 128$ and a PR prototype filter with $M = 128$, $K/M = 1.25$ and $D/M = 20$. Two key observations must be pointed out. We first note that the transition from passband to stopband, i.e. the rolloff, is much steeper with the PR DFT filter bank than with OFDM. Moreover, the attenuation of the first sidelobe is about 43 dB, whereas that of the OFDM system is 13 dB, a difference of 30 dB. In light of all these facts and the results presented in Tables 6.1 and 6.2, we confirm that PR DFT filter banks offer a considerably better spectral containment than OFDM.

If the prototype filter is not subject to the PR constraint, as it is the case in filtered multitone (FMT) [30], the spectral containment can be further improved. We show in Figure 6.4 an example of a non-PR (or near-PR) prototype filter which is designed, as proposed in [35], with the windowing method. We follow the advice given in [35], and, for best performance, we employ a Kaiser window with parameter $\beta = 8.96$ and a cutoff frequency of $\omega_c = \pi(1 + \delta)/K$, $\delta = 0.15$. Despite its impressive spectral properties, the non-PR system requires the use of a computationally demanding equalization scheme, in the form of per-subcarrier decision-feedback equalizers, to mitigate the interference due to

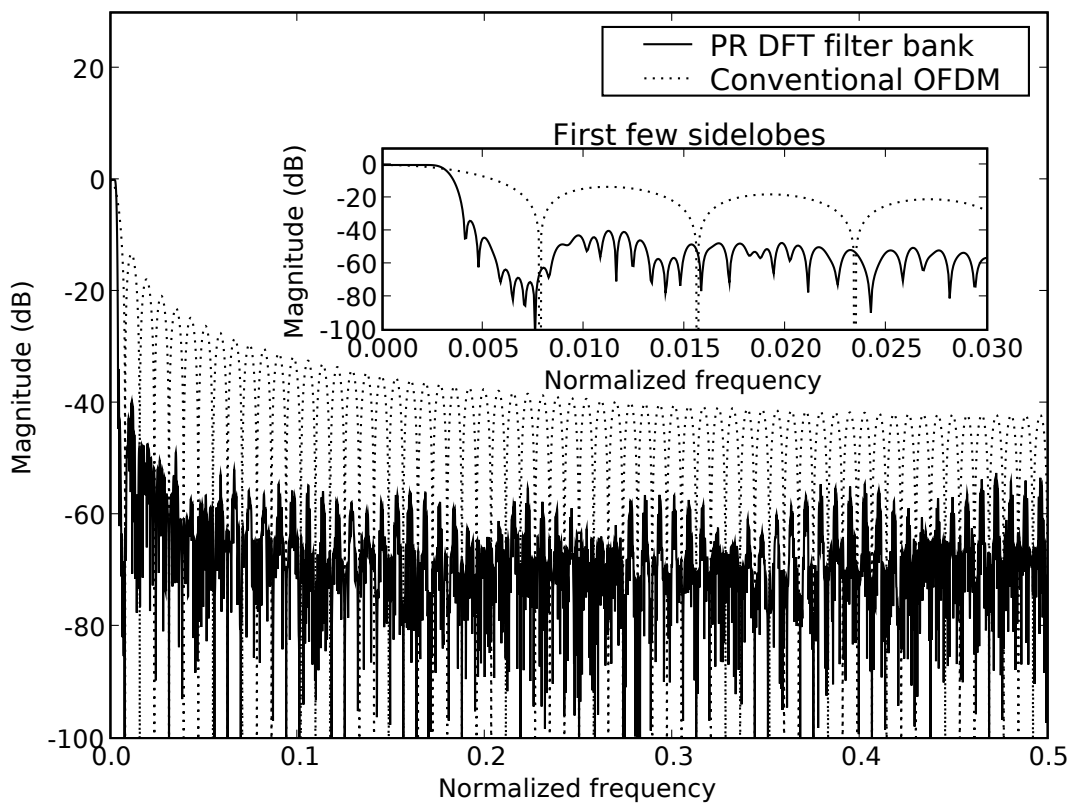


Fig. 6.3 Frequency responses of the PR DFT filter bank with $M = 128$, $K/M = 1.25$ and $D/M = 20$ and of the OFDM prototype filter with $M = 128$.

the non-PR of the filter banks [38]. As reported in Section 6.2, the performance of non-PR systems using simple one-tap equalizers is unacceptable, whereas that of PR systems is very promising (see Figure 6.10).

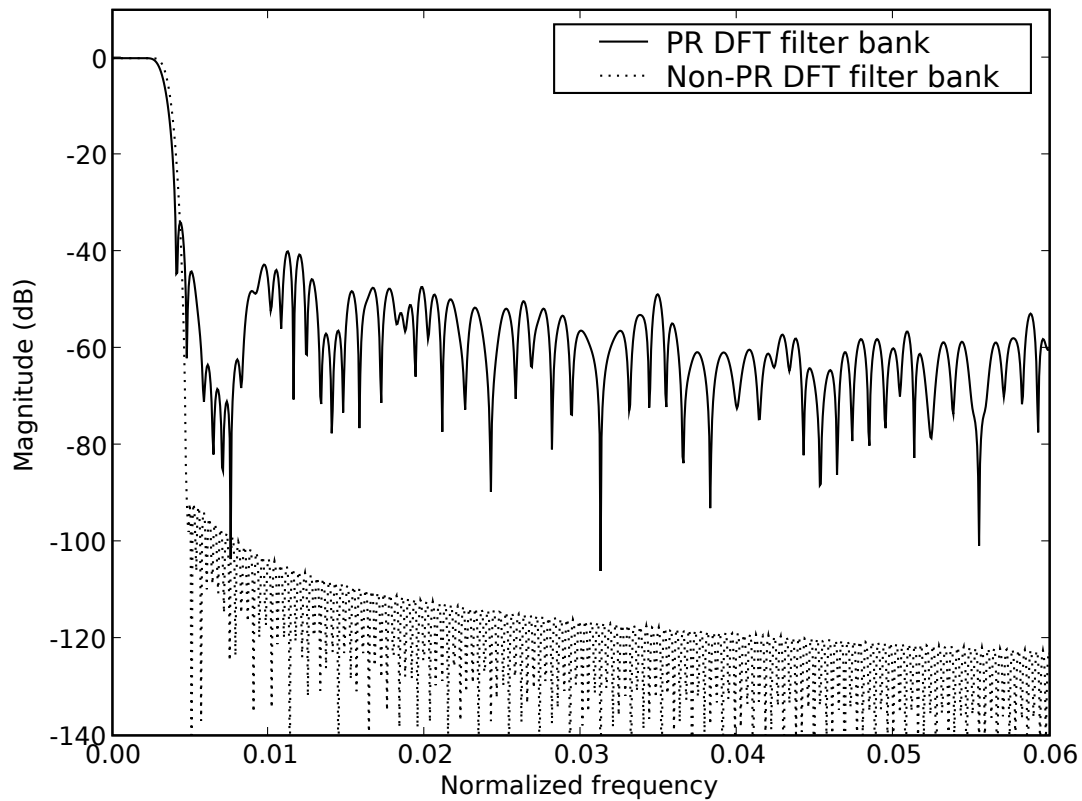


Fig. 6.4 Frequency responses of the first few sidelobes of the PR and non-PR DFT filter banks with $M = 128$, $K/M = 1.25$ and $D/M = 20$.

6.2 Channel Equalization

We now assess the performance of our proposed system using the various equalization schemes proposed in Chapter 4. We consider a DSL environment contaminated by white

noise and by radio frequency interference, modelled as narrowband noise.

6.2.1 Simulation Parameters

A DSL-like environment is simulated using the parameters described below. A sampling rate f_s of 22.08 MHz is selected. We consider two local loops, consisting in a 100-metre or a 200-metre UTP-3 copper wire, whose frequency response is taken from [30]. In DSL, the impulse response of the local loops is normally infinite, and a time-domain equalizer is usually employed to shorten the channel to a finite length [48]. However, for simulation purposes, the frequency response of the local loops is conveniently approximated via two 17-tap FIR filters (i.e. Q , the channel length, is 17) as shown in Figure 6.5.

Two different noisy conditions are considered, corresponding to additive white Gaussian noise (AWGN) and radio frequency interference (RFI). To facilitate comparison, both are set to the same power. In DSL, RFI arises due to the local loops which can pick up nearby radio transmissions. Amateur radio (or, ham) emissions are particularly bad because of their allocated frequency bands, which overlap those used in DSL, and their high allowable power. RFI can be modelled as a narrowband noise located in one of the possible frequency bands reserved for amateur radio usage, which are enumerated in Table 6.3 [16]. The power is generally limited to 400 W or 56 dBm [16]. Under unfavourable conditions, e.g. when the antenna and the local loop are separated by 10 m and run parallel to each other, an ingress power of about -4 dBm can be measured [16]. We thus consider here a -4 dBm narrowband noise, which is centered at 1.8113 MHz and located in the first amateur radio band. The narrowband noise is generated using a second-order autoregressive process, and its power spectral density (PSD) is illustrated in Figure 6.6.

Performance is evaluated in this section by computing the theoretical achievable bit rate in order to maintain an error probability of 10^{-7} . To do so, we first determine the number

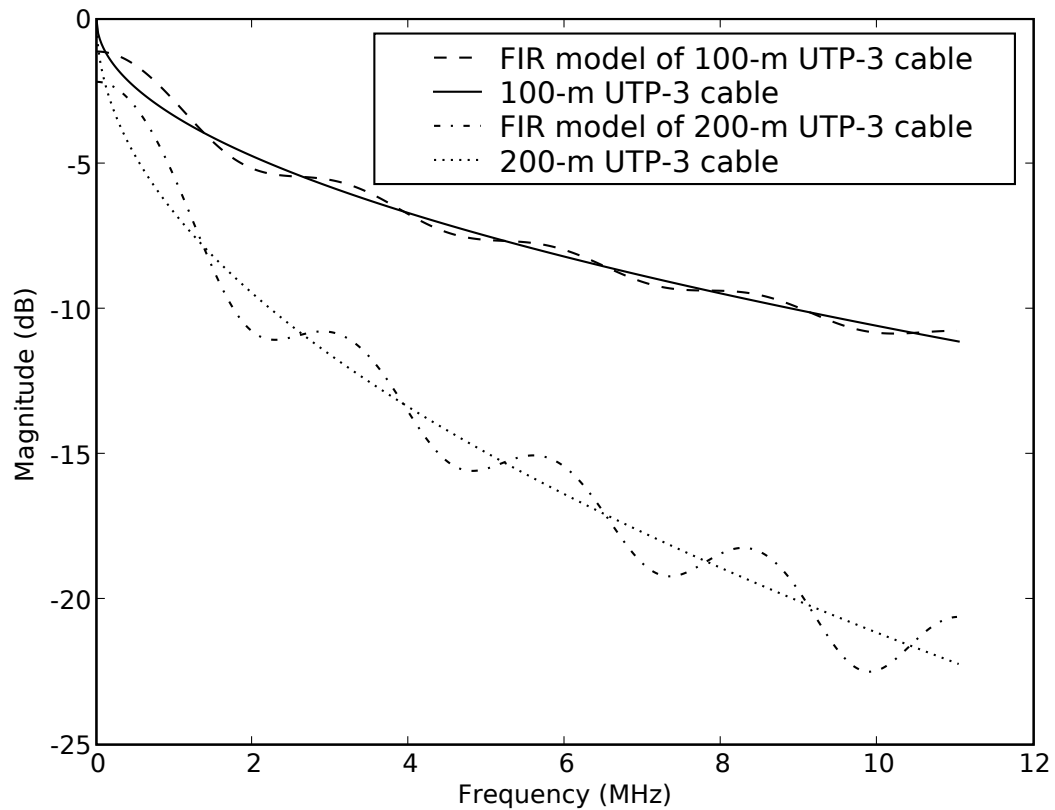


Fig. 6.5 Frequency response of the channels modelling a 100-m and a 200-m UTP-3 cable.

| Category | Start (MHz) | End (MHz) |
|------------|-------------|-----------|
| 160 metres | 1.81 | 2.00 |
| 80 metres | 3.50 | 3.80 |
| 40 metres | 7.00 | 7.10 |
| 30 metres | 10.10 | 10.15 |

Table 6.3 International amateur radio frequency bands (below 11 MHz).

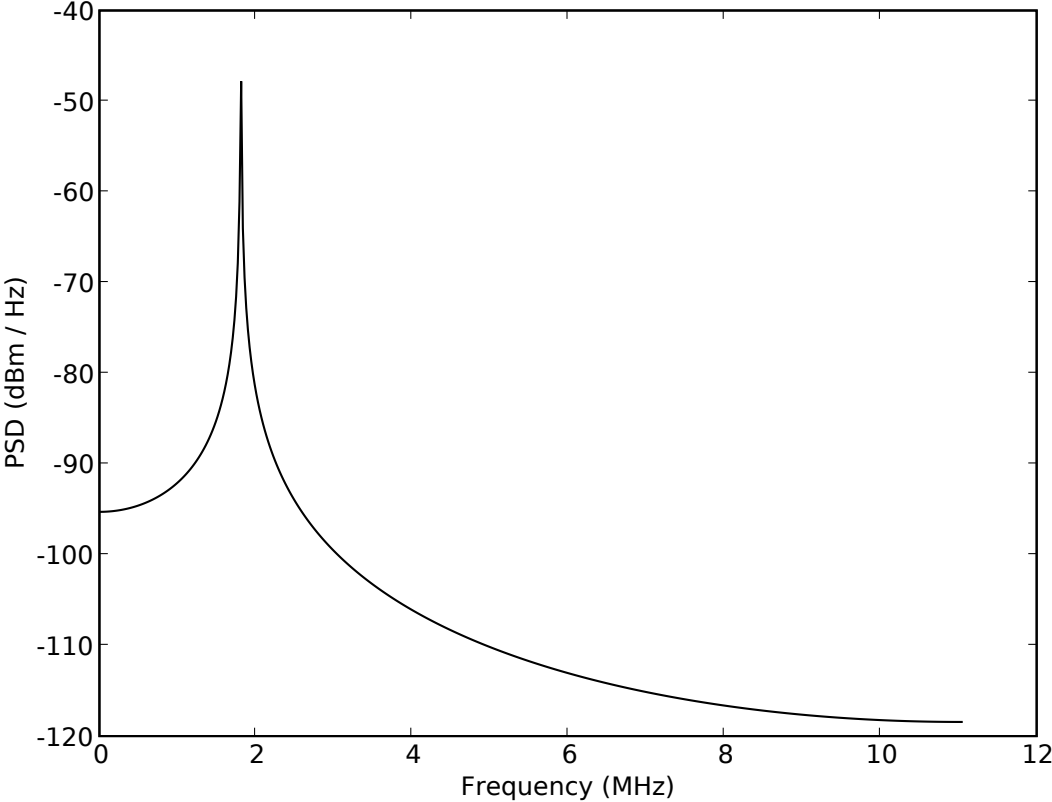


Fig. 6.6 Power spectral density of the radio frequency interference.

of bits b_i allocated for each subcarrier using the relation proposed in [46]:

$$b_i = \log_2 \left(1 + \frac{\text{SNR}_i}{\Gamma} \right), \quad i = 0, \dots, M - 1, \quad (6.1)$$

where SNR_i is the subchannel SNR, which can be obtained using (4.36) as detailed in Chapter 4, and Γ is the SNR “gap”. By assuming an error probability of 10^{-7} and the use of coded QAM symbols, the SNR gap can be obtained as follows [46]:

$$\Gamma = 9.8 + \gamma_m - \gamma_c \text{ [in dB]},$$

where γ_m is the margin, whose purpose is to ensure good performance under unforeseen conditions, and γ_c is the coding gain. Here, we select $\gamma_m = \gamma_c$. We also assume that the available power budget is divided equally among all subcarriers. Finally, the overall achievable bit rate is given by

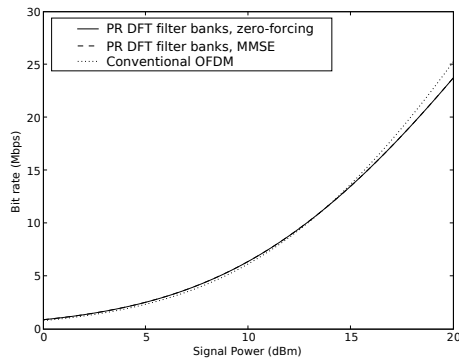
$$R = \frac{f_s}{N} \sum_{i=0}^{M-1} b_i, \quad (6.2)$$

where N is the length of the transmitted multicarrier frame, taking into account the redundancy introduced by the filter bank, zero-padding (if used) or the length of the cyclic prefix in the case of OFDM.

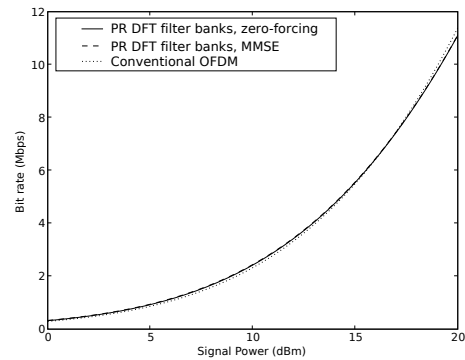
6.2.2 Equalization with Zero-Padding

Using (6.1) and (6.2), we now compute the achievable bit rate of the PR DFT filter bank transceiver with $M = 128$, $K/M = 1.25$ and $D/M = 20$ (see Figure 6.3 for the frequency response of the prototype filter). Equalization is first performed using zero-padding with a block length of $B = Q - 1 = 16$ and a block linear equalizer, as discussed in Section 4.1. Both the zero-forcing and the MMSE solutions, i.e. (4.5) and (4.11), respectively, are

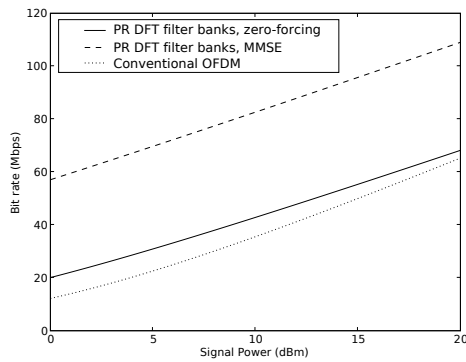
considered. Results, presented in Figure 6.7, also include the performance of a conventional 128-subcarrier OFDM system whose cyclic prefix length is set to $B = 16$ taps. Note that the zero-padding (or the cyclic prefix in the case of OFDM) is taken into account in the computation of the signal power.



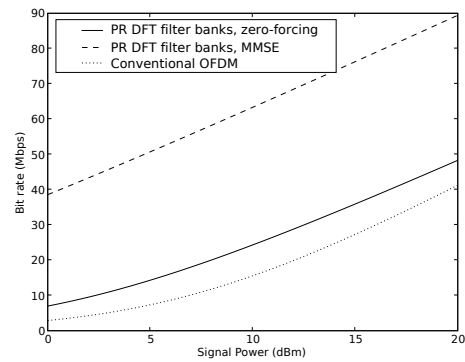
(a) AWGN and 100-m loop.



(b) AWGN and 200-m loop.



(c) RFI and 100-m loop.



(d) RFI and 200-m loop.

Fig. 6.7 Achievable bit rate of the OFDM system and the proposed transceiver using zero-padding and a block linear equalizer with a zero-forcing and a MMSE solution.

We can observe in Figure 6.7 that, in the presence of AWGN, the achievable bit rate of the zero-padded PR DFT filter bank transceivers is comparable to that of the conventional OFDM system, despite the bandwidth penalty due to the over-interpolation of the filter

bank. However, in environments contaminated by RFI, the proposed transceiver outperforms the OFDM system for both the 100-metre and the 200-metre local loop, especially when the MMSE solution is employed. For instance, with a signal power of 20 dBm, the achievable bit rate attained by using the MMSE solution is about 1.6 and 1.9 times larger than that of the OFDM system for a 100-metre and 200-metre local loop, respectively.

Let us now consider the situation where the guard length (either the zero-padding in the proposed transceiver or the cyclic prefix in OFDM) is insufficient, i.e. shorter than the channel impulse response. As discussed in Section 4.1, a modified MMSE solution can be derived and is given by (4.16). In order to focus on the insufficient guard length problem, we use here a highly dispersive 17-tap channel¹ whose impulse response $c[m]$ is given by

$$\{-0.006, 0.006, 0.063, 0.032, -0.014, 0.072, 0.004, 0.078, -0.038, \\ -0.158, 0.056, 0.006, 0.012, -0.072, -0.114, 0.040, -0.025\}.$$

Figure 6.8 shows the performance of the OFDM system and PR DFT filter bank transceiver with the modified MMSE solution and the zero-forcing solution when the guard length B is limited to 6 taps.

By inspecting Figure 6.8, one may immediately notice the poor performance of the zero-padded filter bank when the zero-forcing solution is implemented and the guard length is insufficient. In contrast, the modified MMSE solution maintains the same performance as the OFDM system under AWGN, and it allows a considerable improvement in the presence of RFI. For instance, with a signal power of 0 dBm or 20 dBm, the achievable bit rate of the modified MMSE solution is respectively about 5.2 or 1.3 times faster than that of the

¹This channel will only be considered for the particular case of insufficient guard length. As previously discussed, all other results presented in this chapter use a channel that either models a 100-m or a 200-m UTP-3 copper wire.

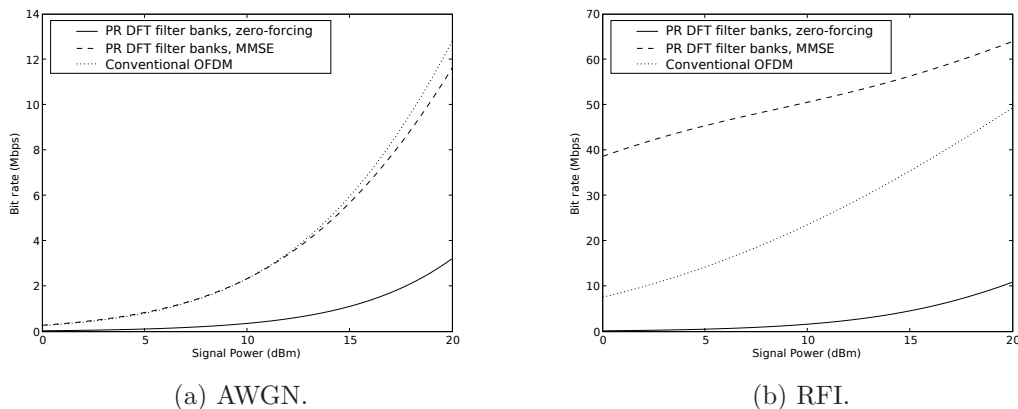


Fig. 6.8 Achievable bit rate of the OFDM system and the proposed transceiver using zero-padding and a block linear equalizer with insufficient guard length ($B = 6$).

OFDM system.

6.2.3 Equalization with One-Tap per Subcarrier

We now consider the one-tap per subcarrier equalization scheme proposed in Section 4.2.

We first examine the three possible approaches to compute the equalizer coefficients e_0, \dots, e_{M-1} .

The three possibilities include the approximate zero-forcing and MMSE solutions, corresponding to (4.23) and (4.27), respectively, and the optimal MMSE solution, corresponding to (4.31). Results presented in Figure 6.9 show the symbol mean square error (MSE) of all three solutions. The symbol mean square error is obtained via the expression

$$\text{Symbol MSE} = \frac{1}{N_f M} \sum_{n=d}^{N_f+dM-1} \sum_{i=0}^{M-1} \frac{1}{\sigma_{x_i}^2} |y_i[n] - x_i[n-d]|^2, \quad (6.3)$$

where N_f is the number of frames sent to estimate the error, and $\sigma_{x_i}^2$ is the power of the constellation symbol x_i . We employ the same prototype filter as we did in the assessment of the zero-padding equalizer, namely, a PR prototype filter with $M = 128$, $K/M = 1.25$

and $D/M = 20$ whose frequency response is illustrated in Figure 6.3.

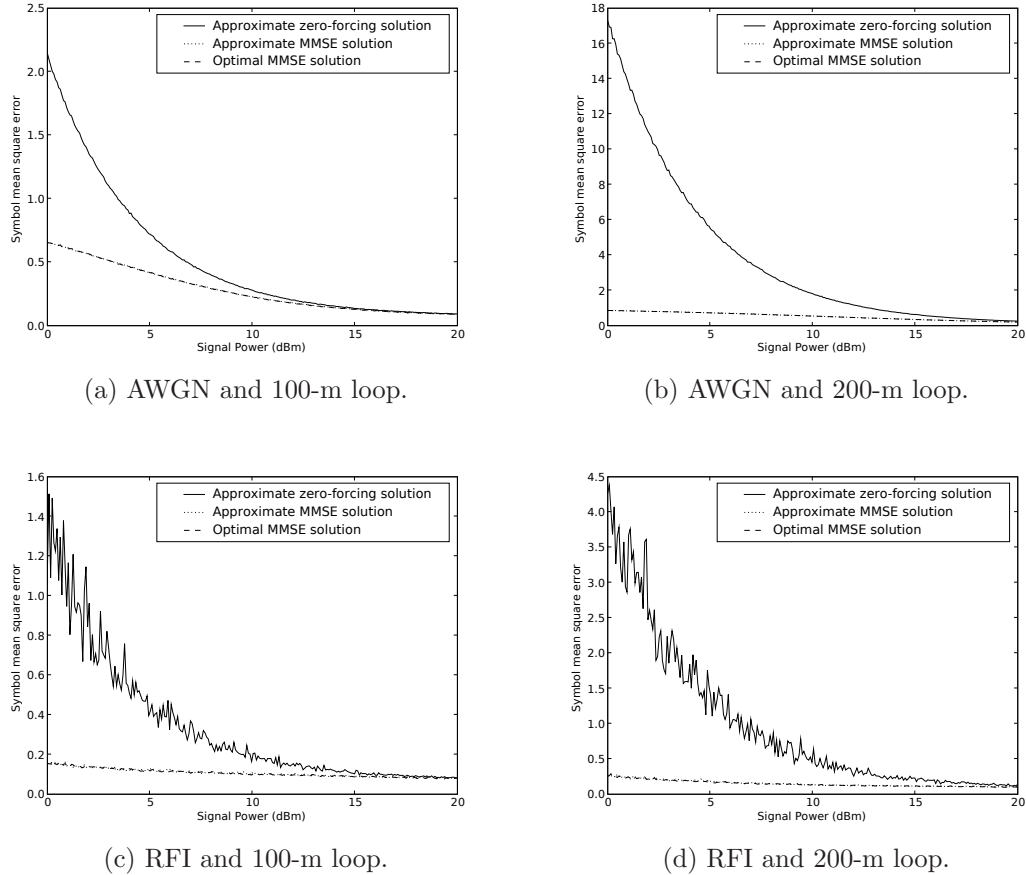


Fig. 6.9 Symbol mean square error using a one-tap per subcarrier equalizer.

We can observe from Figure 6.9, that the performance of optimal MMSE solution is almost identical to that of the approximate MMSE one. However, the computation of the optimal solution involves several multiplications of large matrices, as shown in (4.31) and (4.35), which entail a highly prohibitive computational cost (see Tables 4.7 and 4.8). In comparison, the approximate MMSE solution only requires a FFT to compute the equalizer coefficients. Since the performance loss between the two solutions is marginal, we prefer to employ the approximate solution due to its low computational complexity.

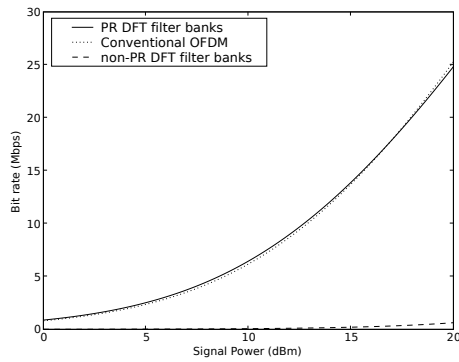
Concerning the zero-forcing solution, its performance is considerably less than the MMSE ones when the SNR is low. At high SNRs, however, all solutions are equivalent. In this case, the zero-forcing solution might be preferable as it is simpler to implement (e.g. we do not have to estimate the noise power, etc.).

Finally, we compute the achievable bit rate of the proposed PR DFT filter bank transceiver using a one-tap per subcarrier equalizer. Figure 6.10 shows the bit rate obtained by varying the signal power of the following transceivers: the proposed PR DFT filter bank transceiver, a similar transceiver using a non-PR prototype filter, and an OFDM system. We employ the PR and the non-PR prototype filters that are depicted in Figure 6.4.

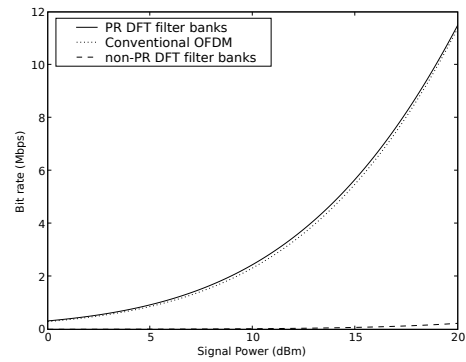
Figure 6.10 confirms that a non-PR prototype filter is not suitable for one-tap equalization schemes, since the achievable bit rate of the transceiver employing such a filter is very poor. As reported in [38], non-PR filter banks generally produce too much ISI to be mitigated by a single tap. The PR DFT filter bank transceiver, however, exhibits a performance comparable to that of the OFDM system when AWGN contaminates the communication channel. Under a RFI impairment, the proposed PR DFT filter bank transceiver outperforms the OFDM system, with a difference of about 10 Mbps between the two.

6.2.4 Comparison Between the Proposed Equalization Schemes

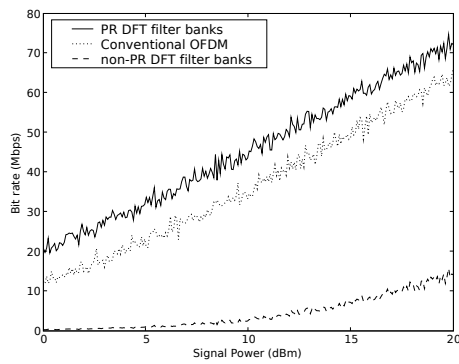
According to Figures 6.7 and 6.10, the highest achievable bit rate is obtained using a zero-padding scheme combined with a MMSE block linear equalizer. Such solution is, however, very costly in terms of computational resources. For instance, based on the results presented in Table 4.8, we note that the best solution requires about 1.82 Mflops for the computation of the equalizer coefficients and 0.118 Mflops per frame for the equalization itself. By comparison, the zero-forcing one-tap equalizer necessitates 0.0045 Mflops for the coefficient computation and 0.00077 Mflops for the equalization. The computational cost is thus two



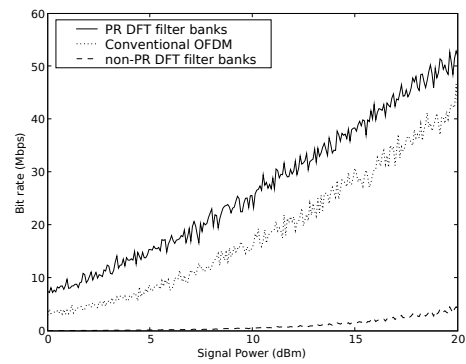
(a) AWGN and 100-m loop.



(b) AWGN and 200-m loop.



(c) RFI and 100-m loop.



(d) RFI and 200-m loop.

Fig. 6.10 Achievable bit rate of the OFDM system and the proposed transceiver using a one-tap per subcarrier equalizer (approximate zero-forcing solution) with a PR and a non-PR prototype filter.

orders of magnitude less than the cost of the zero-padded block linear approach.

We also note that the achievable bit rate of the one-tap equalizer is similar to that of the zero-padded equalizer under AWGN. Although, under RFI, the zero-padded method outperforms the one-tap equalizer, the latter still offers a significant improvement when it is compared to the OFDM system. If we balance the computational complexity of the solution versus the bit rate improvement, the one-tap equalizer appears to be the overall best solution.

6.3 Blind Channel Identification

In this section, we evaluate the blind channel identification technique proposed in Chapter 5. The simulation environment is first described. We then investigate the convergence of the estimated channel coefficients using different sets of cycle frequencies. We also compare the solutions obtained via the inverse iteration method and the SVD.

6.3.1 Simulation Parameters

We consider a DSL-like environment, similar to the one used in Section 6.2. The communication channel represents a 100-metre local loop, modelled by a 17-tap FIR filter as illustrated in Figure 6.5. The noise PSD is flat and corresponds to -140 dBm/Hz, whereas the signal power is fixed to 15 dBm. The sampling rate f_s is set to 22.08 MHz. We employ the prototype filter shown in Figure 6.3 which is characterized by the following parameters: number of subbands $M = 128$, excess bandwidth $K/M = 1.25$, number of filter taps per subcarrier $D/M = 20$.

One of the relevant performance metric in this section is the channel coefficient mean

square error (MSE). It can be computed via the relation

$$\text{Channel MSE} = \frac{1}{Q} \|\alpha \hat{\mathbf{c}}[n] - \mathbf{c}\|^2, \quad \alpha = \pm \frac{\|\mathbf{c}\|}{\|\hat{\mathbf{c}}[n]\|},$$

where $\hat{\mathbf{c}}[n]$ is the channel estimate after the n -th frame has been sent. The scaling factor α is necessary to compensate for the gain ambiguity present in blind channel estimation techniques, as discussed in Chapter 5.

6.3.2 Channel Coefficient Estimation

We first explore how the choice of k in (5.14) can influence the overall convergence of the channel estimate $\hat{\mathbf{c}}[n]$. Figure 6.11 shows the time-averaged channel MSE using the one-cycle scheme with different cyclic frequencies, i.e. $k = 1, \dots, 159$. Results are obtained by solving (5.14) directly via the SVD. We note that the lowest estimation error is obtained with the frequency cycles corresponding to $k = 1$ and $k = 159$. From Figure 6.11, we see that the choice of a proper frequency cycle is critical to have the best possible performance.

Let us now investigate the MSE of the channel coefficients with respect to time. We consider a one-cycle scheme with $k = 1$, representing one the best choice for k according to the previous results, and a multiple-cycle scheme with $k_r = r + 1$, $r = 0, \dots, 6$ (see (5.16)). The resulting estimation error is illustrated in Figure 6.12 for the two schemes. Figure 6.12 also shows the MSE of the cyclic autocorrelation $R_v[k]$. We must be careful about the number of cyclic frequencies R in the multiple-cycle approach, since it is proportional to the size of the matrix Φ in (5.16). A large R would increase the number of flops and the memory requirements considerably.

Results presented in 6.12 indicate that the one-cycle solution is almost identical to the multiple-cycle solution, a convenient outcome since the one-cycle scheme has a lower

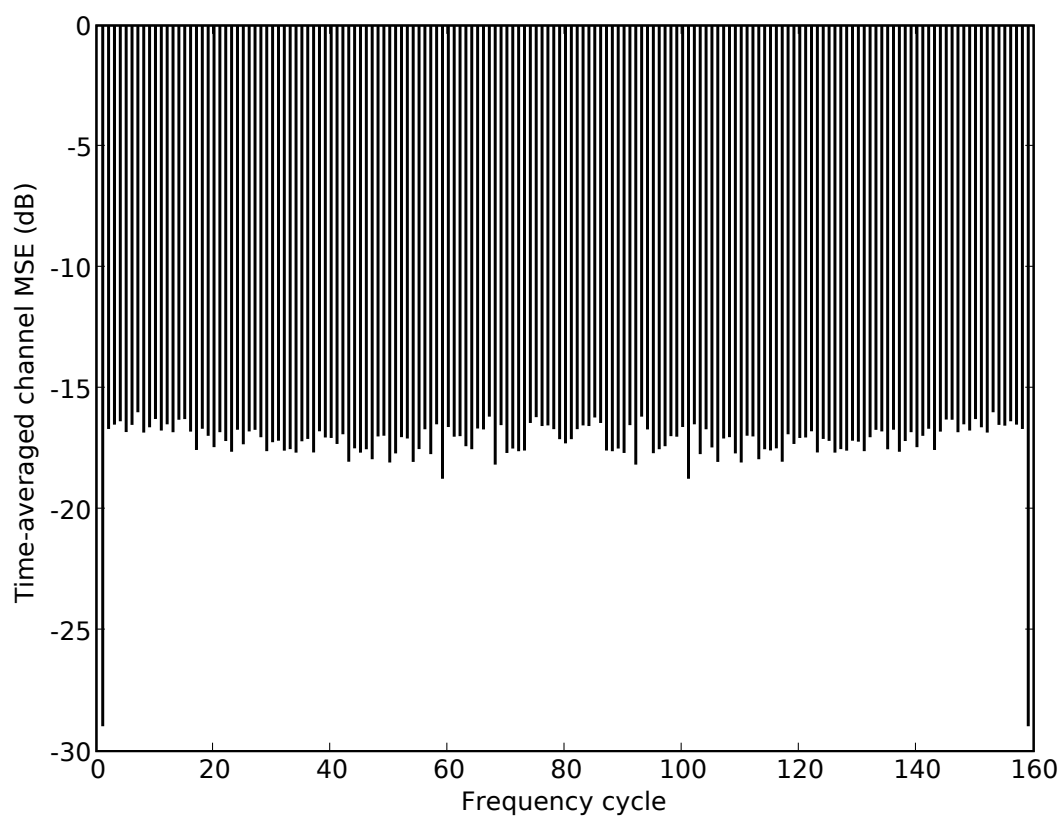


Fig. 6.11 Time-averaged channel MSE using different cyclic frequencies.

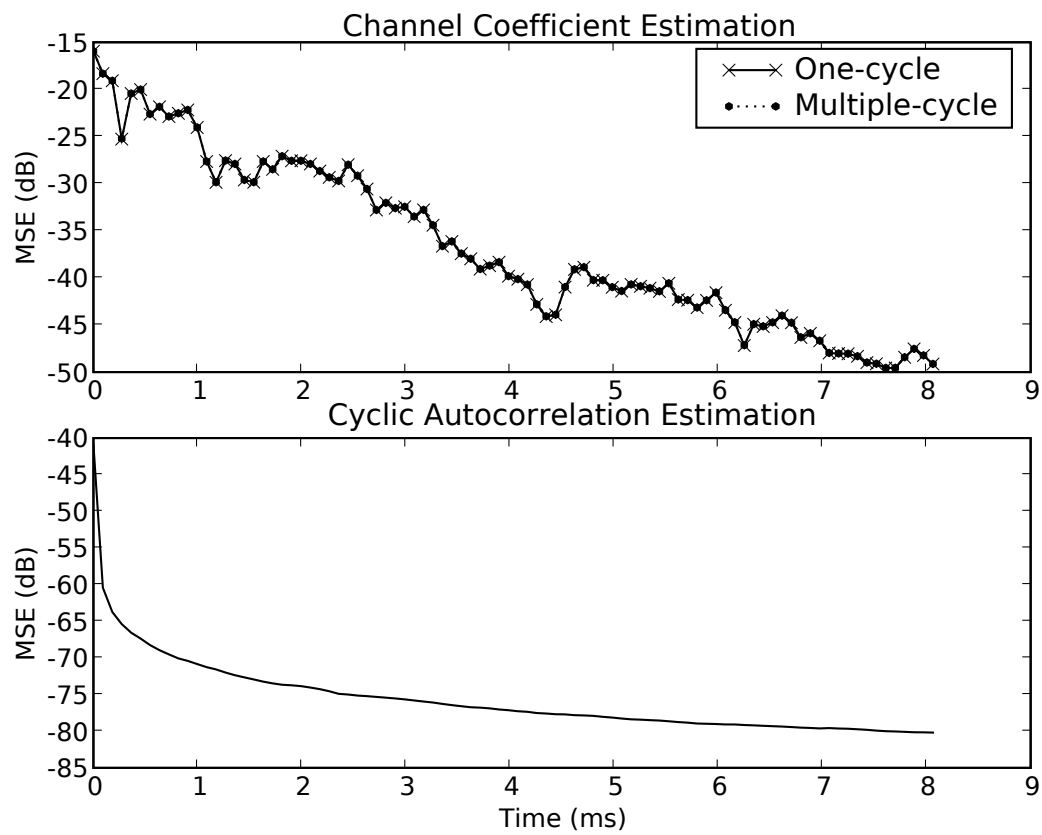


Fig. 6.12 Estimation of the cyclic autocorrelation and the channel coefficients using a one-cycle and a multiple-cycle approach.

computational complexity. We also observe that error between the real and estimated channel coefficients can be reduced by more than 30 dB after a time interval of 8.15 ms, which represents the transmission of 180,000 frames. The convergence of the estimated channel coefficients requires a relatively large number of frames, which is compatible with the assumption of a DSL environment where the channel varies slowly with time.

We next consider the symbol MSE, defined in (6.3), of a transceiver equalized by a one-tap method, as proposed in Section 4.2. The channel is estimated blindly by computing the SVD of (5.14) with $k = 1$ (one-cycle). The resulting symbol MSE with respect to time is illustrated in Figure 6.13 using both the estimated and the true channel coefficients. We may observe that the symbol MSE obtained using the estimated channel coefficients converges towards the error obtained using the true coefficients. The estimated coefficients' error curve reaches that of the true coefficient after a time period of about 4 ms.

Finally, in order to avoid doing a computationally expensive SVD each time we want to estimate the channel coefficients, we proposed in Chapter 5 to use the inverse iteration method. Since this method is iterative and we perform only a single iteration per received frame (see Table 5.2), one may be concerned about the precision of the resulting solution. We thus compare in Figure 6.3.2 the mean square error of the blind estimation technique using the SVD and the inverse iteration algorithm. The one-cycle scheme with $k = 1$ is employed.

As shown in Figure 6.3.2, the solution obtained using the inverse iteration follows the same trend as the one generated by the SVD. Even after a single iteration, the difference between the two solutions is marginal, and does not change the overall precision of the resulting solution. These results validate the fact that the convergence of the inverse iteration method is very fast [50].

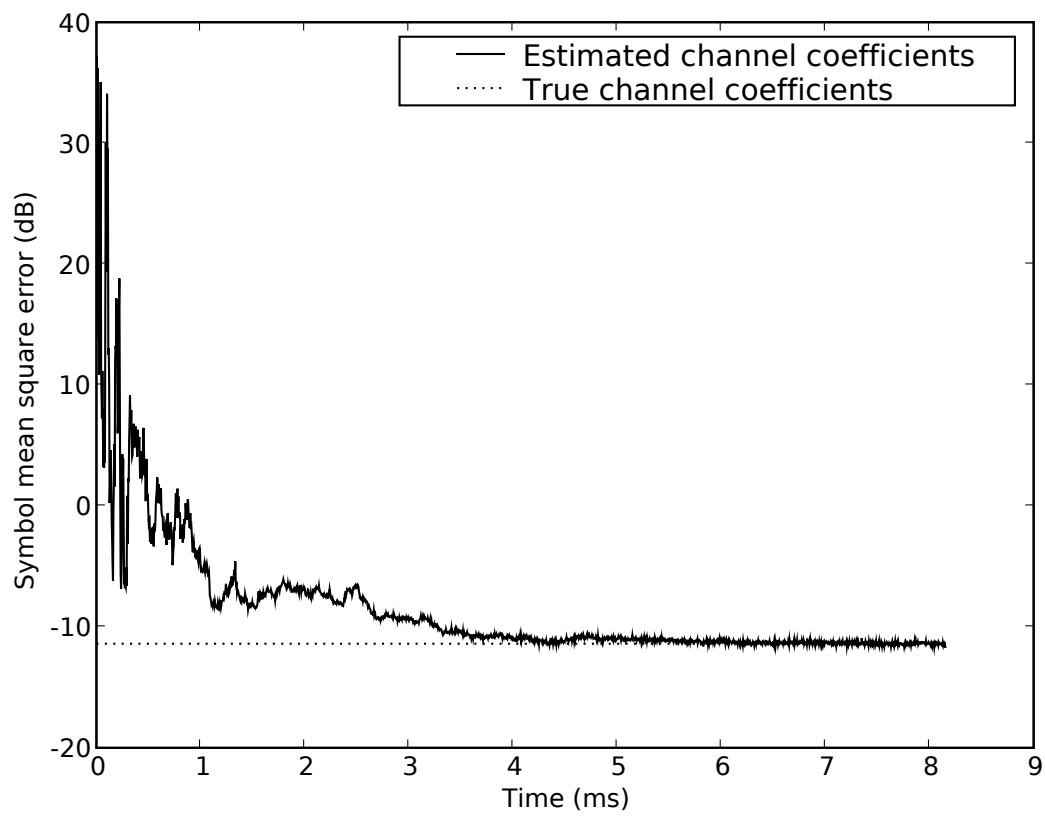


Fig. 6.13 Symbol mean square error of the transceiver using a one-tap equalizer.

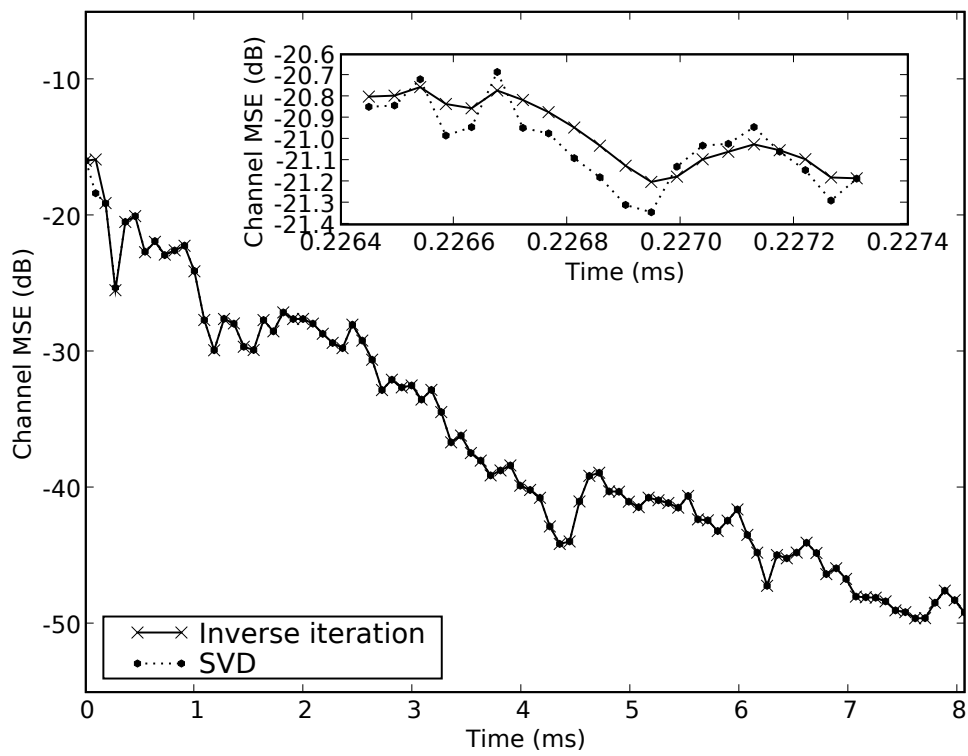


Fig. 6.14 Channel coefficient estimation using the inverse iteration method and the SVD.

6.4 Chapter Summary

In this chapter, we have conducted many computer experiments to assess the performance of the algorithms proposed throughout this thesis. We first designed several PR prototype filters and we measured some of their spectral features. A good compromise between over-interpolation, spectral containment, and filter length was obtained by considering a 128-subcarrier system with an upsampling factor of 160 and a filter length of 20 taps per subcarrier, i.e. $M = 128$, $K/M = 1.25$ and $D/M = 20$. We then obtained the achievable of such a system using two proposed equalization schemes: a zero-padded block linear equalizer and a one-tap per subcarrier equalizer. The best performance was actually achieved using the zero-padded equalizer, but its huge computational cost would prevent its use in practice. The one-tap per subcarrier equalizer, still performing substantially better than the conventional OFDM system, was thus preferred. Finally, we tested the blind channel identification algorithm. It was reported that the channel coefficients would indeed converge to their true values provided that proper frequency cycles were selected.

Chapter 7

Conclusion

We conclude by first summarizing the results and contributions presented in this thesis. Ideas for future work are then proposed.

7.1 Summary of our Work

Background information on multicarrier modulation (MCM) and DFT filter banks was first given in Chapter 2. The OFDM transceiver, which is, despite its poor spectral containment, the most widely deployed MCM system, was described. The role of the cyclic prefix in such a transceiver was also explained. To improve the spectral containment in MCM systems, we proposed to consider the use of filter banks. The concepts of polyphase representation, over-interpolation, paraunitaryness, and perfect reconstruction (PR) were thus discussed. In order to reduce the computational complexity associated with unstructured filter banks, we also looked at the theory of DFT modulated filter banks. Algorithms for the implementation of transmitting and receiving DFT filter banks were given in Tables 2.1 and 2.2, respectively. Finally, it was noted the computational complexity of the DFT filter bank was equal to the

FFT cost and twice the length of the prototype filter. As a comparison, the computational complexity of the OFDM system is solely determined by its FFT cost.

In this work, we specifically focused on PR DFT filter banks as an alternative to OFDM. PR DFT filter banks were designed using a novel method which was presented in Chapter 3. The proposed method was based in part on the parametrization of the impulse response of the prototype filter by a set of real parameters. The parametrization was carried out such that the resulting polyphase matrix of the DFT filter bank is paraunitary, which guarantees that the PR property is satisfied. To select the proper set of real coefficients, we formulated the problem as an unconstrained optimization problem where the goal is to maximize the spectral containment of the filter bank, or, equivalently, to minimize the stopband energy of the prototype filter. The stopband energy was computed via the autocorrelation of the prototype filter's impulse response.

In Chapter 4, we considered suitable equalization schemes for PR DFT filter bank transceivers. By advantageously taking into account the PR property of the filter banks, two equalization methods were proposed. The first method was based on the use of zero-padding and a block linear equalizer. Efficient algorithms implementing a zero-forcing and a MMSE solution were given in Tables 4.1 and 4.2, respectively. We also considered the case when the guard interval (i.e. zero-padding) is insufficient. In such case, a MMSE-based solution was derived, and was referred to as the “modified MMSE” solution. A much more computationally simpler method, employing one-tap per subcarrier equalizers, was then proposed. Provided that the prototype filter had a low stopband energy and a narrow passband, i.e. the filter bank was characterized by a large number of subcarriers, we proved that the channel could approximately be modelled as a simple per-subcarrier gain. Both the zero-forcing and MMSE solutions were derived. The optimal solution for non-ideal prototype filters was also determined. It was observed that the computational complexity

of the one-tap equalizer was equivalent to the low complexity cyclic prefix scheme used in OFDM.

A blind estimation algorithm for the channel impulse response was described in Chapter 5. The statistical properties of the proposed DFT filter bank transceiver were first determined. It was proved that the transmitted and received signals were wide-sense cyclostationary, a property emanating from the periodicity of their autocorrelation function. By properly exploiting the cyclostationarity of the signals and by choosing a set of cyclic frequencies, we showed that a homogeneous system of linear equations, whose solution corresponds to the channel coefficients, could be built. Solving such a system required the determination of its null space, an operation which is equivalent to the tracking of the eigenvector associated with the lowest eigenvalue. It was proposed to use the inverse iteration method for this task.

Finally, we presented in Chapter 6 computer simulations and experimental results in order to assess the performance of the proposed transceiver and to validate the algorithms presented throughout this thesis. We first showed various examples of PR prototype filters designed using the method given in Chapter 3. A good tradeoff between computational complexity, excess bandwidth and spectral containment was obtained by considering a 128-subcarrier system with an excess bandwidth of 1.25 and a prototype filter of 20 taps per subcarrier. In this case, the spectral containment of the resulting filter bank was considerably better than that of the OFDM system. The two equalization methods proposed in Chapter 4 were then considered. It turned out that, for both methods, the achievable bit rate in a DSL-like environment contaminated by AWGN was similar to the bit rate achieved by an OFDM system. Under RFI, however, the proposed transceiver outperformed the OFDM system by a considerable margin. Lastly, the blind channel identification algorithm developed in Chapter 5 was implemented and tested. We confirmed that the estimated

channel coefficients would indeed converge to their true values, under the condition that a proper set of cyclic frequencies was chosen. We also observed that the inverse iteration method is capable of properly tracking the channel coefficients even after having performed only one iteration.

7.2 Future Work

We describe in this section future directions for research work on PR DFT filter bank transceivers.

As proposed in Chapter 3, to design a suitable PR prototype filter, we need to solve an optimization problem (see (3.7)). However, solving the problem as the number of subcarriers M increases becomes more and more difficult due to the large number of parameters that must be optimized. With $M > 128$, the convergence of the optimization algorithm is poor, and a solution is hard to obtain. To solve this problem, one needs to reduce the number of coefficients that parametrize the prototype filter. A option would be to set certain parameters to a determined value, or to find an alternate parametrization.

Among the two proposed equalization schemes in Chapter 4, the zero-padded block linear equalizer was the method that yielded the highest achievable bit rate. However, its computational complexity is high, and the other solution, the one-tap equalizer, was preferred even though its achievable bit rate was lower. It would thus be a good investment to further investigate the zero-padded block linear equalizer in order to bring its computational cost closer to the cost of the one-tap equalizer. A good starting point would be to consider the single-carrier cyclic prefix (SCCP) block linear equalizer, which can be efficiently implemented using an FFT/IFFT pair [68].

In order estimate the channel coefficients, we proposed in Chapter 5 to find the null

space of a specially crafted matrix. However, computing the null space of a matrix remains a computationally expensive operation even if, as suggested in Table 5.2, we employ the inverse iteration method. The main problem is the QR factorization in Table 5.2 and its cubic-order complexity. Other null space tracking methods should thus be investigated. As a first step, the adaptive method in [69] should be considered.

Appendix A

Entries of the Polyphase Matrix $U(z)$

We prove in this appendix that the entries of $U(z)$ are given by (3.1), provided that $\alpha_{i,k}$, given in (3.2), exists. Let us first recall that $U(z)$ can be written as

$$U(z) = L_1 \Lambda_f L_0(z).$$

Let us consider $M \times K$ matrices F_l , $l = 0, \dots, D/K - 1$, as a partition of $L_1 \Lambda_f$, i.e.

$$\begin{bmatrix} F_0 & \dots & F_{D/K-1} \end{bmatrix} = L_1 \Lambda_f. \quad (\text{A.1})$$

Then, the matrix $U(z)$ in (2.21) can also be written as

$$U(z) = \begin{bmatrix} F_0 & \dots & F_{D/K-1} \end{bmatrix} L_0(z) = \sum_{l=0}^{D/K-1} F_l z^{-l}. \quad (\text{A.2})$$

Let us now consider the expression

$$l = nL + \alpha,$$

where $\alpha \in \{0, \dots, L-1\}$ and $n \in \{0, \dots, D/P-1\}$. We can then re-write (A.2) as

$$\mathbf{U}(z) = \sum_{n=0}^{D/P-1} \sum_{\alpha=0}^{L-1} \mathbf{F}_{nL+\alpha} z^{-nL-\alpha}, \quad (\text{A.3})$$

where, according to (A.1), we have

$$[\mathbf{F}_{nL+\alpha}]_{i,k} = \begin{cases} f_0[nP + \alpha K + k] & \text{if } \alpha K + k \equiv i \pmod{M} \\ 0 & \text{otherwise.} \end{cases}$$

We may notice that $[\mathbf{F}_{nL+\alpha}]_{i,k}$ can only be non-zero for a specific value of α since $\alpha K + k \equiv i \pmod{M}$ can only be satisfied for a given $\alpha \in \{0, \dots, L-1\}$. We denote this value of α by $\alpha_{i,k}$. This implies that

$$\sum_{\alpha=0}^{L-1} [\mathbf{F}_{nL+\alpha}]_{i,k} = [\mathbf{F}_{nL+\alpha_{i,k}}]_{i,k},$$

and, using (A.3), we have

$$U_{i,k}(z) = z^{-\alpha_{i,k}} \sum_{n=0}^{D/P-1} [\mathbf{F}_{nL+\alpha_{i,k}}]_{i,k} z^{-nL} \quad (\text{A.4})$$

Finally, from (A.4), we can observe that if there exists $\alpha_{i,k} \in \{0, \dots, L-1\}$ such that

$$\alpha_{i,k} K + k \equiv i \pmod{M},$$

then

$$U_{i,k}(z) = z^{-\alpha_{i,k}} \sum_{n=0}^{D/P-1} f_0[nP + \alpha_{i,k} K + k] z^{-nL}.$$

Otherwise,

$$U_{i,k}(z) = 0.$$

Note that if $\alpha_{i,k}$ exists, we can show that it is unique.

References

- [1] I. Kalet, "The multitone channel," *IEEE Trans. Commun.*, vol. 37, no. 2, pp. 119–124, Feb. 1989.
- [2] J. A. C. Bingham, "Multicarrier modulation for data transmission: an idea whose time has come," *IEEE Commun. Mag.*, vol. 28, no. 5, pp. 5–14, May 1990.
- [3] H. Liu and G. Li, *OFDM-Based Broadband Wireless Networks: Design and Optimization*. John Wiley & Sons, 2005.
- [4] *Wireless LAN Medium Access Control (MAC) and Physical Layer (PHY) specifications, High-speed Physical Layer in the 5 GHz band*, IEEE standard 802.11a, 1999.
- [5] *Wireless LAN Medium Access Control (MAC) and Physical Layer (PHY) specifications, Further Higher-Speed Physical Layer Extension in the 2.4 GHz Band*, IEEE standard 802.11g, 2003.
- [6] *Digital Video Broadcasting (DVB); Framing structure, channel coding and modulation for digital terrestrial television*, ETSI EN 300 744 V1.5.1, Nov. 2004.
- [7] *Asymmetric digital subscriber line (ADSL) transceivers*, ITU-T Recommendation G.992.1, Jul. 1999.
- [8] *Very high speed digital subscriber line transceivers*, ITU-T Recommendation G.993.1, Jun. 2004.
- [9] J. S. Chow, J. C. Tu, and J. M. Cioffi, "A discrete multitone transceiver system for HDSL applications," *IEEE J. Sel. Areas Commun.*, vol. 9, no. 6, pp. 895–908, Aug. 1991.
- [10] A. J. Coulson, "Bit error rate performance of OFDM in narrowband interference with excision filtering," *IEEE Trans. Wireless Commun.*, vol. 5, no. 9, pp. 2484–2492, Sep. 2006.
- [11] P. P. Vaidyanathan, "Filter banks in digital communications," *IEEE Circuits Syst. Mag.*, vol. 1, no. 2, pp. 4–25, Second Quarter 2001.

-
- [12] ———, *Multirate Systems and Filter Banks*. Prentice-Hall, 1993.
- [13] J. Cioffi, P. Silverman, and T. Starr, “Digital subscriber lines,” *Computer Networks*, vol. 31, no. 4, pp. 283–311, Feb. 1999.
- [14] J.-J. Werner, “The HDSL environment,” *IEEE J. Sel. Areas Commun.*, vol. 9, no. 6, pp. 785–800, aug 1991.
- [15] K. B. Song, S. T. Chung, G. Ginis, and J. M. Cioffi, “Dynamic spectrum management for next-generation DSL systems,” *IEEE Commun. Mag.*, vol. 40, no. 10, pp. 101–109, Oct. 2002.
- [16] J. A. C. Bingham, “RFI suppression in multicarrier transmission systems,” in *Proc. Global Telecommunications Conf.*, vol. 2, Nov. 1996, pp. 1026–1030.
- [17] M. Vetterli and J. Kovacevic, *Wavelets and Subband Coding*. Prentice-Hall, 1995.
- [18] M. Vetterli, “Perfect transmultiplexers,” in *Proc. IEEE Int. Conf. on Acoustics, Speech, and Signal Processing*, vol. 11, Apr. 1986, pp. 2567–2570.
- [19] Y.-P. Lin and S.-M. Phoong, “ISI-free FIR filterbank transceivers for frequency-selective channels,” *IEEE Trans. Signal Process.*, vol. 49, no. 11, pp. 2648–2658, Nov. 2001.
- [20] P. Vaidyanathan, Y.-P. Lin, S. Akkarakaran, and S.-M. Phoong, “Discrete multitone modulation with principal component filter banks,” *IEEE Trans. Circuits Syst. I*, vol. 49, no. 10, pp. 1397–1412, Oct. 2002.
- [21] M. A. Tzannes, M. C. Tzannes, J. Proakis, and P. N. Heller, “DMT systems, DWMT systems and digital filter banks,” in *Proc. IEEE Int. Conf. on Communications*, May 1994, pp. 311–315.
- [22] A. D. Rizos, J. G. Proakis, and T. Q. Nguyen, “Comparison of DFT and cosine modulated filter banks in multicarrier modulation,” in *Proc. IEEE Global Telecommunications Conf.*, vol. 2, Dec. 1994, pp. 687–691.
- [23] S. D. Sandberg and M. A. Tzannes, “Overlapped discrete multitone modulation for high speed copper wire communications,” *IEEE J. Sel. Areas Commun.*, vol. 13, no. 9, pp. 1571–1585, Dec. 1995.
- [24] V. Couturier-Doux, J. Lienard, B. Conq, and P. Gallay, “Efficient implementation of discrete wavelet multitone in DSL communications,” in *Proc. EURASIP Conf. on Video/Image Processing and Multimedia Communications*, vol. 1, Jul. 2003, pp. 393–398.

-
- [25] B. Farhang-Boroujeny, "Multicarrier modulation with blind detection capability using cosine modulated filter banks," *IEEE Trans. Commun.*, vol. 51, no. 12, pp. 2057–2070, dec 2003.
- [26] B. Farhang-Boroujeny and L. Lin, "Analysis of post-combiner equalizers in cosine-modulated filterbank-based transmultiplexer systems," *IEEE Trans. Signal Process.*, vol. 51, no. 12, pp. 3249–3262, Dec. 2003.
- [27] —, "Cosine modulated multitone for very high-speed digital subscriber lines," in *Proc. IEEE Int. Conf. on Acoustics, Speech, and Signal Processing*, vol. 3, Mar. 2005, pp. 345–348.
- [28] G. Cherubini, E. Eleftheriou, and S. Olcer, "Filtered multitone modulation for VDSL," in *Proc. IEEE Global Telecommunications Conf.*, vol. 2, Dec. 1999, pp. 1139–1144.
- [29] G. Cherubini, E. Eleftheriou, S. Oker, and J. M. Cioffi, "Filter bank modulation techniques for very high speed digital subscriber lines," *IEEE Commun. Mag.*, vol. 38, no. 5, pp. 98–104, May 2000.
- [30] G. Cherubini, E. Eleftheriou, and S. Olcer, "Filtered multitone modulation for very high-speed digital subscriber lines," *IEEE J. Sel. Areas Commun.*, vol. 20, no. 5, pp. 1016–1028, June 2002.
- [31] S.-M. Phoong, Y. Chang, and C.-Y. Chen, "DFT-modulated filterbank transceivers for multipath fading channels," *IEEE Trans. Signal Process.*, vol. 53, no. 1, pp. 182–192, Jan. 2005.
- [32] B. Borna and T. N. Davidson, "Efficient filter bank design for filtered multitone modulation," in *Proc. IEEE Int. Conf. on Communications*, vol. 1, Jun. 2004, pp. 38–42.
- [33] —, "Efficient design of FMT systems," *IEEE Trans. Commun.*, vol. 54, no. 5, pp. 794–797, May 2006.
- [34] I. Berenguer and I. J. Wassell, "FMT modulation: Receiver filter bank definition for the derivation of an efficient implementation," in *Proc. Int. OFDM Workshop*, Sep. 2002.
- [35] A. Lim, H. H. Dam, and S. Nordholm, "Filter bank design for DFT based transmultiplexers," in *Proc. Asia-Pacific Conf. on Communications*, Oct. 2005, pp. 965–968.
- [36] Y. Gao, Z. Gao, W. Zhu, and X. Yang, "The research on the design of filter banks in filtered multitone modulation," in *Proc. IEEE Wireless Communications and Networking Conf.*, vol. 1, Mar. 2005, pp. 584–588.

-
- [37] A. Tonello, "Time domain and frequency domain implementations of FMT modulation architectures," in *Proc. IEEE Int. Conf. on Acoustics, Speech and Signal Processing*, vol. 4, May 2006, pp. 625–628.
- [38] N. Benvenuto, S. Tomasin, and L. Tomba, "Equalization methods in OFDM and FMT systems for broadband wireless communications," *IEEE Trans. Commun.*, vol. 50, no. 9, pp. 1413–1418, Sep. 2002.
- [39] J. G. Proakis and D. G. Manolakis, *Digital Signal Processing: Principles, Algorithms, and Applications*, 3rd ed. Prentice-Hall, 1996.
- [40] A. Scaglione, G. B. Giannakis, and S. Barbarossa, "Redundant filterbank precoders and equalizers. I. Unification and optimal designs," *IEEE Trans. Signal Process.*, vol. 47, no. 7, pp. 1988–2006, Jul. 1999.
- [41] P. P. Vaidyanathan and B. Vrcelj, "Transmultiplexers as precoders in modern digital communication: a tutorial review," in *Proc. Int. Symp. on Circuits and Systems*, vol. 5, May 2004, pp. 405–412.
- [42] A. Scaglione, G. B. Giannakis, and S. Barbarossa, "Redundant filterbank precoders and equalizers. II. Blind channel estimation, synchronization, and direct equalization," *IEEE Trans. Signal Process.*, vol. 47, no. 7, pp. 2007–2022, Jul. 1999.
- [43] G. B. Giannakis, "Filterbanks for blind channel identification and equalization," *IEEE Signal Process. Lett.*, vol. 4, no. 6, pp. 184–187, Jun. 1997.
- [44] K. Kajita, H. Kobayashi, S. Muramatsu, A. Yamada, and H. Kiya, "A design method for oversampled paraunitary DFT filter banks using householder factorization," in *Proc. European Signal Processing Conf.*, Sep. 1996, pp. 192–195.
- [45] R. W. Heath and G. B. Giannakis, "Exploiting input cyclostationarity for blind channel identification in OFDM systems," *IEEE Trans. Signal Process.*, vol. 47, no. 3, pp. 848–856, Mar. 1999.
- [46] J. M. Cioffi, "A multicarrier primer," Amati Communication Corporation and Stanford University, T1E1 contribution T1E1.4/97-157, Nov. 1991.
- [47] P. S. Chow, J. M. Cioffi, and J. A. C. Bingham, "DMT-based ADSL: concept, architecture, and performance," in *Proc. IEE Colloquium on High speed Access Technology and Services*, Oct. 1994, pp. 3/1 – 3/6.
- [48] R. K. Martin, K. Vanbleu, M. Ding, G. Ysebaert, M. Milosevic, B. L. Evans, M. Moonen, and C. R. Johnson Jr., "Unification and evaluation of equalization structures and design algorithms for discrete multitone modulation systems," *IEEE Trans. Signal Process.*, vol. 53, no. 10, pp. 3880–3894, Oct. 2005.

-
- [49] F. Gao and A. Nallanathan, "Blind channel estimation for OFDM systems via a generalized precoding," *IEEE Trans. Veh. Technol.*, vol. 56, no. 3, pp. 1155–1164, May 2007.
- [50] G. Golub and C. V. Loan, *Matrix Computations*, 3rd ed. Johns Hopkins University Press, 1996.
- [51] X.-G. Xia, "New precoding for intersymbol interference cancellation using nonmaximally decimated multirate filterbanks with ideal FIR equalizers," *IEEE Trans. Signal Process.*, vol. 45, no. 10, pp. 2431–2441, Oct. 1997.
- [52] S. Weiss and R. W. Stewart, "Fast implementation of oversampled modulated filter banks," *Electronics Letters*, vol. 36, no. 17, pp. 1502–1503, Aug. 2000.
- [53] Y.-J. Chen, S. Orantara, and K. Amaratunga, "Dyadic-based factorizations for regular paraunitary filterbanks and m-band orthogonal wavelets with structural vanishing moments," *IEEE Trans. Signal Process.*, vol. 53, no. 1, pp. 193–207, Jan. 2005.
- [54] Z. Cvetkovic and M. Vetterli, "Tight Weyl-Heisenberg frames in $l^2(z)$," *IEEE Trans. Signal Process.*, vol. 46, no. 5, pp. 1256–1259, May 1998.
- [55] T. M. Apostol, *Introduction to Analytic Number Theory*. Springer, 1976.
- [56] J. Nocedal and S. J. Wright, *Numerical Optimization*, 2nd ed. Springer, 2006.
- [57] R. H. Byrd, P. Lu, and J. Nocedal., "A limited memory algorithm for bound constrained optimization," *SIAM Journal on Scientific and Statistical Computing*, vol. 16, no. 5, pp. 1190–1208, 1995.
- [58] C. Zhu, R. H. Byrd, and J. Nocedal., "L-BFGS-B: Algorithm 778: L-BFGS-B, FORTRAN routines for large scale bound constrained optimization," *ACM Transactions on Mathematical Software*, vol. 23, no. 4, pp. 550–560, 1997.
- [59] M. R. Wilbur, T. N. Davidson, and J. P. Reilly, "Efficient design of oversampled NPR GDFT filterbanks," *IEEE Trans. Signal Process.*, vol. 52, no. 7, pp. 1947–1963, Jul. 2004.
- [60] M. R. B. Shankar and K. V. S. Hari, "Reduced complexity equalization schemes for zero padded OFDM systems," *IEEE Signal Process. Lett.*, vol. 11, no. 9, pp. 752–755, Sep. 2004.
- [61] J. R. Magnus and H. Neudecker, *Matrix Differential Calculus with Applications in Statistics and Econometrics*. John Wiley, 1999.

-
- [62] B. Muquet, Z. Wang, G. B. Giannakis, M. de Courville, and P. Duhamel, "Cyclic prefixing or zero padding for wireless multicarrier transmissions?" *IEEE Trans. Commun.*, vol. 50, no. 12, pp. 2136–2148, Dec. 2002.
- [63] D. H. Brandwood, "A complex gradient operator and its application in adaptive array theory," *Proc. Inst. Elect. Eng.*, vol. 130, no. 1, pp. 11–16, Feb. 1983.
- [64] W. A. Gardner, A. Napolitano, and L. Paura, "Cyclostationarity: Half a century of research," *Signal Processing*, vol. 86, no. 4, pp. 639–697, Apr. 2006.
- [65] A. V. Oppenheim and R. W. Schaffer, *Discrete-Time Signal Processing*, 2nd ed. Prentice-Hall, 1999.
- [66] C. K. Ho, B. Farhang-Boroujeny, and F. Chin, "A comparison of blind channel estimation schemes for OFDM in fading channels," in *Proc. Int. Conf. on Commun. Systems*, Singapore, Nov. 2000.
- [67] I. C. F. Ipsen, "Computing an eigenvector with inverse iteration," *SIAM Review*, vol. 39, no. 2, pp. 254–291, Jun. 1997.
- [68] C. Y. Chen and S. M. Phoong, "Zero forcing cosine modulated filter bank transceivers with cyclic prefix," in *Proc. Int. Workshop on Spectral Methods and Multirate Signal Processing*, Sep. 2002.
- [69] G. Dong and R. W. Liu, "An orthogonal learning rule for null-space tracking with implementation to blind two-channel identification," *IEEE Trans. Circuits Syst. I*, vol. 45, no. 1, pp. 26–33, Jan. 1998.